Czech Technical University in Prague
Faculty of Electrical Engineering
Department of Electromagnetic Field

Michael Písařík – Doctoral Thesis

November 2016

Czech Technical University in Prague

Faculty of Electrical Engineering - Department of Electromagnetic Field

Rare Earth Doped Fiber Lasers for Spectral Region about 2 Micrometers

Doctoral Thesis

by

Michael Písařík

Prague, November 2016

Ph.D. Programme: Electrical Engineering and Information Technology
Branch of Study: Radioelectronics

Supervisor: Prof. Stanislav Zvánovec

Supervisor specialist: Dr. Pavel Peterka

Contents

Declaration of originality

I, the undersigned, hereby declare that this doctoral thesis is the result of my research in our research team and my contribution corresponds to that specified at the beginning of each research chapter. The thesis was written under the professional supervision of Prof. Stanislav Zvánovec, Dr. Pavel Peterka, using the literature and resources listed in the Bibliography and References.
In Prague, 31. November 2016,

……..

Ing. Michael Písařík

ACKNOWLEDGEMENTS

Special thanks to:

Prof. Stanislav Zvánovec and Dr. Pavel Peterka for their friendship, insight, optimism, opportunity to make something unique and a lot of discussions pushing us more forward.

So many great colleagues from the SQS Fiber Optics, the Institute of Physics, the Czech Academy of Sciences, the Department of Electromagnetic Field, Faculty of Electrical Engineering, Czech Technical University in Prague and the Institute of Photonics and Electronics, the Czech Academy of Sciences.

Finally, to my family, my wife, my daughter and my son for loving me.

The research presented in this thesis was supported by:

The Ministry of Industry of the Czech Republic, grants number FR-TI3/797 and FR-TI4/734.

The Technology Agency of the Czech Republic, grants number TA03020439, TA04010220, TA04011017, TH01010567, TH01010997 and TE02000202.

Abstract

Previous fiber laser research was strictly targeted for high efficiency, economical and exceedingly thin-disk lasers within beam quality parameters. Ytterbium doped silica fiber was the preferred fiber for most industrial applications. However, rest of rare earth doped active fibers were only demonstrated in basic principles via laboratory experiments, suggesting that many interesting solutions have yet to be studied. The purpose of this thesis is to develop methodology of key fiber laser components for wavelength range of 1.7 µm to 2.2 µm and to evaluate applications of these components to basic fiber lasers concepts further to explore and exploit their potential uses.

Keywords

Fiber laser, Mid-IR, Thulium doped fiber, 2 µm laser source, 2 µm broadband source, 2 µm fiber components, Compact fiber laser, High power fiber laser, Fiber laser applications

Abstrakt

Předchozí výzkumy vláknových laserů byly nekompromisně směrovány na vysoce účinné ekonomicky dostupné lasery překonávající tenko diskové lasery v parametrech kvality svazku. Ytterbiem dopovaná skla byla primární volba pro průmyslové aplikace. Ačkoliv množství vláken dopovaných vzácnými zeminami zůstalo pouze demonstrovaných v základních konfiguracích v rámci laboratorních experimentů, mnoho zajímavých možností zůstalo neprostudováno. Účelem této disertační práce je vyvinutí klíčových vláknových součástek pro lasery určených pro práci v rozsahu 1.7 µm do 2.2 µm a jejich další analýza pro prozkoumání jejich použitelnosti v rámci vláknových laserů.

Klíčová slova

Vláknový laser, střední infračervená oblast, 2 µm laserové zdroje, 2 µm širokopásmové zdroje, 2 µm vláknové součástky, kompaktní vláknový laser, vláknový laser s vysokým výkonem, aplikace vláknových laserů

Abbreviations list

ASE - Amplified spontaneous emission

ESA – Excited state absorption

CW – Continuous wave

NIR – Near infrared

MIR – Middle infrared

YAG – Yttrium Aluminum garnet

TDF – Thulium doped fiber

HDF – Holmium doped fiber

EDFA – Erbium doped amplifier

FBG – Fiber Bragg grating

DP – Diode-pumped

TP – Tandem-pumped

CBC – Coherent beam combination

FSO – free-space optics

LaWS – Laser weapon systems

CD – chemical deposition

MCVD – modified chemical vapor deposition

DC – Double cladding fiber

MC – Multi cladding fiber

SM – Single mode fiber

MM – Multi mode fiber

TAP – Tapered fiber

FBT – Fused bi-conical tapering

TFB – Tapered fiber budle

WDM – Wavelength division multiplexer

MOPA – Master oscillator power amplifier

1. Introduction

Shortly after the groundbreaking method of producing coherent light from a ruby crystal by Theodore Maiman [1] fiber lasers were first developed in 1960 by Elias Snitzer who used an optical fiber doped by neodymium [2] as an active medium for amplification. The first fiber laser was constructed as a fiber wound around a discharge tube within a coherent light generation around 1.06 μm. In the forthcoming years there came the huge advance of solid state lasers, and fiber lasers shelved and were nearly forgotten as a technical or laboratory curiosity. Meanwhile, rapid progress in computer science set strict requirements for a high speed telecommunication medium. Optical fiber had outmatched all other telecommunication mediums by best function parameters and boast an incomparable low price. In the late 1980s, a team headed by David N. Payne from Southampton university in UK demonstrated the amplification effect of erbium ions of signal with a wavelength around 1550 nm [3] (the wavelength with minimal attenuation in single mode optical fiber) and largely ignored fiber laser assumed the mantle as key signal amplifier for telecommunication in the form of Erbium Doped Fiber Amplifier (EDFA). Development in EDFA become a key component for long distance communication and presented an opportunity to create a large scale broadband computer network – the Internet.

At beginning of the 1990s dramatic political changes in Europe took place and group of scientists emerged from the eastern bloc and resumed their work in a centralized Germany. One such scientist was Denis V.Gapontsev who founded the IPG company in the reunited nation. Until the late 1990s, industries relied upon gas lasers, mostly in the form of carbon dioxide CO_2. Disk lasers offered a great range of benefits, such as improved beam quality, which led to rapid market change to solid state lasers. Moreover, fiber lasers offered better beam quality and efficiency than disk lasers. V.Gapontsev and his group subsequently patented a key component of fiber lasers to mix the pump and signal [4]. Since the 2001 crisis in telecommunication markets, a lot of people have been looking for other possible applications of telecommunication components and a popular area of investment has been the development of a fiber laser made by optical fibers doped by Ytterbium. No other type of a solid state laser can match efficiency and beam quality of fiber lasers.

Nowadays lasers are used in many applications in industry, medicine, communication and science, though they have low energy efficiency when transferring electric energy into coherent optical laser emission [5]. Typical power efficiency of most laser types is just a few percentage points. Semiconductor laser diodes have greater efficiency, up to 50% in energy conversion [6], but they have wide divergent emissions with poor beam quality which is a limiting factor for wide class of applications. Optical fiber allows poor quality light emitted from laser diodes to be converted into a high-quality coherent optical emission resulting in a high power laser with a conversion efficiency of up to 90% (Yb dopped fiber lasers)[6,7]. Other benefit of fiber lasers is their long active mass length which reduces cooling requirements and decreases the outer dimension.

Most powerful fiber lasers are constructed with Ytterbium-doped fibers which offer one of the highest efficiencies and optical continuous wave (CW) output power up to several tens of kilowatts at an emitting wavelength of around 1 μm [6, 7]. This is hazardous as even relatively low energy in the near infra-red (NIR) region close to the visible spectrum can cause permanent eye damage because it can be focused by the eye's optical system [8]. This

problematic issue places additional demands upon work safety, as staff must be fully aware of the risks and anyone working with the application must do so in a strictly controlled environment. Wavelengths longer than 1.4 μm are safer to the eye with dangerous power limits higher by 10 000 times contrary to shorter wavelengths due to their high absorption in water (i.e., in the so-called eye safe region). Another common fiber laser with an efficiency of about 40% is the Erbium doped fiber laser [9]. Erbium fiber lasers are widely used in telecommunications for amplifying. Last year saw an efficiency up to 70% by thulium doped fiber [10] which made such a solution comparable with ytterbium fiber lasers [11]. The benefit of Thulium-doped fiber lasers stems from a wider tunable wavelength, from 1850 nm up to 2050 nm in comparison with 1020-1100 nm for Ytterbium-doped fiber lasers.

The thesis is focused on the methodology of novel fiber laser design and their applications. It is divided into following sections: first, the State of art briefly describes the benefits of fiber lasers with emissions around 2 μm, their potential applications, lasing principles, mode of operations and design architecture. Then, the motivation of the PhD thesis is given. Next, the core of the thesis provides a Collection of published journal papers from the research of key components for fiber lasers around 2 μm demonstrating, as well new principles of lasers and their limits. Finally, the Future directions of my research work, my Final conclusion and a summarization of the achieved results of this thesis are provided.

2. State-of-art

2.1. Fiber laser application

Knowledge of the target application is essential for setting up the operating conditions of fiber laser. For a successful transfer of research to a real application in industrial conditions it is essential to acquire an understanding of the user or applications requirements. In my work I focused on a methodology of development for selected applications for fiber lasers featuring wavelength around 2 µm. These applications can be found in the field of materials processing, communications, safety and medicine. The most desirable benefits of fiber lasers around 2 µm introduce eye-safety and high energy efficiency with the widest possible frequency band. Disadvantages include higher prices for the basic materials Thulium and Holmium oxides in comparison with Yb or Eb oxides.

The main benefit of fiber lasers is their excellent beam quality, good energy and economic efficiency that is difficult to match with gas or thin-disk lasers. Fiber lasers are powered by pump laser diodes modules, so they cannot be more efficient than diode lasers. For this reason fiber lasers are not competitive with diode lasers when beam quality is not essential. Thin disk lasers have same efficiency and worse beam quality than fiber lasers. However, problematic issues of thin disk lasers include pointing stability, cooling problems of the active medium and mirrors, thermal lenses and power stability. One of disadvantages of fiber lasers in comparison with thin disk lasers is higher waveguide dispersion which can be limiting for pulse duration. Rod lasers offer high output power but all have the aforementioned disadvantages of previous laser types including poor slope efficiency. High-power fiber laser sources operating in the 2 µm wavelength region have been intensively studied as promising sources for many applications, including materials processing, medicine, eye-safe LIDAR, and chemical and environmental sensing [6][10]. Particularly important applications are in nonlinear frequency conversions to mid-infrared wavelength, e.g., in optical parametric oscillators and in supercontinuum broadband sources [5][12]. Such fiber lasers require a novel active fiber design as well as composition changes.

Eye safety is a key advantage of all lasers operating at wavelengths longer than 1.4 µm. Contrary to them, higher frequencies are not so attenuated by water in vitreous and are focused your lens to the retina. NIR frequencies around 1.0 µm should be considered seriously because retina is not sensitive to this NIR spectrum and the iris would not reduce incident light intensity. Even brightness of 10 µW per square cm could cause irreversible chemical changes in retina after one hour of exposure as was reported in studies on rats [13].

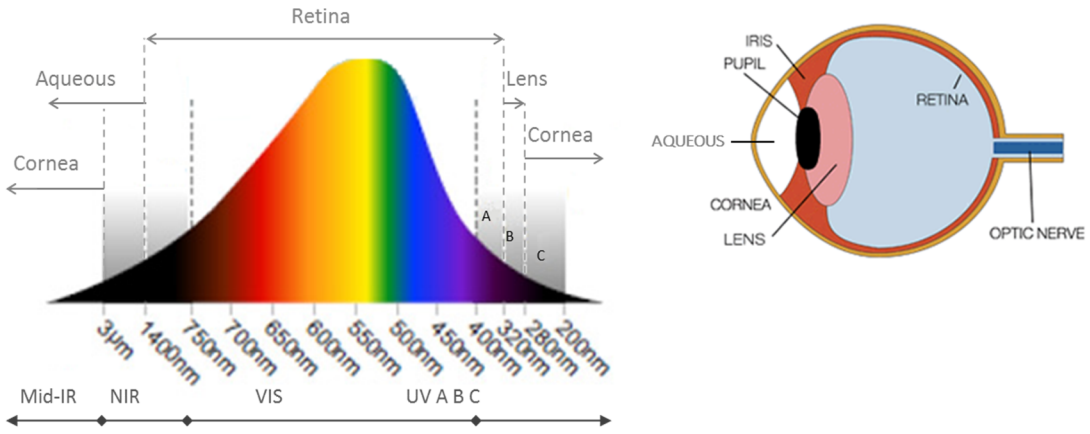

Figure 1. Eye hazard by various spectra of light

A high risk of potential damage of an eye (see Fig.1) by infrared light increases the cost of the additional protection of production cells and limits a lot of applications, such as free space communications or medical applications.

Thulium fiber lasers have all the requirements to become industrial standard in a few years, but it is necessary to develop components and investigate behavior of standard components for emitting wavelengths around 2 µm [6][7]. It is also necessary to investigate techniques for increase of efficiency as well as immediate and average output power.

2.1.1. Fiber lasers for materials processing

Materials processing by lasers could be divided into four purposes – cutting, wielding, precise-manufacturing and materials modifications. Most of applications are based on direct laser impact, but interesting applications can also be found including laser marking or laser shock peening with indirect laser impact.

Cutting and wielding applications are mostly done by continuous laser mode. Raw power is often needed to cut materials and because the typical working distance is quite short (up to 160 mm) and focal spot quite large, the beam quality is not as important as raw power energy. The required power for metal cutting is typically from 500 W to several kilowatts. Some materials like transparent polymers have low absorption up to 1.7 µm. Therefore they need additives (dopants) to rapidly increase absorption around 1.0 µm. The typical power for cutting of transparent polymers is in the range from 50 W up to 400 W.

Contrary to the afore mentioned applications, precise manufacturing by lasers needs a minimal effect of thermal ablation in impact zone and excellent Gaussian beam with M^2 close to 1. To reduce thermal ablation significantly, lasers cannot operate in continuous wave mode and need pulses shorter than 5 ps. The typical average power for micro shaping is not high, only 20-50 W but with a high repetition rate close to 1 MHz. Micro-machining requires higher energy in pulse (i.e. higher than 1 mJ) with smaller repetition frequency and pulse length shorter than 10 ps. It is important to keep in mind that single fiber laser cannot accumulate more energy for the pulse than a few µW.

Laser marking represents the most basic fiber laser application of materials processing and is mostly processed by pulses longer than 10 ns. For fiber lasers, the most interesting wavelength areas are around 1 μm for metals and non-transparent polymers, 2 μm for transparent polymers as PMMA, PC, PET, PVA or PLLA. The main benefits of the 2 μm region are associated with laser safety which is of high importance due to the low technical skills of laser technology users from previous projects (e.g., repair and maintenance centers in Africa and small companies). Another benefit is absorption in polymers mostly caused by residential OH ions from the polymerization or extrusion process. Heating OH ions or carbonization cause unwanted material changes like yellow color by CO2 lasers. Wielding transparent and non-transparent plastic is required by the automotive industry or in bio-medical applications like labeling.

2.1.2. Free space optical communications

Increases in astronomical sensors and improvements in picture recognition have dramatically increased requirements for the bandwidths of RF transmission from satellites so that up to 40% of data cannot be sent in real time meaning data have to be erased in the next orbital cycle. National Aeronautics and Space Administration (NASA) and European Space Agency (ESA) task groups have exploited a solution to increase possible communication time by establishing a network of geostationary communication satellites while maintaining communication by free-space optics (FSO) [14]. There are suitable windows for communication in the atmosphere and one of them was suggested as a possible application of the Holmium fiber amplifier targeting window at 2.17 μm see in Figure 2 [6].

Another project for long range communication was launched by NASA to increase data bandwidth for long range transmissions between a satellite in lunar orbit, the Lunar Atmosphere and Dust Environment Explorer, and ground stations on the Earth where a demonstrator was constructed on behalf of the Lunar Laser Communication Demonstration (LLCD) project [14]. The required optical power could easily reach multi-Watt level as determined by overview demonstrator results designed at a 1550 nm window with 1 W average power [15], however the ultimate goal is to change to 2.17 μm or 4 μm window and increase average power as the bandwidth develops.

Holmium fiber lasers, which could be used for long range FSO communication and have unique broadband emissions from 2.05 μm to 2.2 μm, with proper modulation could be applied in a communication window at 2.17 μm, but the required output power is difficult to achieve by semiconductor lasers and the price is too high.

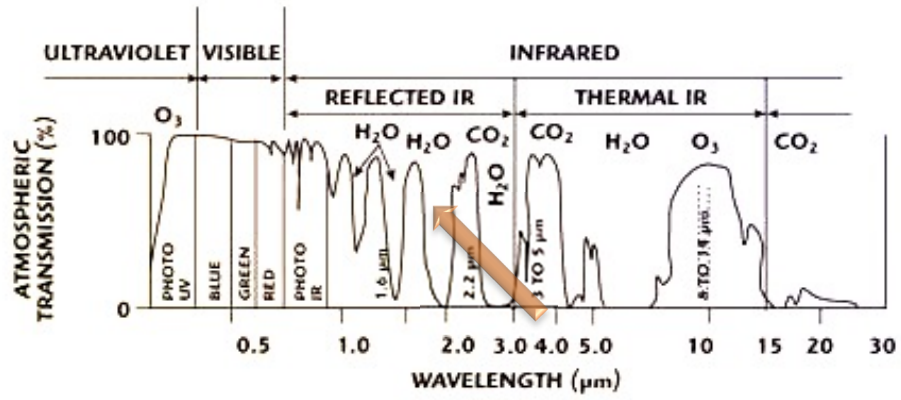

Figure 2. Atmosphere transmission and communication windows [6]

High IR absorption of fused silica at 2.17 μm limits all silica fiber lasers to maximum power of 100 W. Techniques, such as the coherent combination with an active phase controlling, will be deeply investigated for this purpose. In addition, the lack of a high-speed, high-power modulator will become serious problem.

2.1.3. Fiber lasers for medical applications

Lasers have found their way into surgery and they have been widely used for cutting or modifying tissue in wide areas since the 1980s. Pulsed lasers, like femtosecond and picosecond lasers, are ideal for eye surgery or lithotripsy [16]. CW lasers are ideal for cutting and stressing materials like tissue. Basic difference between CW and pulsed lasers is a thermal condition. With pulse durations shorter than 5 ps we can change the mechanism of laser ablation and we can significantly change area of laser treatment to reduce penetration depth which is also highly wavelength dependent.

For example, significant works with lasers has been done in urology [17] where results from this field of application show better achieved results by laser in proximity of 2 μm wavelength because they had a penetration depth lower than 0.5 mm in comparison with 1 μm lasers with up to 2 mm penetration depth. The average human cell measures about 30 μm and a typical fiber coupled laser for surgery has a multimode step-index optical fiber with a core size of 200 μm. By simple calculation the minimal interaction zone is 500 to 1 000 cells.

The use of ablative techniques for the treatment of renal masses has evolved from oncological successes including nephron-sparing surgery and the need for a minimally invasive technique with a learning curve less steep than that of a partial nephrectomy. Cryoablation and radiofrequency ablation are at the forefront of this category, but laser interstitial therapy has also been investigated [18].

In light of extended clamping times during laparoscopic partial nephrectomy, which results in uncompensated tissue hypoxia, alternative techniques using lasers have been developed to simplify the excision of renal cell carcinomas in a bloodless manner without renal vessel clamping. The thulium laser is a continuous or pulsed solid state laser that emits a wavelength of 1900-2040 nm and penetrates tissue to a depth of 0.5 mm. A single center prospective study, provided in [19], of 10 high-risk patients found thulium thin-disk

(thulium:YAG exciting at 2011 nm) laser-assisted enucleation for RCC to be a feasible, safe, and effective procedure, with no positive surgical margins and without blood loss exceeding 40 mL. Similarly, a pilot study, presented in [20], of 15 patients who underwent zero-ischemia LPN using thin-disk thulium:YAG showed minimal blood loss, negative tumor margins, and the preservation of renal function was The results of these preliminary studies are promising but have yet to be conclusively determined and need further analysis.

2.1.4. Military applications

The potential of using lasers for military purposes has been intensively investigated by military since the "Star Wars" project in 1984 to 1992 [21]. Lasers were studied for anti-ballistic and anti-missile systems, but it was not until 2011 that a feasible system was produced. Today, solid state lasers, such as fiber lasers and thin-disk lasers, offer good efficiency and excellent beam quality, so most projects typically combine a number of lasers using incoherent combination technique to create the raw power needed for anti-piracy missions in the Somalia seas [22].

The US navy combines 6 industrial Ytterbium fiber lasers with 5.5 kW output power to produce 33 kW laser output power in its Laser Weapon System (LaWS) [23]. LaWS was installed on the USS Ponce in 2014 and successfully demonstrated in December, 2014. More powerful 100 kW version will come to duty in the year 2017.

Another successful HEL project was a point defense anti-drone and anti-missile system by Rheinmetall as demonstrated in 2013 [24]. 4-Barrel Laser Gatling Gun system is based on coherent combination of 5.4 kW Ytterbium fiber lasers from IPG Photonics. Concept has the potential to come to service around year 2020.

Because military lasers are operating on distances longer than 2 km, successful projects depend on Ytterbium fiber lasers, Nd-YAG rod type lasers. It is just a question of time when drones and missiles will be covered by a reflection coating and the requirements for the raw laser power for this purpose will then be quickly changed to requirement for high pulse energy above laser inducted damage threshold of the drone's reflective coating. To satisfy this new requirement there will be general change from CW mode operation to pulsed operation. Some interesting projects such as particle acceleration or debris removal systems have recently started. An interesting demonstrator has already been built by Thales Optronique using 19 fiber lasers in femto-second regime as will be described in chapter 2.7.4 [25].

Forming plasma in the laser beam path could cause a random scattering of the laser beam as in materials processing. Eye safety will also probably become serious problem also military applications like anti-drone laser batteries in urban places as pulse optimization for propagating inside atmosphere [26].

2.2. Fiber laser lasing

A basic component for lasing in optical fiber is rear-earth-doped optical fiber. The rare-earth cations in covalently bonded glasses, like silica, to form inter-network regions [6] comprised of rare-earth cations. Cations bond ionically to non-bridging oxygen [6] which consists of atoms that interface with the main covalently bonded network regions. Because their large cationic field strength (defined as Z/r^2, where Z is the atomic number and r is the radius of the ion) requires a high coordination number, rare-earth cations tend to cluster in the inter-network regions to share non-bridging oxygen atoms.

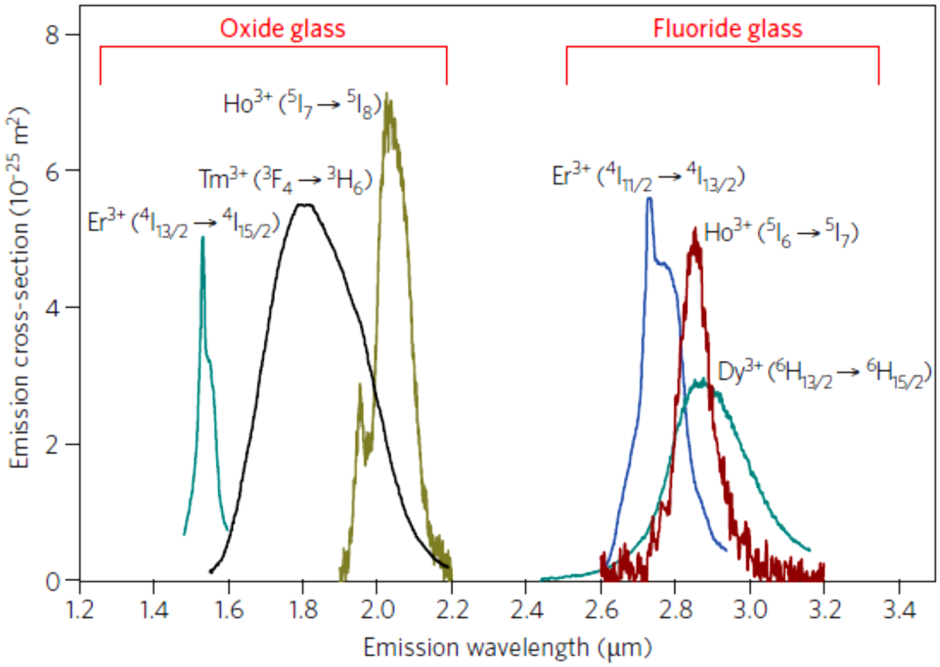

Figure 3. Fluorescence spectra of the rare-earth cation - laser transitions emitting at wavelengths greater than 1.5 μm. The oxide glass is silicate. The fluoride glass is ZBLAN [6].

Figure 3 depicts the fluorescence spectra of the NIR transitions from rare earth fiber lasers emitting in wavelengths longer than 1.5 μm. Achieved power towards high power mid-infrared laser is summarized in figure 4 [5]. The quasi-three-level transitions [27] of the rare-earth cations Tm3+, Ho3+ and Er3+ are responsible for the highest powers available in silicate glass with wavelength λ > 1.5 μm. Tm3+ doped fiber lasers with emission at around 2 μm are one of the most powerful and efficient fiber lasers. These devices are excited with established diode lasers emitting at 0.79 μm, and their output can be tuned from at least 1.86 μm to around 2.09 μm [28]. With the implementation of Tm3+ concentrations exceeding 2.5 wt%, combined with cluster-reducing co-dopants that mitigate gain-lowering energy transfer upconversion processes, cross-relaxation between neighbouring Tm3+ cations can nearly double slope efficiency [29]

.

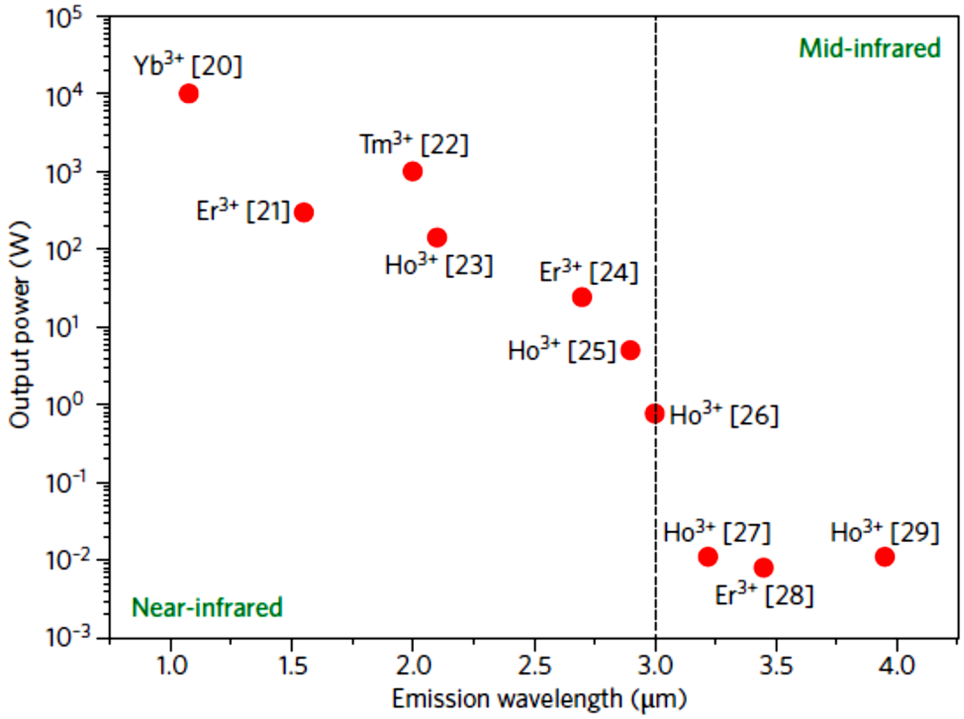

Figure 4. Output power of infrared fiber lasers as a function of the emitted wavelength. The reduction in output power with increasing emission wavelength is caused primarily by the growing quantum defect between the pump photon energy and laser photon energy. [30]

Dopant(s)	Host matrix	Pump Wavelength (um)	Laser Wavelength (um)	Transition	Output Power (W)	Slope efficiency (%)
Tm3+	Silicate	0.793	2.05	$^3F_4$ -> $^3H_6$	1050.000	53
Tm3+, Ho3+	Silicate	0.793	2.10	$^5I_7$ -> $^5I_8$	83.000	42
Ho3+	Silicate	0.458	2.05	$^5I_7$ -> $^5I_8$	0.046	1.7
Ho3+	Silicate	1.950	2.14	$^5I_7$ -> $^5I_8$	140.000	55
Er3+	ZBLAN	0.975	2.80	$^4I_{11/2}$ -> $^4I_{13/2}$	24.000	13
Er3+	ZBLAN	0.653	3.45	$^4F_{9/2}$ -> $^4I_{9/2}$	0.011	2.8
Tm3+	ZBLAN	1.064	2.31	$^3H_4$ -> $^3H_5$	0.150	8
Ho3+	ZBLAN	1.150	3.002	$^5I_6$ -> $^5I_7$	0.770	12.4
Ho3+	ZBLAN	0.532	3.22	$^5S_2$ -> $^5F_5$	0.011	2.8
Ho3+	ZBLAN	0.890	3.95	$^5I_5$ -> $^5I_6$	0.011	3.7

Table 1.The rare earth ion transition [6]

Laser transitions of Tm3+, Er3+ and Ho3+ are shown in Fig. 5 [31][32]. Tm3+ cations have decent absorption at wavelength 1610 nm. The Er3+ fiber amplifier EDFA, with CWDM laser diode operating at 1611 nm, is a great source of single mode high power signal and is ideal as a master oscillator source [33]. A disadvantage is its low efficiency by multiple down-conversion from pumping EDFA – 55% efficiency of 920 nm laser diodes, 45% Er3+ fiber laser, and by low slope efficiency.

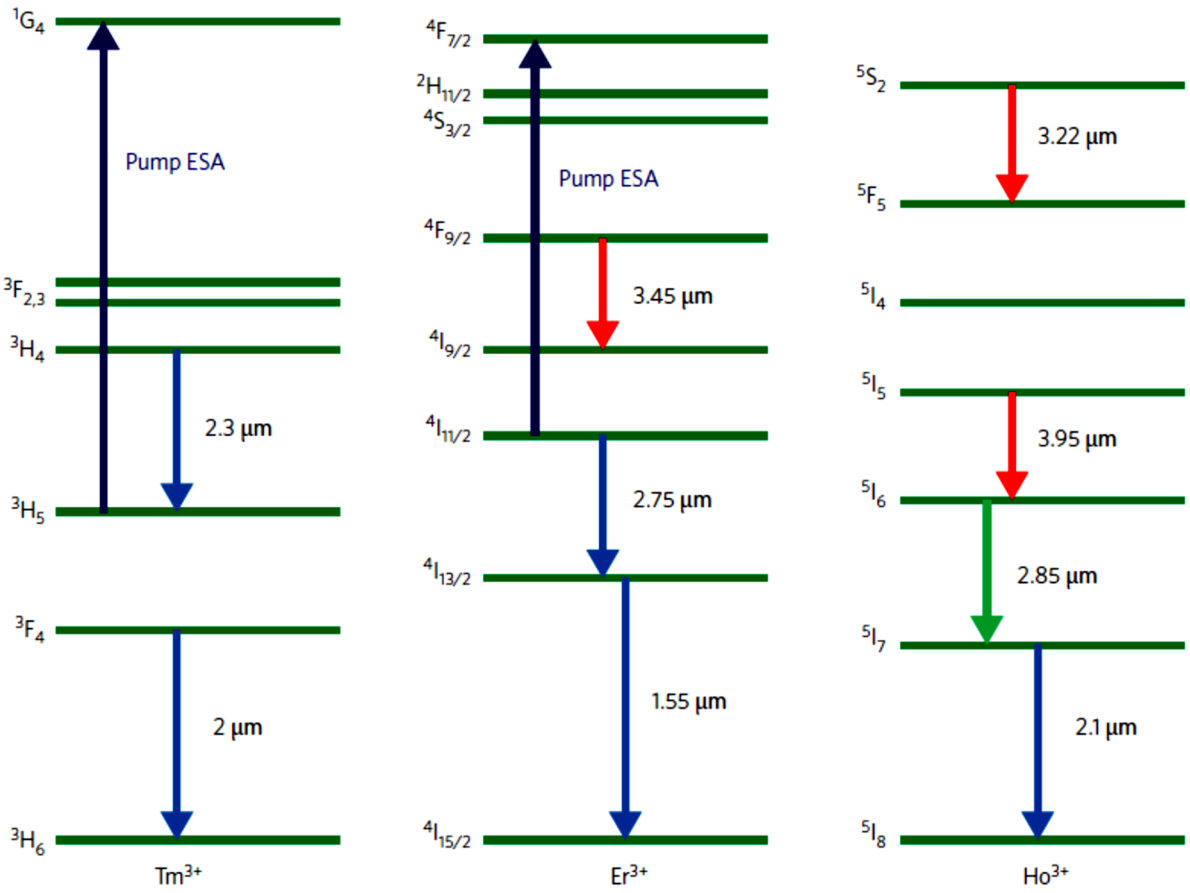

Figure 5. Laser transitions of rare-earth cations that produce emission wavelengths longer than 1.5 µm. The figure shows NIR (blue arrows), MIR (red arrows) and both (green arrows) electronic transitions, together with the primary lasing wavelength for each transition. ESA, excited state absorption. [6]

Holmium fiber lasers were demonstrated in [34] by pumping a Thulium fiber laser at 1950 nm with a basic transitions diagram at Figure 7. Ho3+ has strong absorption at 1950 nm as shown in Fig. 6.

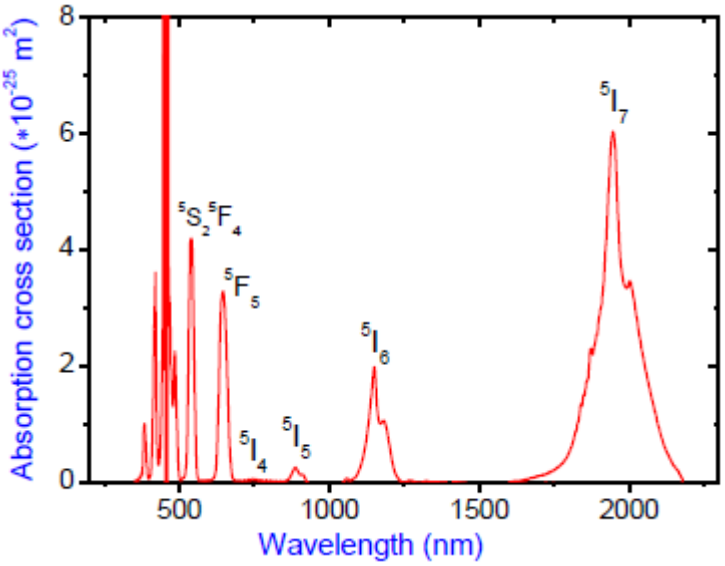

Figure 6. Ho3+ absorption in silicate [32]

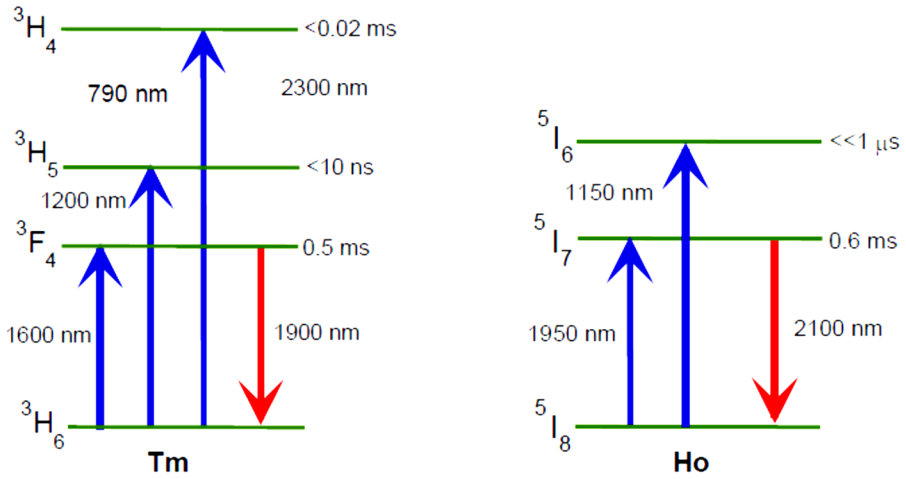

Figure 7. Laser energy transitions in silicate glass

A solution by co-doping silica glass by Tm3+ and Ho3+ ions was suggested in studies [35], but this solution offers a lower slope efficiency, 42%, as referred in Tab. 1 and Fig. 4. A more efficient solution is by direct pumping by Thulium fiber laser.

For high power Holmium fiber laser pumped by new branch of laser diodes operating at 1150 nm has been demonstrated [34]. InGaAs Quantum Wells, with an efficiency rate higher than 50%, are not available on the market.

An excimer Argon laser operating at 457.9 nm for pumping Ho3+ ions has been used in studies [36], but it achieved a slope efficiency of only 1.7%.

2.3 Suitable material base for fiber lasers around 2 μm

Every fiber laser component is limited by the material it is made from. Silica fibers are, for many reasons, the best for optical communications as they are made by drawing a preform made by MCVD (Modified chemical vapor deposition) process where the refraction index is modified by germanium dioxide (GeO_2) or aluminum oxide (Al_2O_3) to increase or decrease refraction index by fluorine or boron trioxide. Silica fibers have a broad band spectrum from UV 250 nm, though silica with high OH measures transparency up to 2.3 μm and parameters of silica and all silica fibers around 2 μm (see fig. 8 and table 2) is important for WDM and signal/pump combiners. Silica glass has lowest attenuation in single mode fibers close to 0.15 dB/km for a light with a wavelength of 1550 nm being one of highest laser inducted damage thresholds by CW value 0.5 W/μm^2 calculated [37], 1.7 W/ μm^2 to 20.0 W/ μm^2, as validated through experimental investigation [38]. In pulse mode of operation, safe brightness or fluency for silica fibers is typically 40-60 J/cm^2 for pulses 1 ps or 10 ns long [39], is more suitable [40]. A special kind of silica fibers are micro-crystal fibers where air gaps are used as low refraction index zones.

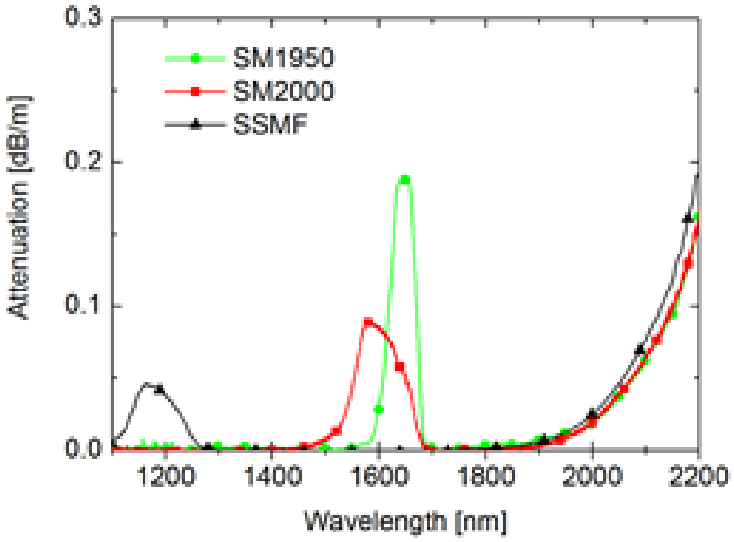

Figure 8. Spectral attenuation measurement of the three selected fiber samples.

	SSMF (KDP)	SM2000 (Thorlabs)	SM1950 (Nufern)
Core diameter (FWHM) [μm]	8.28	11.0	6.6
Δn_{max} [×10^{-3}]	5.0	4.9	12.8
NA_{max} [1]	0.121	0.120	0.194
Cutoff estimated from ESI [nm]	1308	1723	1672
Theoretical cutoff [nm]	1315	1680	1650
Effective cutoff [nm]	1300	1680	1680
Cable cutoff [nm]	1160	1510	1650
Attenuation at 2000 nm [dB/m]	0.04	0.02	0.02
Attenuation at 2200 nm [dB/m]	0.25	0.15	0.16

Table 2. Basic characteristics of the three silica fibers suitable for 2000 nm transmission.

For many reasons optical fibers made from silica are primary material choice. Silica fibers could be used for the transmission of light up to 2.2 μm where attenuation is reasonable still.

Fluoride glass is made from non-oxide fluorides of various metals. It's very difficult to avoid crystallization while processing fluoride glass because they have low viscosity. Heavy metal fluoride glasses have extremely low optical attenuation even lower than in silica glass. Fluoride glass has many disadvantages though, such as fragility, poor resistance to moisture and other environmental attacks [41].

An example of a heavy metal fluoride glass is ZBLAN glass composed of zirconium, barium, lanthanum, aluminum and sodium fluorides. Some components could be manufactured as a planar waveguide, but it is important to state that this components lack time stability and, due to poor chemical stability (hydroscopic), shielding reduces laser inducted damage. Their main advantage is low attenuation from 2.0 μm to 4 μm which ensures that they will be an interesting material in this wavelength region.

Chalcogenide fibers are made from arsenide and sulfur, selenium and tellurium. It's important to say that, due to higher attenuation, toxicity (proven carcinogen) and fragility, every operation should precede with extreme caution. When processing chalcogenide materials [42], it is also important to avoid crystallization, though this process is very difficult. Due to a high viscosity slope, even higher than ZBLAN fibers, they have a sublimation tendency, so all processing should be done under inert atmosphere conditions using gasses such as N_2 or Ar.

2.4. Fiber laser architecture

The basic principle of fiber lasers is pumping active earth ions by optical power with specific wavelength. Nowadays, solid state lasers are pumped by diodes. Focusing diode stacks to an optical fiber has some geometrical limits. Coupled diodes by single mode fiber are quite expensive so they are not ideal solutions for pumping high power fiber lasers. There are two basic architectures available to perform pumping. The first one is based on fused wavelength division multiplexers (WDM) [7]. The second is inline (monolithic) solution where pump is coupled to doped fiber with fiber Bragg grating (FBG)[43][44]. Double or triple clad optical fibers are ideal for pumping fiber laser, because it's much easier and cheaper to do coupling from diode stacks.

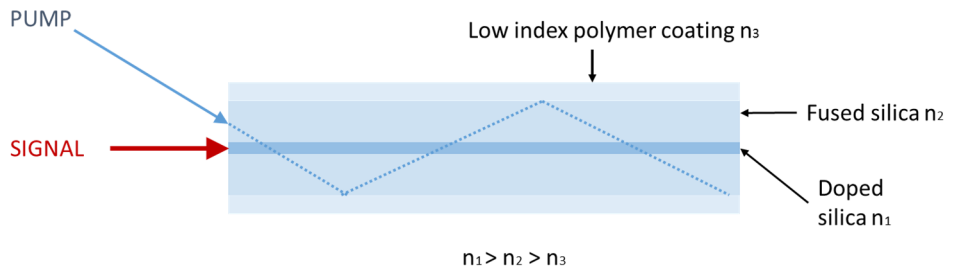

Figure 9. Double clad fiber for fiber lasers

Another way to pump a fiber laser is with a high brightness source naturally coupled to a single mode fiber. As an example for Tm3+ ions, we could use power Erbium doped fiber amplifier (EDFA) as a pump or an Ho3+ fiber laser could be effectively pumped by a Thulium fiber laser with emission close to 1.95 µm. Main difference between these two types of pumping is mixing the signal with the pump. Double clad (DC) and multi clad (MC) optical fibers, see Fig. 9., requires geometrical solution for coupling, which is practically wavelength independent instead of being a wavelength multiplexer for core pumping. We could combine both principles and make a powerful high brightness pump by using fiber lasers as a pump for multi clad fibers – tandem pumping see Fig. 10 [45].

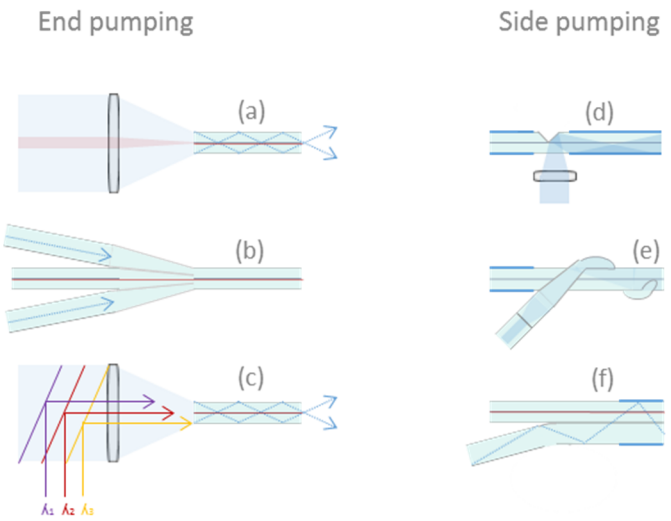

Figure 10. Elementary principles of pumping active multi-clad fiber a) to c) end-pumping, d) to f) side-pumping.

There are six fundamental principles how to guide the diode pump to active multi-clad fibers. Figure 10(a) shows free-space geometric combination of pump modules [46] with usage of dichroic mirror. This configuration is widely used as a research setup, but rarely in practical applications due to laser point stability [47]. Fig. 10(b) shows a scheme based on a Tapered Fiber Bundle (TFB) [48][49]. The number of combined free space or fiber-coupled pump modules depends on the cladding diameter and NA and is restricted by the etendue conservation principle applied to circular shape of fiber [50][51]:

$$B = \frac{P}{(\pi\, r\, NA)^2} = \frac{P}{(M^2\lambda)^2} \tag{1}$$

where B is brightness, P optical power, r radius of optical fiber, NA numerical aperture of fiber, M^2 beam quality parameter and λ wavelength. Fig. 10(c) shows the pumping scheme by free space optics and a wavelength multiplexer unit mostly used in assisted pumping [52]. Side pumping by scratch mirror in Fig. 10(d) brings a lot of practical problems like fiber fragility. Fig. 10(e) shows schematics patented by V.Gapontsev [53] which is very effective due to zero insertion loss of signal. The last schematic Fig. 10(f) shows exotic construction which requires an expensive low refraction index tube (fluoride doped silica) and reducing pump absorption due to increased profile and straight geometry.

2.5. Fiber lasers functionality and modes of operation

In down-conversion, energy is accumulated as an excitation valent electron to free orbital. An electron in excitation state will remain in this orbital for some time with some probability of spontaneously returning back and exciting the equivalent photon with energy equal to the differences in energy of each state with respect of a quantum mechanical model of an atom (with lower energy). The median time of an electron spent in an excitation state is called excitation time. The spectrum generated by this spontaneously emission is called Amplified Spontaneously Emission (ASE) and it's not coherent. The opposite of ASE is stimulated emission which is generated by amplifying the oscillator signal with frequency corresponding to valid laser transition.

All of these effects are greatly affected by host material (fused silica, ZBLAN, phosphate glass) and the dopant rate or method of deposition chemical vapor deposition (CVD) and modified chemical vapor deposition (MCVD) [54]. So it's required to measure these parameters for every type of active fiber. For example, the acidity of silica glass is a defining, stable oxidation number of a rare-earth element and free excitation state. Denying it could result in the making of problematic clusters.

The oscillating signal is propagated by an optical fiber and if corresponding photon hits an excited electron of dopant, second photon with the same energy is generated and goes back, according laser transition, to its original state. Thus, the signal is affected – amplified by probability of photon collision with excited electron. Also, in optical fibers it is crucial to conclude waveguide characteristics like dispersion and other linear or nonlinear effects for pulse propagation [55].

The shape of an oscillation signal defines mode of operation. The simplest mode of operation is continuous wave mode where stable fiber lasers keep this signal continuously amplified. If we have pulse shaped oscillating signal, the absorbed energy of the pump is accumulated in an excited dopant electron when actual oscillating signal power cannot form an avalanche. The pulsed mode of operation could be done by modulating the oscillating signal, pump or other stimulated emission.

Mode-locking is a technique in photonics that produces extremely short pulses of light down to femtosecond duration [56]. The basis of the technique is to induce a fixed-phase relationship between the longitudinal modes of the laser's resonant cavity. The laser could be 'phase-locked' [57] or 'mode-locked' [58] depending on the type of this relationship. Interference between these modes causes the laser light to be produced as a train of pulses.

It's important to state that in pulse mode or mode locking peak power energy due to high accumulated energy, active optical fiber could easily outreach the necessary power density to form an self-focusing phenomena (nonlinear effect) causing a domino effect and the formation of plasma inside optical fiber or pump modules (the most expensive parts of a laser).

2.6. Fiber ring lasers or all fiber ring resonator as master oscillators

A Fiber ring fiber laser represents a basic technique to construct a stable, self-stimulated, or self-modulated fiber laser [59]. Basic idea for this concept was to use ASE to form a coherent oscillating signal by increasing the chance of stimulating an emission by the most powerful part of ASE repeatedly until selected frequency bandwidth becomes dominant. By adding a saturable absorber with optical limiting effect in to the ring [58] it could be more exploited as stable a oscillator in passive Q-switch mode for fs or ps pulse source.

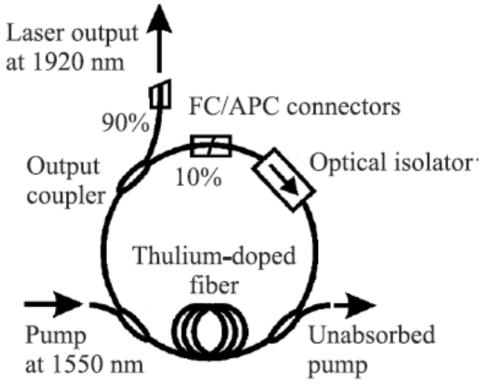

Figure 11. Thulium ring fiber laser with connector pair for modifying it to passive Q-switch by saturable absorber

Basic components from the ring laser schematic (Fig. 11) are the Wave Division Multiplexer (WDM) or bi-directional combiner to mix/separate pump and signal, the optical isolator to keep one directional output, a fiber TAP to get the split of laser signal and an oscillating signal and active medium (rare-earth doped fiber) [58-59].

Many variants of this schematic have been published with Erbium and Ytterbium doped fiber lasers using Bragg gratings to tune the output signal wavelength or reduce the chirp effect, polarization maintaining components to create a stable output, etc. [60-62]

2.7. Scaling-up the power of fiber laser

According [63], fiber technology has grown quite diverse and mature in the last decade and can provide an excellent platform for fabricating powerful, robust, high performance laser systems. The core and cladding structures can be appropriately tailored to control the beam modality, optical nonlinearities and scale-up the power.

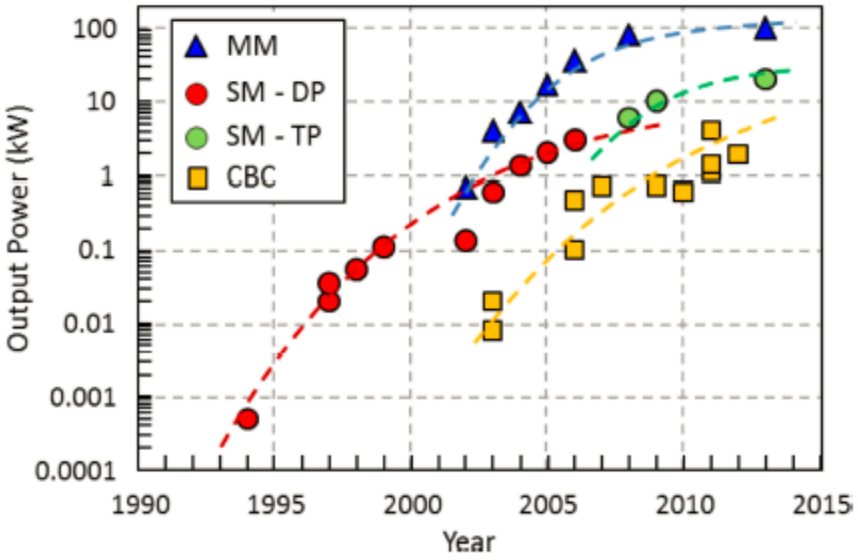

Figure 12. Power evolution with time in high-power Yb3+ -doped clad-pumped fiber lasers. Multimode (MM), single-mode diode pumped (SM - DP), single-mode tandem pumped / MOPA (SM - TP), and coherent beam combination (CBC)[64].

The fiber laser development, in power by different techniques, shows a logarithmic dependency of power in time – see in Fig. 12. Most interesting result is that multi-mode (MM), tandem-pumped (TP) and diode pumped (DP) fiber lasers are reaching their maximum limit but coherent combination is far from its limit and with high probability it will reach MM fiber lasers in the year 2028, see Fig. 13.

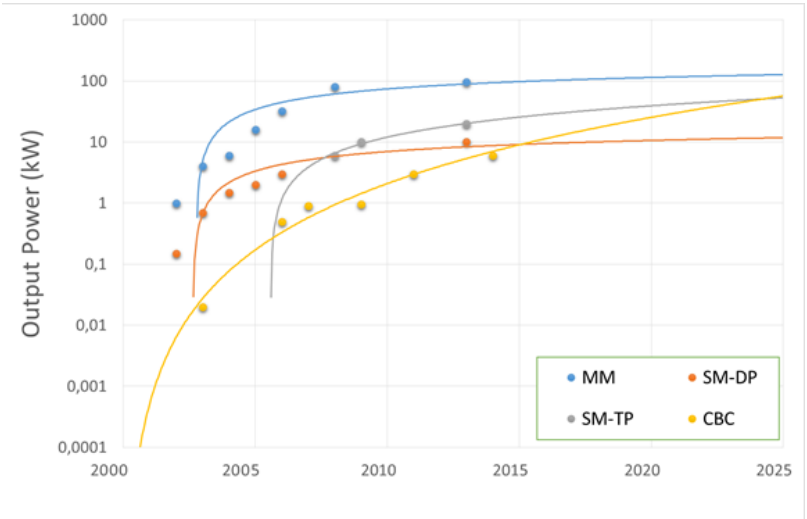

Figure 13. Estimation of fiber laser average power evolvement towards 2025

2.7.1. Incoherent beam combination technique for fiber lasers

The incoherent beam combination of lasers [65] is one of power scaling technique where we combine multiple fiber lasers to a multi-mode fiber or focus them by optics to one spot. By increasing the raw power of laser and keeping beam brightness intact while dramatically reducing beam quality due to the non-Gaussian beam profile.

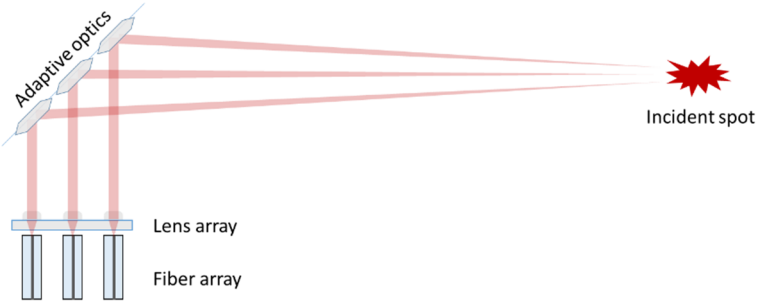

Figure 14. Incoherent beam combination

This concept is really interesting for cutting, wielding, marking and modifying materials like metals where raw power is required. But generally, fiber lasers are reduced for the fiber delivery of optical power generated by diode lasers and this technique is not sufficient for precise cutting and materials processing, medical applications or long distance applications. Still this concept is interesting for fiber lasers when increased pump power is required and a single pump cannot be more powerful due to cost or technical reasons. There are no power limits to increase output power up to nonlinear restrictions. Using large mode area (LMA) optical fibers allowed combinations of multiple lasers, but using LMA fibers limits output power to 10 kW with 35 µm core size due to self-focusing limit. For this technique there are no civil applications for output power higher than 50 kW.

2.7.2. Master oscillator power amplifier technique

Master oscillator power amplifier (MOPA) is one of the most popular ways of achieving power scalability. The master oscillator produces a highly coherent beam whose power is then amplified by several levels of amplifiers. The master oscillator has no need to be powerful or energy efficient but it could offer versatility, shape forming capability or stability.

As promising platform for the development of Thulium high power fiber laser, there is the Ytterbium fiber laser schematic which we adapted for Tm3+ in the MOPA [27] whose configuration can be seen in Fig. 15.

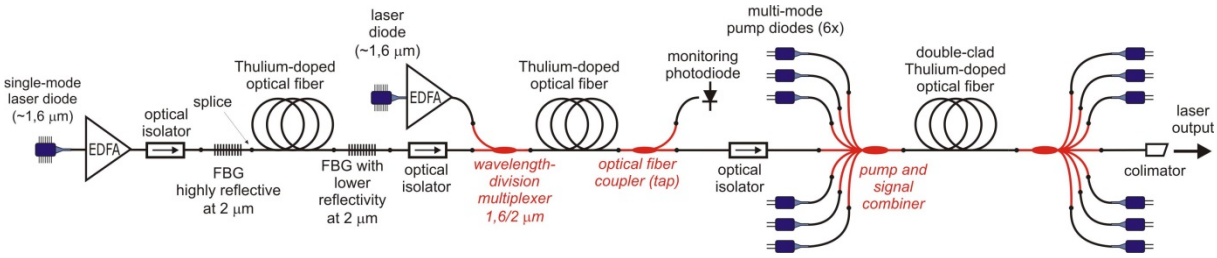

Figure 15. Scheme of the fiber laser in a master oscillator power amplifier configuration where typical applications of the fused fiber components (labeled in italics) are shown.

The main limits for this technique are nonlinear effects including Brillouin scattering. The most powerful fiber laser constructed by this technique reached a power of up to 10 kW [65]. For a single mode operation M^2 parameter varied from 1.2 in single mode fibers to 1.42 for LMA fibers.

2.7.3. Coherent addition/combination technique for fiber lasers

The coherent combination of lasers is power scaling techniques which can be done passively [66] or actively [67]. Typical coherent combination by fiber laser is made up of 2 lasers through passive phase synchronization [68]. Some experiments tried to do combination of 10 fiber lasers [69] but some of key fiber components for lasers like FBG cannot withstand such high continuous wave power. Also the requirements for lasers bandwidth are increasing exponentially with number of lasers in addition.

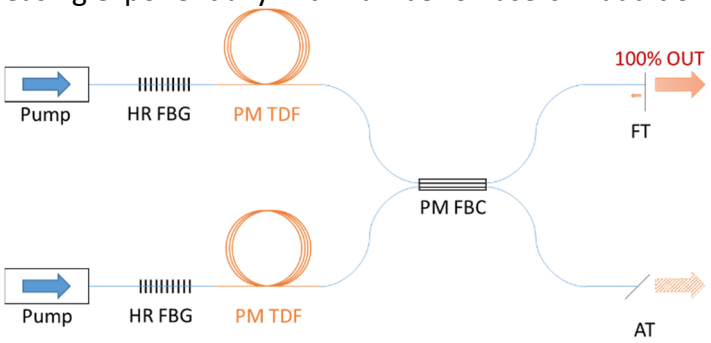

Figure 16. Scheme of two Thulium fiber lasers coherently combined, HR FBG – high reflective fiber Bragg grating, PM TDF – polarization-maintaining Thulium-doped-fiber, PM FBC – 50% polarization-maintaining fused-biconical-coupler, FT – flat termination, AT – angled termination.

Successful combination of two Thulium fiber lasers [70] shows great potential for low cost CW applications. Coherent addition shares limits such as the MOPA scheme and for pulsed mode of operation it requires active phase synchronization. Limited output power by thermal handling of components and peak power by nonlinear effects like Brillouin scattering lead to the use of up to four lasers in an addition in this scheme. Coherent addition lasers have similar beam quality M^2 as MOPA lasers.

2.7.4. Coherent combination in the far-field

As described in previous section, output power for fiber lasers is limited by conditions such as thermal handling and nonlinear effects including Brillouin scattering and self-focusing phenomena. In single mode fibers limits are 10 kW for beam combination and up to 10 kW for a master oscillator power amplifier or coherent addition. But nuclear science, cosmic science and military applications require much higher peak powers. Fiber lasers could be combined coherently by tiling output in to an array of phase controlled lasers across a laser head end face [71]. Each beam of fiber laser is focused individually to fit the aperture to form a central peak and side lobes [72] see Fig 17.

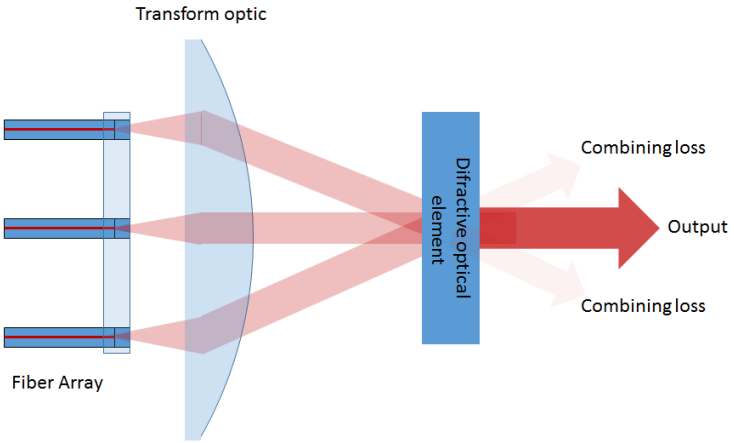

Figure 17. Coherent combination by tilting output using diffractive optical element

If we could implement monitoring of phase and controlling of phase of each laser, the addition of lasers would be nearly limitless. In some projects there is a plan to do active addition of up to 91 lasers by disk lasers but there is a problem with synchronization, cooling and space requirements [73]. Power scaling could be up to 1 PW in peak power in a few years with combination of fiber lasers [74] see Fig 18.

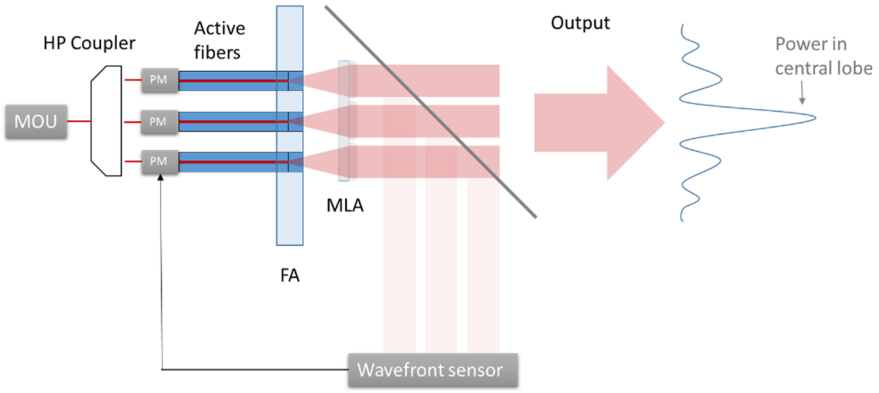

Figure 18. Tiled-aperture coherent beam combination of X-CAN project, FA - fiber array, MLA – micro lens array, MOU – master oscillator unit

The Lincoln-Northrop group found in [75] that tiling concentrated 58% of the total power in the desired central lobe for inputs up to 4 kW. In theory, tiling should increase the

on-axis intensity by a factor equal to the square of the number of emitting elements, but they found that tiling with eight emitters increased it by only a factor of 64, indicating that beam combining had an efficiency of 78%. Using the same fiber laser array, feed laser, and phase-control system with the aperture-filling approach and a five-element diffractive optical element, they reported beam combining at an efficiency of 79% when maximum power of the five beams was used. A feasibility study, I-CAN, led by l'École Polytechnique shows modification of the Lincoln-Northgroup approach and has led to a successful demonstration of a large-scale combination in the France X-CAN project, led by Thales Optronique s.a (where the author of this thesis participated as a subcontractor of fiber array development), led to an unlimited scale of coherent combination [76].

A typical setup requires a regular hexagonal or square arrangement of lasers with excellent precision of about 1 μm cumulative error of fiber core displacement and a tilting error better than 1 mrad. Mechanical precision requirements for a tilting error are at the limit of current technology. A tilting error for a beam emitted by active fiber is higher than these limits. Technology limits were responsible for the limit reported by the Lincoln-Northrop group [75]. By combining techniques such as active aligning and precise laser drilling, this tilting error is significantly reduced as demonstrated by the X-CAN project. A high thermal load of fiber matrix, due to the scattered unabsorbed pump, is the source of thermal shift.

Combining efficiency is in relation with the beam quality M^2 parameter of each fiber in combination because spatial combination by tiling output could be provided only with excellent beam quality M^2 close to 1 (near-diffraction-free). As was mentioned in chapter 2.7.2., the master oscillator power amplifier technique chapter, the typical beam quality M^2 of MOPA laser with LMA fiber is 1.4.

2.8. Supplement components for fiber lasers

Fiber lasers require the development of various novel passive components suitable for the corresponding spectral region which withstand high power operation with good thermal handling. An important group of components can be produced by the so called Fused Bi-conical Tapering (FBT) process, e.g., wavelength multiplexers (WDMs), couplers, taps for optical power monitoring, and pump and signal combiners. Application examples of such components in a fiber laser are shown in Fig. 15. Components fabricated by the FBT process have the advantages of low insertion losses, high power capability, low costs and a high reliability. Since they are all-fiber components, they have inherently good compatibility with optical fibers.

The first optical fiber couplers were fabricated by the FBT method in the early 1980s [77]. Basic technological and theoretical principles and advancements have been documented in several review papers, e. g., by Tekippe [78]; Pal et al. [79]; Abebe et al. [80]; Birks and Li [81]; Mortimore and Arkwright [82]. Numerical simulations of such devices were performed by using the coupled-mode theory [9][79][83], the beam-propagation method [84] as well as the finite-element method [85]. With the advent of new applications of optical fibers and fiber lasers, new technological and theoretical challenges have appeared for fiber coupler manufacturers. These challenges include advanced miniaturization [86], high-power operation in both single-mode [87] and multi-mode regime [88], applications in telecommunication signal multiplexing in multicore [89] and few-mode optical fibers [90] amongst others. Fiber couplers made out from non-silica fibers for mid IR devices have been tested, e.g., chalcogenide fibers that provide good transparency in the mid IR [42]. The preparation of fused fiber components in the 2 µm spectral region was investigated with the aim to achieve multiplexing wavelengths in the range of 795 and 1980 nm with a single-mode guidance for each respective wavelength [91]. Newly developed components will be described in detail in chapter 4.1.

.

3. Objectives of the thesis

This thesis has the following goals:

- To propose and form novel key components for mixing the pump and signal, and signal processing required for high-power fiber lasers and amplifiers around 2 μm
- To form a methodology of novel designs of light sources and fiber lasers around 2 μm

In order to achieve this goal, the following milestones have been set:

- Evaluate this influence of SMF28, SM1950 and SM2000 fibers for splicing losses, fabrication of Fused Biconical Components and bend losses for 2 μm applications
- Develop Fused Biconical Taper technology for the fabrication of key components such as the Wave Division Multiplexer and Taps for core pumped fiber lasers around 2 μm
- Develop Fiber Bundle technology to produce Pump-Signal combiners for clad pumped fiber lasers around 2 μm
- Investigate current 2 μm fiber lasers and light source applications requirements
- Investigate new possible applications of 2 μm fiber lasers and light sources

4. Achieved results

4.1. Results

Results of the research presented in this thesis were published in a number of papers in scientific journals and conference proceedings (see the list of author's publications). The core of the dissertation is composed of four journal papers [A1 – A4] in the main part of the dissertation, and three papers [A5 – A7] in the Appendix. Full bibliographic citations, contributions of the candidate, and acknowledgments are stated at the beginning of each chapter.

Chapter 4.2 describes the review of the development of 2 µm Fused Biconical Tapers (FBT) for signal pump combining and signal processing. At the beginning of my work FBT, including WDM, which are key components for single mode mixing of pump with signal and taps for dividing part of signal were not available. Before 2013 dichroic mirrors in an end-pumping layout and direct end pumping through FBG had been mostly used. The absence of 2 µm components and data relevant to manufacturing them from standard SMF28 fiber and newly developed SM1950 (Nufern), SM2000 (Thorlabs) fibers was also a key factor. Developing FBC components for a wavelength of 2 µm was the key for making compact sized fiber lasers and slope efficiency. The influence of bend sensitivity for different optical fibers required stable applications and components fabrication was also investigated in the article.

Chapter 4.3 provides a review of the development of pump signal combiners with a Mode-Field adapter (MFA) for mixing a pump at 790nm with a signal of 1900 – 2100 nm. By tapering a fiber bundle with signal and pumping signal fibers, we are increasing additional losses and reducing slope efficiency and maximal output power. MFA reduces this loss and it's important for medium- to high-power fiber lasers. Pump signal combiners optimized for EDFA (1550 nm) will have insertion loss in the vicinity of 2 µm up to 2 dB (37%) in splice areas with 5 W of maximum safe thermal load of 220 µm double clad fiber limiting maximum pump power to 13 W. By adding the Mode-Field Adapter we reduce splice loss to 0.02 dB (0.5%) and actually increase this limit up to a fiber limit of over 1 kW. Research and development work was done with the influence of splicing different and modified optical fibers investigated in the article also.

Chapter 4.4 presents the design of new ultra-compact 2 µm fiber laser architecture. The article provides a novel design of an ultra-compact fiber laser and a successfully demonstrated combination of methods for fiber drawing with direct deep ultra-violent fiber Bragg grating writing at 266 nm pumped through newly developed FBC components – wavelength division multiplexers from powerful EDFA amplifier at 1611 nm using 3F4 -> 3H6 transition - is given.

Chapter 4.5 introduces the final results from the research and development of 2 µm laser sources for industrial and medical areas suitable for components characterization, LIDAR, laser surgery and diagnostics.

4.2. Fused fiber components for „eye-safe“ spectral region around 2 micrometers

This chapter is a version of published manuscript:

M. Pisarik, P. Peterka, S. Zvanovec, Y. Baravets,F. Todorov, I. Kasik, P. Honzatko, Fused fiber components for „eye-safe“ spectral region around 2 micrometers, *Optical and Quantum Electronics*, vol. 46, pp. 603-611, 2014.

Connection with my PhD. work:

At the beginning of my work no Fused Biconical Components, such as WDM which are key components for single mode mixing of pump with signal and taps for dividing part of signal, had been available. Before 2013, dichroic mirrors in end-pumping layout and direct end pumping through FBG were mostly used. The absence of 2 μm components and data relevant to manufacturing them from standard SMF28 fiber and newly developed SM1950 (Nufern), SM2000 (Thorlabs) fibers was significant. The development of FBC components for wavelength 2 μm of compact size for future fiber lasers was in its infancy.

Opt Quant Electron (2014) 46:603–611
DOI 10.1007/s11082-013-9801-2

Fused fiber components for "eye-safe" spectral region around 2 μm

M. Písařík · P. Peterka · S. Zvánovec · Y. Baravets · F. Todorov · I. Kašík · P. Honzátko

Received: 22 August 2013 / Accepted: 7 October 2013 / Published online: 20 October 2013

Abstract Thulium-doped fiber lasers operating at wavelengths around 2 μm are rapidly developing a new class of coherent light sources with a high slope efficiency reaching 70 %. The 2-μm radiation sources have many advantages over the 1-μm sources, e.g., better eye-safety, relaxed non-linear limits and often more efficient material processing. Particularly important application of 2-μm fiber lasers is in a highly-efficient generation of wideband mid-infrared radiation through third order nonlinear effects in soft-glass fibers. In this paper we report on the development of passive components intended for fiber laser operation around 2 μm, namely fiber couplers and wavelength division multiplexers for combination of 1.6- and 2-μm radiation. Three commercially available fibers were used for the preparation of these components. The measured characteristics of the components are compared and the limitations are discussed, particularly the two-mode operation and high bend loss. Specific fiber designs are proposed in order to optimize the performance of the wavelength division multiplexer.

Keywords Optical fiber coupler · Wavelength division multiplexer · Fused biconical tapered method · Fiber lasers

M. Písařík (✉) · S. Zvánovec
Department of Electromagnetic Field, Czech Technical University in Prague, Technická 2, 16627 Prague, Czech Republic

M. Písařík
Research and Development, SQS Vláknová optika, a.s., 50901 Nová Paka, Czech Republic

P. Peterka · Y. Baravets · F. Todorov · I. Kašík · P. Honzátko
Institute of Photonics and Electronics, Academy of Sciences of the Czech Republic, v.v.i., Chaberská 57, 182 51 Prague, Czech Republic
e-mail: peterka@ufe.cz

1 Introduction

High power fiber laser sources operating in the 2 μm wavelength region are being intensively studied as promising sources for many applications including material processing, medicine, eye-safe LIDAR, and chemical and environmental sensing (Jackson 2012; Honzatko et al. 2013). Particularly important applications are in nonlinear frequency conversion to mid-infrared wavelength, e.g., in optical parametric oscillators and in supercontinuum broadband sources (Kulkarni et al. 2011; Heidt et al. 2013). Such fiber lasers require a novel active fiber design as well as composition changes. They also require the development of various novel passive components suitable for the respective spectral region which withstand high power operation. An important group of components can be produced by the so called Fused Biconical Taper (FBT) process, e.g., wavelength multiplexers (WDMs), couplers, taps for optical power monitoring, and pump and signal combiners. Application examples of such components in a fiber laser are shown in Fig. 1. Components fabricated by the FBT process have the advantages of low insertion losses, a high power capability, low costs and a high reliability. Since they are all-fiber components, they have inherently a good compatibility with optical fibers.

First optical fiber couplers were fabricated by the FBT method already in the early eighties (Kawasaki et al. 1981). Basic technological and theoretical principles and advancements have been documented in several review papers, e. g., by Tekippe (1990), Pal et al. (2003), Abebe et al. (1988), Birks and Li (1992), Mortimore and Arkwright (1990). Numerical simulations of such devices were performed by using coupled-mode theory (Bures et al. 1983; Pal et al. 2003; Peterka and Kanka 2001), beam-propagation method (Du and Chiou 2013) as well as finite-element method (Chiang 1985). With the advent of new applications of optical fibers and fiber lasers, new technological and theoretical challenges have appeared to fiber coupler manufacturers. These challenges include advanced miniaturization (Jiang et al. 2011), high-power operation in both single-mode (Theeg et al. 2011) and multi-mode regime (Xiao et al. 2011), applications in telecommunication signal multiplexing in multicore (Zhu et al. 2010) and few-mode optical fibers (Saitoh et al. 2010) and others. Fiber couplers made out from non-silica fibers for mid IR devices have been tested, e.g., chalcogenide fibers that provide good transparency in the mid IR (Athanasiou et al. 2013). Preparation of fused fiber components in the 2-μm spectral region was investigated with the aim to achieve multiplexing wavelengths in the range of 795 and 1,980 nm with a single-mode guidance for each respective wavelength (Pelegrina-Bonilla et al. 2012).

In this paper, we report on the development of WDMs and couplers made by the FBT method that are suitable for thulium-doped fiber lasers emitting at around 2,000 nm. Specific characteristics of WDMs developed from three different types of fibers are presented and compared together. Two of the used fibers were designed for operation at around 2 μm and

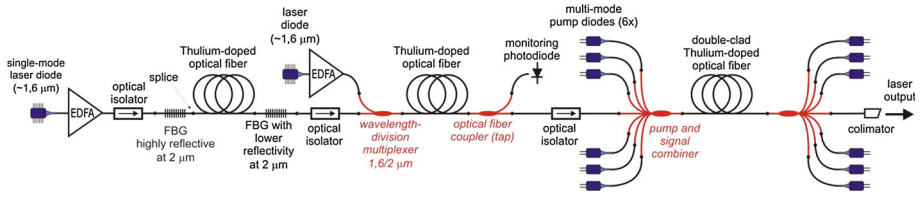

Fig. 1 Scheme of the fiber laser in a master oscillator power amplifier configuration where typical applications of the fused fiber components (labeled in *italics*) are shown. Legend: EDFA—erbium-doped fiber amplifier, FBG—fiber-Bragg grating

as the third one we utilized a standard single-mode fiber (SSMF) with the first higher-order mode cutoff around 1,300 nm. Particular issues and drawbacks of the developed WDMs are discusses in detail. Fiber designs suitable for the WDMs at 1,600/2,000 nm are proposed.

2 Fiber characteristics

Three types of commercially available fibers were selected for the WDM component preparation. Two of the fibers were designed for operation at around 2 μm, namely SM1950 fiber (Nufern) and SM2000 fiber (Thorlabs). The third fiber was a SSMF obeying the International Telecommunication Union (ITU-T) recommendation G.652 (KDP). The refractive index profiles of all three fibers measured by the refractive near-filed method using York S14 instrument are shown in Fig. 2a. We have calculated the dispersion curves of the guided modes according to the measured profiles, see Fig. 2b. The cutoff of the respective modes is determined by the intersection of the dispersion curve with the zero line. Estimated cutoffs of Nufern and Thorlabs fibers are very close, in the range 1,650–1,690 nm. Figure 3a depicts the spectral attenuation measured by the cut-back method. We used relatively short pieces of fibers, a 60 m in the case of SSMF and SM2000 fibers and 20 m in the case of SM1950 fiber

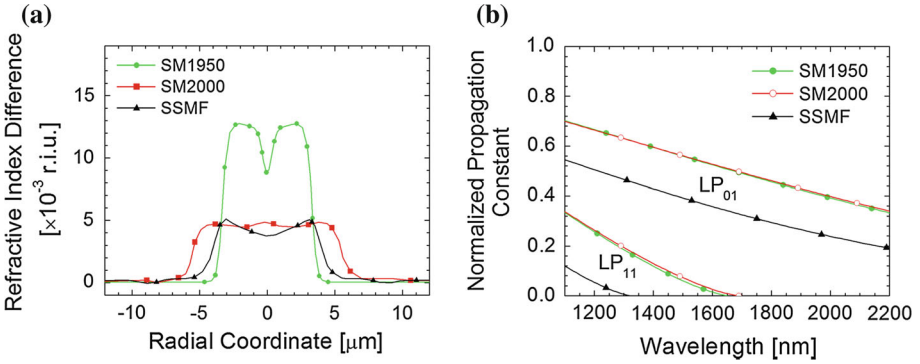

Fig. 2 **a** Measured refractive index profiles of the fibers under investigation. Only the region around the fiber core is shown. **b** Calculated *dispersion curves* of the propagated modes of the three fibers under investigation. The mode is guided when its respective normalized propagation constant is nonzero

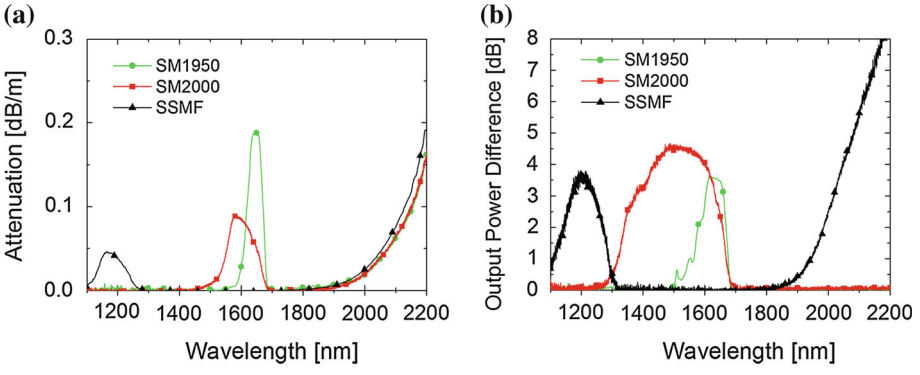

Fig. 3 **a** Spectral attenuation and **b** effective LP_{11} mode cut-off measurement of the three selected fiber samples

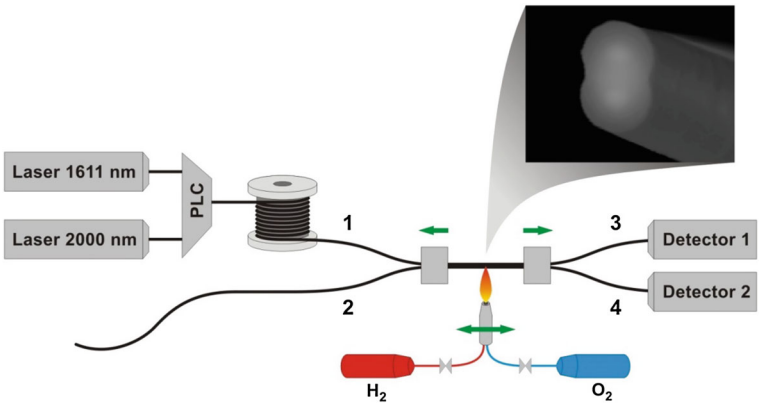

Fig. 4 Scheme of the rig for the FBT fabrication of fiber components. SEM image of the cross section near the waist position of the tapered region is shown in the inset. The waist dimensions are 3.7 × 5.5 μm

Table 1 Basic characteristics of the three fibers used for coupler fabrication

	SSMF (KDP)	SM2000 (Thorlabs)	SM1950 (Nufern)
Core diameter (FWHM) (μm)	8.28	11.0	6.6
Δn_{max} ($\times 10^{-3}$)	5.0	4.9	12.8
NA_{max}	0.121	0.120	0.194
Cutoff estimated from ESI (nm)	1308	1723	1672
Theoretical cutoff (nm)	1315	1680	1650
Effective cutoff (nm)	1300	1680	1680
Cable cutoff (nm)	1160	1510	1650
Attenuation at 2,000 nm (dB/m)	0.04	0.02	0.02
Attenuation at 2,200 nm (dB/m)	0.25	0.15	0.16

in order to measure the spectral attenuation in lossy region around 2 μm. A halogen lamp was used as a wideband source and the spectra transmitted through the fibers were recorded by a Fourier transform infrared (FT-IR) spectrometer.

We analyzed also the cutoff wavelengths of the first higher order mode (LP_{11}). The effective cutoff was measured by a comparison of a spectral transmission of a 2-m long fiber sample with a small loop of about 4 cm in diameter and of the same fiber without the loop, respectively. The differences of the spectral transmission in these two measurements are shown in Fig. 3b for all the three fibers. The measurements are in good correspondence with the theoretically predicted cutoff from the refractive index profiles shown in Fig. 2b. We measured also the so called "cable cutoff wavelength" which estimates the LP_{11} cutoff for propagation in longer fibers. In this case we compared the spectral transmission of several tens of meters of fiber on the spool with a small loop of about 4 cm in diameter and of same fiber without the loop in accordance with the ITU-T recommendation G.650. For the SM2000 and the SSMF fibers, the cable cutoff was found more than 100 nm smaller than the effective cutoff due to increased bending losses. The fiber SM1950 is less bend sensitive because of its higher Δn of the core. Therefore, the cable cutoff of the SM1950 fiber is only about 30 nm below the effective cutoff. Basic characteristics of the three fibers are summarized in the Table 1. The theoretical cutoff is evaluated for the equivalent step-index

profile (ESI) according to relation $\lambda_{\text{cutoff}} = 2\,\pi\ a\ NA_{max}/2.405$, where the core diameter $2a$ is determined as the full width at half maximum (FWHM) of the refractive profile and the numerical aperture is given by $NA_{max} = \sqrt{(n_{max}^2 - n_{min}^2)}$. The theoretical cutoff for the measured refractive index profile is evaluated by using a numerical calculation of the modal dispersion curves.

3 Experimental setup

Schematic deployment of the setup for the FBT fabrication is depicted in Fig. 4. The apparatus is similar to the setup explained in detail by Jiang et al. (2011) but it is modified for wavelengths of 1,610 and 2,000 nm. Laser diodes or fiber lasers (Peterka et al. 2013) can be used as a laser source. For combination of laser sources at 1,610 nm and at 2,000 nm we have developed a planar lightwave coupler (PLC) with spectral uniformity better than 0.5 dB up to 2,000 nm. In the twisted FBT fabrication method, the two optical fibers are twisted at two separate points. The twisted fiber section is then heated with an oscillating torch and slowly stretched to create a taper and enable the mode coupling. Within our approach, a ceramic tube was placed around the fibers to provide their indirect heating. Gas flow was controlled by temperature feedback from ceramic tube to keep the tension stable. The tapering process was stopped at predetermined value of optical power coupled to the other fiber. During the WDM fabrication process for example, the tapering was stopped in the first coupling maximum to enable the developed WDM to achieve the largest bandwidth of the transmission spectrum.

4 Experimental results and discussion

The developed WDMs were characterized in terms of insertion losses of the respective branches of the WDMs and in terms of spectral dependence of the coupling ratio. The insertion losses were measured conveniently just after finishing of the fabrication process at the both respective wavelengths for which the component was designed. The wavelength of 1,610 nm is on the longest wavelength edge of the gain interval covered by L-band EDFAs that are often used for pumping of thulium-doped fiber lasers. The thulium absorption cross section at the wavelength of 1,610 nm is already high and it represents more than 80 % of the thulium peak absorption at around 1,650 nm. The signal wavelength of 2,000 nm was chosen because it falls within the interval of wavelengths where thulium-doped fiber lasers have good efficiency. The measured insertion losses $IL_i = P_i/P_1$ for the respective output branch i are summarized in Table 2. The numbering of the WDM branches is as follows: P_1 is the power in the input (common) port at the respective wavelength, P_3 is the output from 1,610 nm branch and P_4 is the output from 2,000 nm branch of the WDM. The spectral coupling ratio $CR_i = P_i/(P_3 + P_4)$ of the respective WDM's output branch i was measured by using

Table 2 Characteristics of the developed WDMs

Sample No.	Fiber type	IL_3(dB) at 1,610/2,000 nm	IL_4(dB) at 1,610/2,000 nm
WDM1	SM2000 (Thorlabs)	30/0.017	0.017/25.23
WDM2	SM2000 (Thorlabs)	n.a./0.15	0.1/n.a.
WDM3	SM1950 (Nufern)	30/0.03	0.01/23.98
WDM4	SSMF (KDP)	13.98/0.25	0.21/18.86

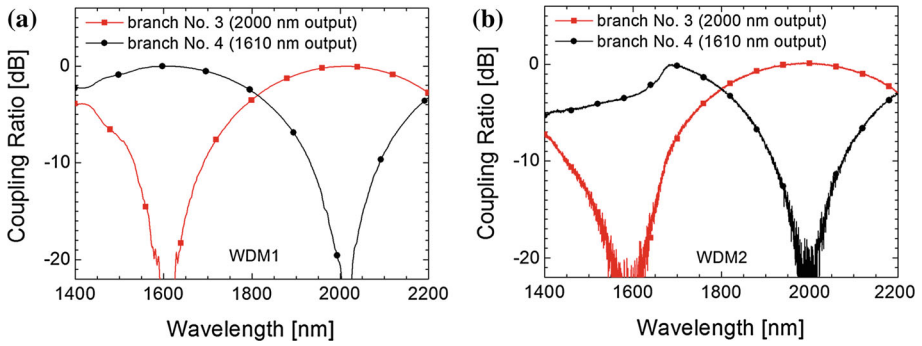

Fig. 5 Spectral characteristics of coupling ratio for WDM1 and WDM2: **a** fundamental mode is dominantly excited and **b** higher insertion below 1,680 nm may arise when first higher order mode is also excited

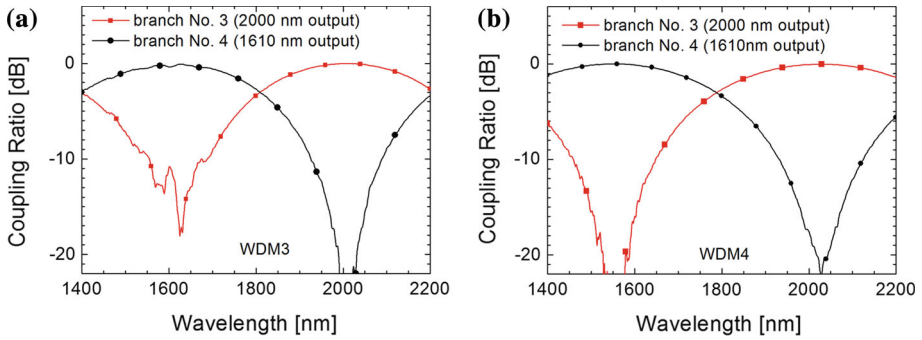

Fig. 6 Spectral characteristics of coupling ratio for WDM3 and WDM4 that were made from: **a** SM1950 fiber and **b** SSMF

a halogen lamp as a wideband source and a FT-IR spectrometer. The results are shown in Figs. 5 and 6, respectively. It should be noted that the spectrally resolved measurement was performed by the combination of a halogen lamp (with a low spectral power density) and a FT-IR spectrometer and therefore the dynamic range was limited to only about 20 dB.

An important issue of the FBT components is the possible multimode operation of the fiber itself. Two of the used fibers, Nufern SM1950 and Thorlabs SM2000 have the LP_{11} cutoff well above 1,610 nm. This fact is clearly manifested on developed WDMs in Figs. 5b and 6a. The spectral ripples arise for wavelengths below cutoffs. For the case of the WDM2 which was made from Thorlabs SM 2000 fiber we measured high insertion loss of about 3 dB. This increase in loss could arise when both modes are almost equally excited, see Fig. 5b. Low insertion losses can be obtained when only the fundamental mode is carefully excited, see Table 2. But it is hard to keep off the possible multimode operation. Excitation of the LP_{11} mode may then cause problems either due to higher insertion losses mentioned above or due to an induced instability of the pump power coupling. It should be noted that even relatively small pump instabilities may cause a detrimental self-Q-switching operation of fiber lasers (Richardson et al. 2010; Peterka et al. 2012b) and users should keep in mind these facts when working with FBT couplers made out of multimode fibers.

Another issue of silica-based fiber components intended for the 2-μm spectral region is their increased losses for longer wavelengths. It is well known that silica-based fibers exhibit exponentially increasing attenuation from its minimum at 1,550 nm towards longer

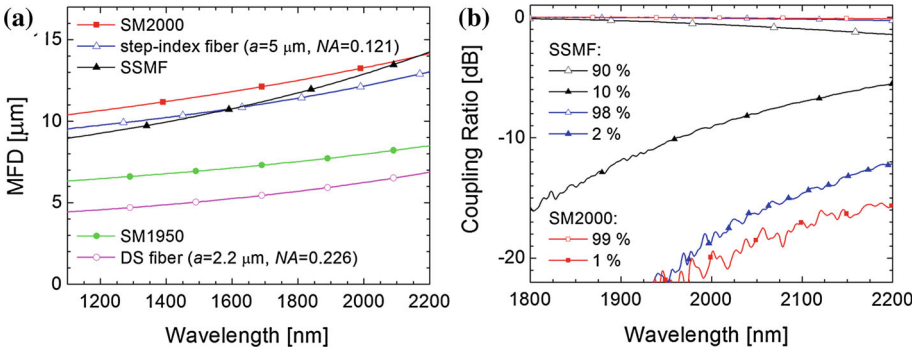

Fig. 7 **a** Spectral dependence of the MFD of the LP_{01} mode for the specially designed step-index fiber, the dispersion-shifted fiber and the fibers tested in WDM fabrication. **b** Spectral transmissions of the 1, 2 and 10 % taps

wavelengths. The attenuation at longer wavelengths can be influenced also by bending losses, especially in fibers with short cutoff wavelength like the standard single-mode fiber with cutoff around 1,300 nm. Therefore, the resulted insertion loss at 2,000 nm for the SSMF fiber is usually slightly higher than for the other two fibers, see Table 1.

Both issues listed above can be solved by a fiber with a special design which would be convenient for the WDM at 1,610/2,000 nm. Such a fiber should have LP_{11} mode cutoff closely below the shorter wavelength and its mode-field diameter (*MFD*) should match the *MFD* of the SSMF fiber at 1,610 nm and eventually should also match the *MFD* of typical fibers for the 2-μm region at the longer wavelengths. Parameters of such a fiber can be estimated from the following approximate formula for the *MFD* (Marcuse 1977):

$$MFD \cong 2a\left(0.65 + \frac{1.619}{V^{1.5}} + \frac{2.879}{V^{6}}\right), \quad V = \frac{2\pi}{\lambda} a\, NA$$

where V stands for normalized frequency, a is the fiber core radius, and NA represents the numerical aperture. For example, a step index fiber with a = 5 μm and NA = 0.121 match the design criteria. Bending insensitivity can be increased by increasing the core's NA like in the so called dispersion-shifted (DS) single-mode fibers according to ITU-T recommendation G.653. A step index fiber with a = 2.2 μm and NA = 0.226 is an example of DS fiber (Keiser 1991). The respective spectral dependence of the *MFD* are shown in Fig. 7a. It can be seen from the Fig. 7a, that better bending insensitivity of the DS fiber is compensated with higher splice losses due to larger *MFD* mismatch.

The fibers solely designed for 2-μm region would be of course suitable for FBT components intended for this spectral region. Examples of the 1-, 2- and 10 % couplers, so-called taps, are shown in Fig. 7b. Lower values of measured coupling ratio are influenced by noise due to limited dynamic range of the measurement setup.

5 Conclusions

In summary, we have presented results of FBT components for the 2 μm spectral region, namely fiber couplers and WDMs for combining light at 1,610 and 2,000 nm. Three different types of silica-based fibers were used for the preparation of WDMs and the characteristics of the prepared WDMs were compared. The two fibers designed for operation at around

2,000 nm exhibited vulnerability to change the insertion losses at 1,610 nm depending on the launching conditions. A change of the insertion loss as much as 3 dB at 1,610 nm was observed. Apparently this vulnerability is caused by the two-mode nature of the propagation below 1,680 nm, the cutoff wavelength of the LP_{11} mode. The WDM made from SSMF does not suffer from possible few-mode operation and therefore it can satify needs of many potential applications. However, such WDM may exhibit higher insertion losses at 2,000 nm due to sensitivity to bending. To overcome these issues, we have discussed other types of fibers for the WDM 1,600/2,000 nm. Firstly, we proposed a fiber with cutoff just below 1,600 nm that would match the mode-field diameters of the SSMF at 1,600 nm and secondly, the dispersion-shifted fiber with good bending insensitivity but higher splice losses with most typical fibers.

Acknowledgments The authors acknowledge fruitful cooperation with experts from Gooch & Housego in Torque, UK. This work was supported in part by the Czech Science Foundation under Grant P205/11/1840, by the Czech Ministry of Industry and Trade under Grant FR-TI4/734 and by the European Commission under the COST action MP1204 TERA-MIR Radiation: Materials, Generation, Detection and Applications.

References

Abebe, M., Villarruel, C.A., Burns, W.K.: Reproducible fabrication method for polarization preserving single-mode fiber couplers. J. Lightwave Technol. **6**, 1191–1198 (1988)

Athanasiou, G.S., Bereś-Pawlik, E., Semczuk, G., Furniss, D., Seddon, A.B., Benson, T.M.: Large core, multimode, chalcogenide glass fibre coupler by side-polishing. Opt. Quantum Electron. **45**, 961–967 (2013)

Birks, T.A., Li, Y.W.: The shape of fiber tapers. J. Lightwave Technol. **10**, 432–438 (1992)

Bures, J., Lacroix, S., Lapierre, J.: Analyse d'un coupleur bidirectionnel à fibres optiques monomodes fusionnées. Appl. Opt. **22**, 1918–1922 (1983)

Chiang, K.S.: Finite-element analysis of optical fibres with iterative treatment of the infinite 2-D space. Opt. Quantum Electron. **17**, 381–391 (1985)

Du, C.-H., Chiou, Y.-P.: Beam propagation analysis using higher-order full-vectorial finite-difference method. Opt. Quantum Electron. **45**, 769–774 (2013)

Heidt, A.M., Li, Z., Sahu, J., Shardlow, P.C., Becker, M., Rothhardt, M., Ibsen, M., Phelan, R., Kelly, B., Alam, S.U., Richardson, D.J.: 100 kW peak power picosecond thulium-doped fiber amplifier system seeded by a gain-switched diode laser at 2 μm. Opt. Lett. **38**, 1615–1617 (2013)

Honzatko, P., Baravets, Y., Todorov, F., Peterka, P., Becker, M.: Coherently combined 20 W at 2000 nm from a pair of thulium-doped fiber lasers. Laser Phys. Lett. 10 (2013)

Jackson, S.D.: Towards high-power mid-infrared emission from a fibre laser. Nat. Photonics **6**, 423–431 (2012)

Jiang, J.-A., Hsu, T.-Y., Liao, W.-B., Liu, M.-Y.: Development of miniature optical fiber hybrid WDM coupler employing the FBT technology. Opt. Fiber Technol. **17**, 568–573 (2011)

Kawasaki, B.S., Hill, K.O., Lamont, R.G.: Biconical-taper single-mode fiber coupler. Opt. Lett. **6**, 327–328 (1981)

Keiser, G.: Optical Fiber Communications, 2nd edn. McGraw-Hill, New York (1991)

Kulkarni, O.P., Alexander, V.V., Kumar, M., Freeman, M.J., Islam, M.N., Neelakandan, M., Chan, A.: Supercontinuum generation from $\sim$ 1.9to4.5 μm in ZBLAN fiber with high average power generation beyond 3.8 μm using a thulium-doped fiber amplifier. J. Opt. Soc. Am. B **28**, 2486–2498 (2011)

Marcuse, D.: Loss analysis of single-mode fiber splices. Bell Syst. Tech. J. **56**, 703–718 (1977)

Mortimore, D.B., Arkwright, J.W.: Theory and fabrication of wavelength flattened $1 \times N$ single-mode couplers. Appl. Opt. **29**, 1814–1818 (1990)

Pal, B.P., Chaudhuri, P.R., Shenoy, M.R.: Fabrication and modeling of fused biconical tapered fiber couplers. Fiber Integr. Opt. **22**, 97–117 (2003)

Pelegrina-Bonilla, G., Hausmann, K., Liu, K., Sayinc, H., Morgner, U., Neumann, J., Kracht, D.: Matching of the propagation constants in an asymmetric single-mode fused fiber coupler for core pumping thulium-doped fiber at 795 nm. Opt. Lett. **37**, 1844–1846 (2012)

Peterka, P., Kanka, J.: Erbium-doped twin-core fibre narrow-band filter for fibre lasers. Opt. Quantum Electron. **33**, 571–581 (2001)

Peterka, P., Navrátil, P., Maria, J., Dussardier, B., Slavík, R., Honzátko, P., Kubeček, V.: Self-induced laser line sweeping in double-clad Yb-doped fiber-ring lasers. Laser Phys. Lett. **9**, 445–450 (2012)

Peterka, P., Honzatko, P., Becker, M., Todorov, F., Pisarik, M., Podrazky, O., Kasik, I.: Monolithic Tm-doped fiber laser at 1951 nm with deep-UV femtosecond-induced FBG pair. IEEE Photonics Technol. Lett. **25**, 1623–1625 (2013)

Richardson, D.J., Nilsson, J., Clarkson, W.A.: High power fiber lasers: current status and future perspectives [Invited]. J. Opt. Soc. Am. B **27**, B63–B92 (2010)

Saitoh, F., Saitoh, K., Koshiba, M.: A design method of a fiber-based mode multi/demultiplexer for mode-division multiplexing. Opt. Express **18**, 4709–4716 (2010)

Tekippe, V.J.: Passive fiberoptic components made by the fused biconical taper process. Fiber Integr. Opt. **9**, 97–123 (1990)

Theeg, T., Hausmann, K., Frede, M., Sayinc, H., Neumann, J., Kracht, D.: High power fused single mode optical fiber coupler. In Conference on Lasers and Electro-Optics Europe and 12th European Quantum Electronics Conference, CLEO EUROPE/EQEC 2011, Article no 5943141 (2011)

Xiao, Q., Yan, P., He, J., Wang, Y., Zhang, X., Gong, M.: Tapered fused fiber bundle coupler capable of 1 kW laser combining and 300 W laser splitting. Laser Phys. **21**, 1415–1419 (2011)

Zhu, B., Taunay, T.F., Yan, M.F., Fini, J.M., Fishteyn, M., Monberg, E.M., Dimarcello, F.V.: Seven-core multicore fiber transmissions for passive optical network. Opt. Express **18**, 11117–11122 (2010)

4.3. Mode-Field Adapter for Tapered-Fiber-Bundle Signal and Pump Combiners

This chapter is a version of a published manuscript:

P. Koska, Y. Baravets, P. Peterka, J. Bohata, M. Pisarik, Mode-Field Adapter for Tapered-Fiber-Bundle Signal and Pump Combiners, *Applied Optics*, vol. 54, no. 4, p. 751-756, 2015.

Connection with my PhD. work:

At beginning of my research there were no low-loss star combiners for mixing a pump and signal adapted to a 790 nm pump and 2 μm signal. By tapering a fiber bundle with signal and pumping signal fibers we increase addional losses and reduce slope efficiency and maximal output power. A Mode-Field adapter reduces this loss which is important for medium- to high-power fiber lasers. Pump signal combiners optimized for EDFA (1550 nm) will have an insertion loss in the 2 μm area up to 2dB (37%) in the splice area with 5 W of maximum safe thermal load of 220 μm double clad fiber limiting maximum pump power to 13 W. By adding the Mode-Field Adapter we reduce splice loss to 0.02 dB (0.5%) and actually increase this limit up to fiber limits over 1 kW.

Mode-field adapter for tapered-fiber-bundle signal and pump combiners

Pavel Koška,[1,2,*] Yauhen Baravets,[1,2] Pavel Peterka,[1] Jan Bohata,[3] and Michael Písařík[3]

[1]Institute of Photonics and Electronics ASCR, v.v.i., Chaberská 57, Prague 18251, Czech Republic

[2]Department of Physical Electronics, Czech Technical University in Prague, Břehová 7, Prague 11519, Czech Republic

[3]Department of Electromagnetic Field, Czech Technical University in Prague, Technická 2, Prague 16627, Czech Republic

*Corresponding author: koska@ufe.cz

Received 28 August 2014; revised 16 December 2014; accepted 16 December 2014; posted 16 December 2014 (Doc. ID 221872); published 26 January 2015

We report on a novel mode-field adapter that is proposed to be incorporated inside tapered fused-fiber-bundle pump and signal combiners for high-power double-clad fiber lasers. Such an adapter allows optimization of signal-mode-field matching on the input and output fibers. Correspondingly, losses of the combiner signal branch are significantly reduced. The mode-field adapter optimization procedure is demonstrated on a combiner based on commercially available fibers. Signal wavelengths of 1.55 and 2 μm are considered. The losses can be further improved by using specially designed intermediate fiber and by dopant diffusion during splicing as confirmed by preliminary experimental results. © 2015 Optical Society of America

OCIS codes: (060.2340) Fiber optics components; (060.3510) Lasers, fiber; (060.2320) Fiber optics amplifiers and oscillators.

http://dx.doi.org/10.1364/AO.54.000751

1. Introduction

High-power fiber lasers are gaining importance in many fields, including industrial material processing, metrology, and health care. The key for high-power operation of fiber lasers is the usage of double-clad fibers (DCFs) as transformers of lower-brightness pumps into high-brightness laser signal beams [1,2]. Pumping radiation needs to be introduced into the first cladding of the DCF while the active core of the DCF often needs to be accessible by dedicated signal fiber. Pump-signal combiners are devices responsible for such coupling and they are thus crucial components of high-power fiber lasers. Several approaches were developed for pump and signal coupling into DCFs [3–18]. Combiners utilizing free-space optics are usually impractical out of the laboratory environment due to lack of robustness [3]. The free-space-optics combiner was used by Elias Snitzer in the first demonstration of a cladding-pumped fiber laser [2] but very soon an all-fiber solution was envisaged by Gapontsev [4] and later demonstrated by using a tapered pump fiber wrapped around the DC fiber [5]. The pump can be coupled from the side of the DC fiber by using a tapered capillary [6], or prism [7]. Pump coupling from the end of the DC fiber can be achieved, e.g., by using a specially designed input fiber (IF) with smaller diameter than the output DC fiber; the IF is surrounded by pretapered multimode fibers for the pump [8]. Low-loss end-pumping was demonstrated by using direct splicing of pump and signal fibers into the DC fiber with stadium-like cross section [9]. Other methods consist of bundling individual and separable pump and signal fibers where the pump radiation couples between the fibers; the fibers are tightly touching thanks to a heat-shrunk tube over the fibers [10] or by twisting

1559-128X/15/040751-06$15.00/0

the fiber bundle [11,12]. Among the most suitable solutions for practical applications are fused fiber bundle combiners [13]. These combiners consist of several multimode pump delivery fibers and a signal fiber. Fibers are bundled together and then fused and tapered to match the output DCF [14]. Instead of multimode-laser-diode pumps, the plurality single-mode fiber lasers can be also combined in the so-called tandem pumping scheme that enables operation of a high-power fiber amplifier to deliver a power of up to 20 kW [15].

Methods for achieving low losses in the signal branch of the combiner are of increasing importance in order to improve efficiency and reliability of fiber laser systems. Reduction of losses requires accurate field profile matching both on input and output of the combiner. Because of tapering, the mode-field profile changes in the signal fiber along the taper and the problem with field profile matching arises. Several approaches addressing this problem were proposed. At first, a special fiber with matched mode-field profile simultaneously on input and output was discussed as a signal fiber in [13]. The signal fiber is connected to the IF before the fused portion of the combiner and to the output fiber (OF) at the end of the fused portion of the combiner in this case. Limitations of the mode-field matching of such a signal fiber connection are obvious from later analysis provided by Kong *et al.* [19]. The second technique consists of fattening of the signal fiber core before bundling and tapering, which is achieved by heating and subsequent dopant diffusion [14]. The third approach is based on vanishing core technology when the special DCF is used as the signal fiber inside the combiner [16,17]. By tapering, the field expands from the core to the first cladding, which is matched to the OF core at the end of the taper. Another approach consists of etched taper conserving core diameter along the taper [18].

In this paper we propose and demonstrate a mode-field adapter that is based on tapered splice between dissimilar fibers inside the bundled pump and signal combiner. A similar technique was also proposed for the reduction of splicing loss between a single-mode fiber and a dispersion-flattened fiber where splice losses were reduced by moderate tapering of the splice itself [20] and for low-loss splice in a wavelength-independent Y-junction beam splitter [21]. Here, we utilized to the best of our knowledge for the first time the splice tapering principle inside the bundled pump and signal combiner. Placement of the splice inside the tapered part of the combiner introduces an additional degree of freedom in comparison with [13]. Optimization of the splice position inside the taper extends the range of possibilities of combiner losses reduction and it provides a way to improve the reliability of the combiners in high-power fiber lasers.

2. Combiner Principle and Design

The proposed tapered fiber bundle combiner is schematically shown in Fig. 1. The bundle combiner consists of several pump delivery fibers and one signal fiber. A single-mode fiber is used as the signal input. Inside the tapered part of the bundle the signal IF is spliced to the appropriate intermediate fiber (MF). The tapered bundle is spliced to active or passive double-clad OF.

The principle of operation is as follows. As the IF is tapered, the field first shrinks and then expands from the core. The mode-field diameter (MFD) becomes even greater than that of the original nontapered fiber below a certain taper ratio. The splice is placed at the point where the IF expanded field profile corresponds to the field profile of the MF tapered with the same ratio. The MF is further tapered with the bundle to the point where the diameter of the bundle corresponds to the diameter of the OF. The MFD in the MF decreases in the progressing down-taper portion. The field profile at the end of the MF must correspond to the field profile of the OF core. Therefore, the choice of the MF is crucial for successful design.

A. Numerical Design

In order to clarify the design procedure let us describe the particular design of geometrically hexagonal $(6+1)\times 1$ combiner signal branch for the wavelengths of 2 and 1.55 μm. We assume standard single-mode fiber according to ITU recommendation G.652 as the IF, e.g., the Corning SMF28 fiber with the numerical aperture (NA) of 0.14, the core diameter of 8.2 μm, and the cladding diameter of 125 μm. On the output, we assume the OF with core mode-field profile matched to SMF28 and cladding diameter of 125 μm. Because the bundle consists of seven fibers, it needs to be tapered to the ratio of 1/3 to match the diameter of the OF. The MF is required to have its field profile matched to the OF at the end of the taper. The easiest way is to use a special fiber with core and cladding refractive indices corresponding to the OF, but a threefold larger core diameter. In a theoretical case, when we neglect perturbations of fiber NA and core diameter due to dopant diffusion during fabrication and splicing processes, such a special fiber fundamental mode will have exactly the

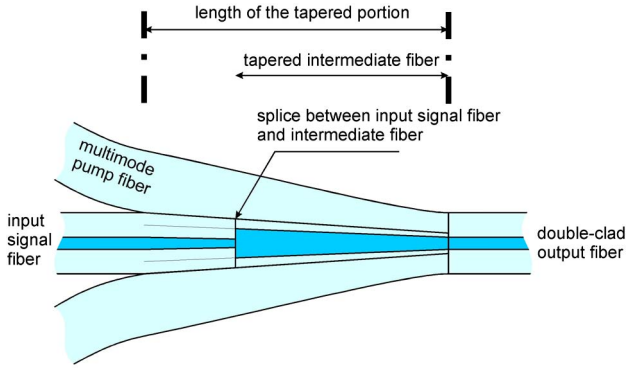

Fig. 1. Schematic illustration of the proposed mode field adapter inside the bundled tapered pump and signal combiner.

same field profile as the OF when tapered to the ratio of 1/3.

Commercially available fiber can be also used instead of a special fiber. The fiber should have approximately a threefold larger core and similar NA with respect to the OF. The suitability of the fiber needs to be verified using numerical simulation. In our particular case, we used CorActive MM-20/125 fiber [22] with NA 0.14 for the wavelength of 2 μm and CorActive SCF-UN 20/125-12 fiber [22] with NA 0.12 for the wavelength of 1.55 μm. We started with the fundamental LP_{01} eigenmode of each fiber and used the finite element beam propagation method [23,24] to calculate the field distribution evolution along the fibers tapered to the ratio of 1/3. The taper had linear shape and the length of the taper was 12 mm, so the taper was gradual and adiabatic [25]. We then calculated the fundamental eigenmode of the standard single-mode fiber, which according to our assumption corresponds to the eigenmode of the OF. Finally, we calculated the overlap integral (1) between OF eigenmode and the propagated field in each propagation step. The result quantifies the field correspondence between the OF and the MF with respect to the tapering ratio. Splice loss is determined by the squared absolute value of the overlap integral [26,27] and it is shown in Fig. 2.

$$a = \frac{\int \vec{E}_1 \vec{E}_2^* \mathrm{d}\Omega}{\sqrt{\int |\vec{E}_1|^2 \mathrm{d}\Omega}\sqrt{\int |\vec{E}_2|^2 \mathrm{d}\Omega}}. \quad (1)$$

Figure 2 shows that minimal splice loss is achieved slightly before the target ratio for both wavelengths, but loss at the ratio of 1/3 is not significantly worse.

The second step is finding the optimal position of the splice between the tapered IF and the MF. The splice must be placed to the point of optimal field matching between both fibers. Again, we started with fundamental LP_{01} eigenmode of each fiber and used the beam propagation method for calculating the field profile evolutions in the tapered input and MFs. Then we calculated the overlap integral

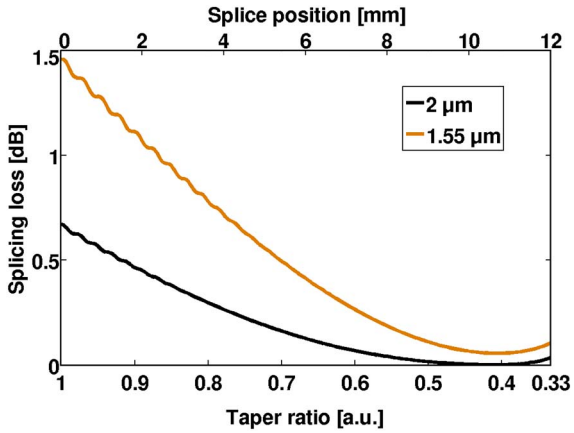

Fig. 2. Estimation of MF—OF splicing loss dependence on MF tapering ratio and splice position.

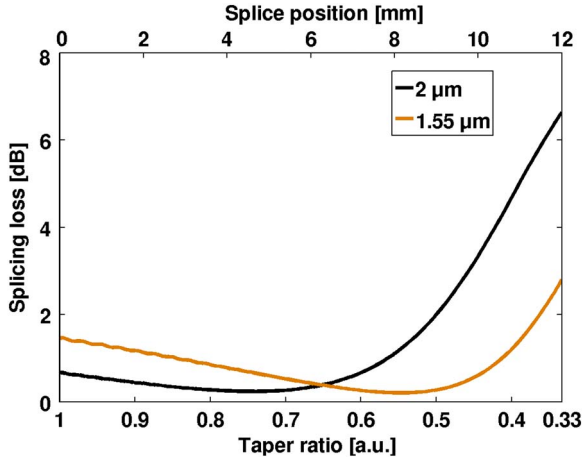

Fig. 3. Estimation of splice loss dependence on taper ratio and splice position between IF and MF based on squared absolute value of overlap integral between fields in fibers.

between fields of these tapered fibers for each taper ratio. Figure 3 shows the dependence of the estimated splice loss on the taper ratio between the IF and the MF.

Minimum loss is achieved for the ratio of 0.74 for 2 μm design and for the ratio of 0.55 in the case of 1.55 μm design. Loss is approximately 0.2 dB in both cases. The actual position of the splice (place of the optimum taper ratio) along the taper depends on the shape of the taper. In our simulations we assumed adiabatic linear taper with the length of 12 mm. So the optimal positions for splices were 4.7 mm from beginning for 2 μm design and 8.2 mm from beginning for 1.55 μm design. In general, the shape of the taper is not important as long as the taper is adiabatic [25].

Finally, we verified the proposed design. We excited the designed adapters by IFs fundamental LP_{01} eigenmodes for both wavelengths and evaluated overlap integrals between fundamental LP_{01} modes of the OFs and fields propagated along the adapters. Evolution of overlap integrals along the adapters is shown in Fig. 4. Transmittances of adapters correspond to the squared absolute value of the overlap integrals values at the end of propagation. Figure 4 shows that the transmittances of −0.27 dB in the case of 2 μm and −0.37 dB for 1.55 μm are achieved between IFs and OFs. The evolution of optical intensity along the taper is illustrated in Fig. 5. It is obvious from Figs. 4 and 5 that at the beginning the field corresponds to the OF LP_{01} eigenmode as we originally assumed. As the core of the IF shrinks, the field profile changes and the overlap integral decreases. The position of the splice is clearly visible. In the tapered MF the field is initially expanded and then compressed back and the overlap gradually increases.

3. Experiment

We performed an experiment in order to verify the design and theoretical results. We limited the

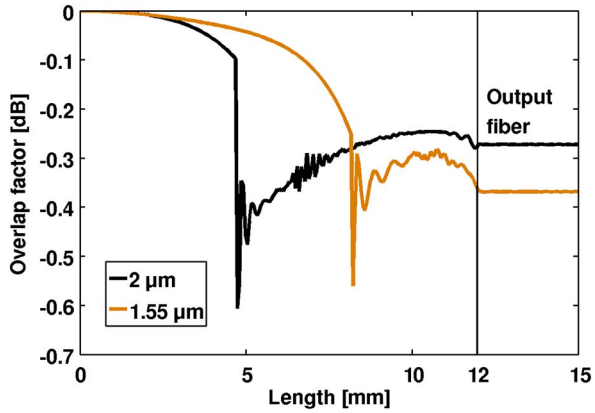

Fig. 4. Evolution of squared absolute value of the overlap integral between the output fiber LP_{01} eigenmode and the field in the taper along the structure.

verification only to the design for the wavelength of 1.55 μm due to ease of instrumentation.

A. Experimental Setup

We did not create the entire combiner in our experiments. We only verified whether tapering according to our design improves splicing loss between IF and MF, which is fundamental for our approach. At first, we spliced SMF28 and SCF-UN 20/125-12 fibers. We then tapered the spliced fibers according to our design using the VYTRAN GPX 3400 glass processing unit, see Fig. 6. The splice was placed in the narrowing part of the taper. The taper then continues and reaches the waist of a specific certain ratio. We created several tapers with different waist ratios. Beyond the waist the taper expands back to the original shape of the SCF-UN 20/125-12. Based on our simulations in Fig. 2, we assume that the field in the waist of the tapers corresponds to the OF field. Therefore, we did not investigate experimentally the connection between the taper and the OF. Instead, we assumed that expanding part of the taper is adiabatic and the transformation of the field to SCF-UN 20/125-12 is lossless. Thus, splicing loss between IF and MF does not depend on the waist diameter in this case.

We measured changes in transmission during the tapering process on the VYTRAN unit. Radiation of the wavelength of 1.55 μm was introduced into the SMF28 fiber. The end of SCF-UN 20/125-12 was connected to an InGaAs detector and its signal was observed using an oscilloscope set to slow time base.

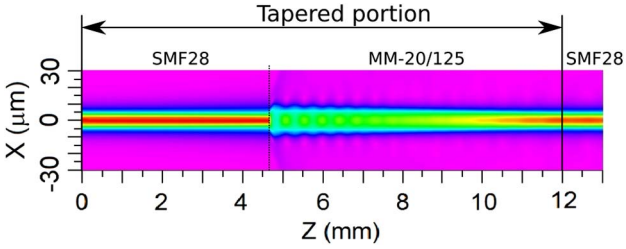

Fig. 5. Optical intensity evolution along the tapered section for the wavelength of 2 μm.

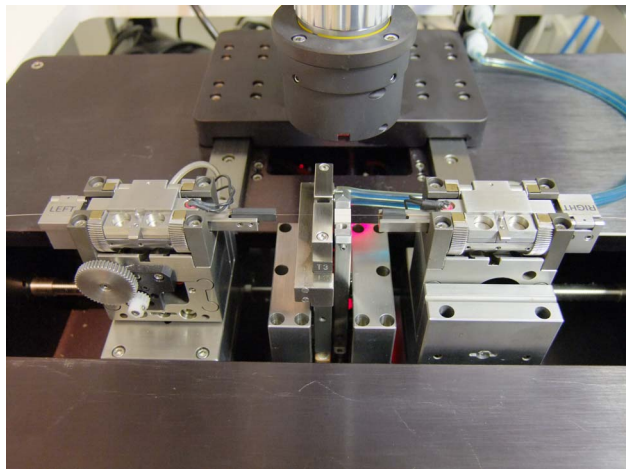

Fig. 6. Photo of the optical fiber tapering rig in the VYTRAN GPX 3400 device. The fiber is heated by an Ω-shaped graphite filament (under the shield in the middle) and pulled by the moveable fiber holders.

B. Experimental Results

The first example of the fabricated tapers (taper 1) had the waist diameter of 69 μm. This waist diameter corresponds to the taper ratio of 0.55. This is according to our simulations an optimal ratio for the splicing point between IF and MF, see Fig. 3.

The splice itself was positioned 3.5 mm before the waist, where the ratio of about 0.61 was achieved. The shape of the tapered splice is shown in Fig. 7. Figure 7(a) is only illustrative, namely the core dimensions are exaggerated and the experimental fiber taper is not strictly linear. Figure 7(b) shows that the taper slope is not continuous across the splice, but there is a step. This is probably because of the different material properties of both fibers. Nevertheless, this step did not cause any decrease in transmission, as is discussed later.

We recorded the transmitted power during the tapering procedure, see Fig. 8. The figure shows an increase in transmittance and thus a reduction

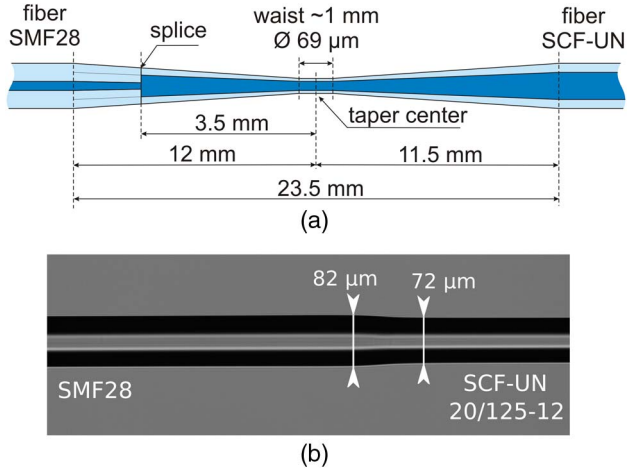

Fig. 7. (a) Dimensions of the taper 1, (b) detail of tapered splice inside the taper 1.

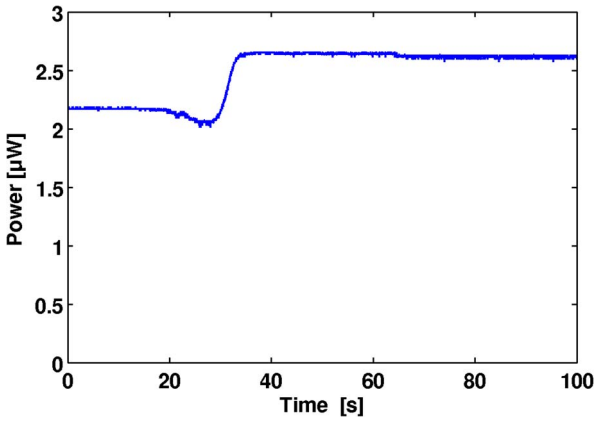

Fig. 8. Oscillogram of the tapering process of taper 1.

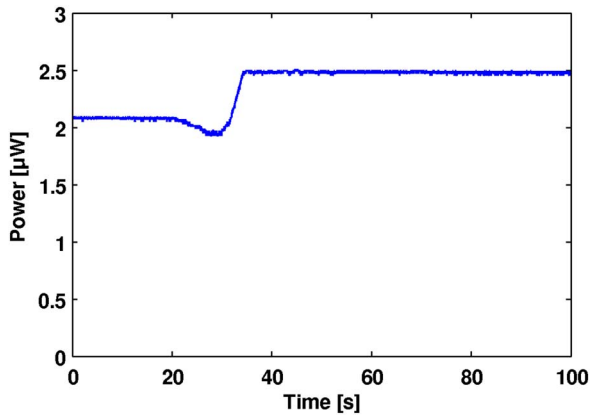

Fig. 10. Oscillogram of the tapering process of taper 2.

of splicing loss as the tapering head with the heat filament crossed the splice. Further phases of the tapering process had no significant impact on transmittance. This proves our assumptions concerning the independence on the waist diameter and the adiabatic field expansion back to SCF-UN 20/125-12.

The second taper example (taper 2) had the waist diameter of 50 μm. This corresponds to the ratio of 0.4, which is according to our simulations optimal for splicing to the OF, see Fig. 2. The position of the splice was 4.4 mm before the waist where the tapering ratio was approximately 0.54. This tapering ratio is very close to the optimal one, see Fig. 3. The taper shape and the tapering process oscillogram are shown in Figs. 9 and 10.

Improvement of splicing loss was slightly worse in taper 2 than in taper 1, as shown in Fig. 10. Taper 2 was thinner in diameter around the splice than taper 1. Although the splice diameter of this taper was closer to the optimal, it had higher loss than taper 1.

Figures 8 and 10 show only the improvement in splicing losses relative to the spliced fibers throughput. Finally, we also measured absolute losses of the tapered splices. A schematic of the measurement setup is shown in Fig. 11 [28]. At first the radiation

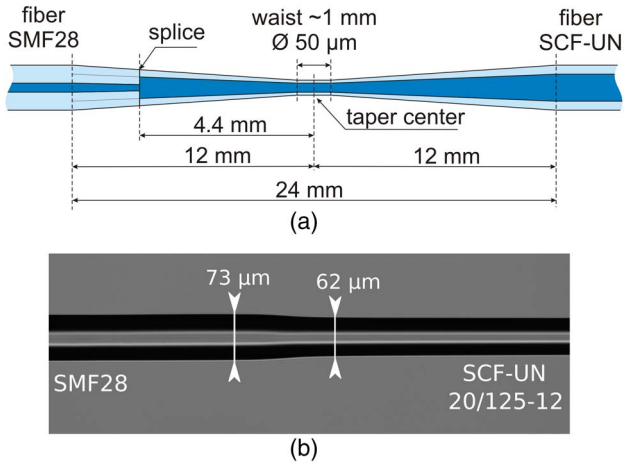

Fig. 9. (a) Dimensions of the taper 2, (b) detail of tapered splice inside the taper 2.

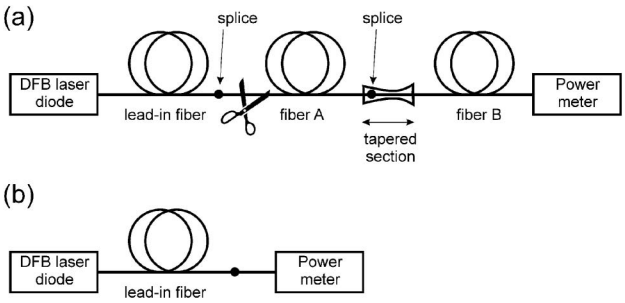

Fig. 11. Setup for the measurement of splice-losses: (a) Measurement of the optical power passing through the spliced dissimilar fiber A and B after tapering, (b) calibration of the input power.

was introduced from lead-in SMF28 fiber into SMF28 IF, and output power was measured at the end of intermediate SCF-UN 20/125-12 fiber. The input SMF28 fiber was then cleaved before taper and the input power was calibrated at this point. The difference of measured powers then gives loss of tapered splice. Lengths of all fibers were about 1 m. Measured losses are summarized in Table 1.

Table 1 shows better performance of the tapered splices than our theoretical simulations (see Fig. 3). Since the numerical simulations do not account for dopant diffusion it was expected that the experimental results should be better than the theoretical predictions based only on the mode-field overlap. While we assumed abrupt change in refractive index profiles between input and MFs in the numerical simulations, in real spliced and tapered structure the transition is more gradual due to dopant diffusion. Indeed, the advantageous impact of diffusion on reduction of splicing losses was also discussed in [20]. The difference between theoretical and experimental

Table 1. Losses of Created Taper Splices

	Measured Loss (dB)
Taper 1	0.02
Taper 2	0.17
Nontapered splice	0.98

results was probably also influenced by the fact that we used estimated equivalent step-index refractive index profiles of the input, intermediate, and OFs. Such approximated refractive index profiles may deviate from the real ones.

4. Conclusions

We presented to the best of our knowledge a novel type of a mode-field adapter for signal branch of pump and signal combiners. The principle and design procedure of the adapter was described using the examples of two particular adapters for the wavelengths of 2 and 1.55 μm and commercially available fibers. Numerical simulations showed insertion losses in the signal branch between the input single-mode fiber and the output DCF of 0.27 dB for the design wavelength of 2 μm and 0.37 dB for the design wavelength of 1.55 μm. The losses could be further improved using specially designed and optimized MFs.

We experimentally verified the fundamental principle of the adapter for the wavelength of 1.55 μm. We created two tapered splices between the IF and the MF. We observed improvement of splicing losses from 0.98 to 0.02 dB for the first taper and 0.17 dB for the second taper. Experimental results show even better performance than theoretical results as expected because of dopant diffusion during the splicing and tapering processes that was not accounted for in the numerical simulations. Especially, the important splice between significantly dissimilar input and MFs profits from dopant diffusion. The presented numerical and experimental results of the proposed mode-field adapter are promising for fabrication of high-power combiners with low signal losses.

This work was supported by the Czech Science Foundation, Project No. P205/11/1840, and by the Ministry of Industry and Trade of the Czech Republic, Project No. FR-TI4/734.

References

1. D. J. Richardson, J. Nilsson, and W. A. Clarkson, "High power fiber lasers: current status and future perspectives [Invited]," J. Opt. Soc. Am. B **27**, B63–B92 (2010).
2. E. Snitzer, H. Po, F. Hakimi, R. Tuminelli, and B. C. McCollumn, "Double-clad, offset core Nd fiber laser," in *Optical Fiber Sensors*, Vol. **2** of OSA Technical Digest Series (Optical Society of America, 1988), paper PD5.
3. F. Gonthier, L. Martineau, N. Azami, M. Faucher, F. Séguin, D. Stryckman, and A. Villeneuve, "High-power all-fiber components: the missing link for high power fiber lasers," Proc. SPIE **5335**, 266–276 (2004).
4. V. P. Gapontsev and L. E. Samartsev, "High-power fiber laser," in *Advanced Solid State Lasers*, G. Dube, ed., Vol. **6** of OSA Proceedings Series (Optical Society of America, 1990), paper LSR1.
5. V. P. Gapontsev and I. Samartsev, "Coupling arrangement between a multi-mode light source and an optical fiber through an intermediate optical fiber length," U.S. patent 5,999,673 (7 December 1999).
6. C. Jauregui, S. Bohme, G. Wenetiadis, J. Limpert, and A. Tünnermann, "Side-pump combiner for all-fiber monolithic fiber lasers and amplifiers," J. Opt. Soc. Am. B **27**, 1011–1015 (2010).
7. T. Weber, W. Lüthy, and H. Weber, "Side-pumped fiber laser," Appl. Phys. B **63**, 131–134 (1996).
8. Q. Xiao, P. Yan, H. Ren, X. Chen, and M. Gong, "Pump-signal combiner with large-core signal fiber feed-through for fiber lasers and amplifiers," Appl. Opt. **52**, 409–414 (2013).
9. P. Peterka, I. Kasik, V. Matejec, V. Kubecek, and P. Dvoracek, "Experimental demonstration of novel end-pumping method for double-clad fiber devices," Opt. Lett. **31**, 3240–3242 (2006).
10. P. Polynkin, V. Temyanko, M. Mansuripur, and N. Peyghambarian, "Efficient and scalable side pumping scheme for short high-power optical fiber lasers and amplifiers," IEEE Photon. Technol. Lett. **16**, 2024–2026 (2004).
11. A. B. Grudinin, J. Nilsson, P. W. Turner, C. C. Renaud, W. A. Clarkson, and D. N. Payne, "Single clad coiled optical fibre for high power lasers and amplifiers," in *Conference on Lasers and Electro-Optics*, OSA Technical Digest (Optical Society of America, 1999), paper CPD26.
12. M. N. Zervas and C. A. Codemard, "High power fiber lasers: a review," IEEE J. Sel. Top. Quantum Electron. **20**, 219–241 (2014).
13. D. J. DiGiovanni and A. J. Stentz, "Tapered fiber bundles for coupling light into and out of cladding-pumped fiber devices," U.S. patent 5,864,644 (26 January 1999).
14. F. Gonthier, F. Seigun, A. Villeneuve, M. Faucher, N. Azami, and M. Garneau, "Optical coupler comprising multimode fibers and method of making the same," U.S. patent 7,046,875 (16 May 2006).
15. V. P. Gapontsev, V. Fomin, and N. Platonov, "Fiber laser system," U.S. patent 7,848,368 (7 December 2010).
16. D. Neugroschl, J. Park, M. Wlodawski, J. Singer, and V. I. Kopp, "High-efficiency (6+1) × 1 combiner for high power fiber lasers and amplifiers," Proc. SPIE **8601**, 860139 (2013).
17. D. Noordegraaf, M. D. Maack, P. M. W. Skovgaard, S. Agger, T. T. Alkeskjold, and J. Lægsgaard, "7 + 1 to 1 pump/signal combiner for air-clad fiber with 15 μm MFD PM single-mode signal feed-through," Proc. SPIE **7580**, 75801A (2010).
18. B. G. Ward, D. L. Sipes, Jr., and J. D. Tafoya, "A monolithic pump signal multiplexer for air-clad photonic crystal fiber amplifiers," Proc. SPIE **7580**, 75801C (2010).
19. L. Kong, J. Leng, J. Cao, S. Guo, and H. Jiang, "The comparison between MFD and MOI on the simulation of combiner insertion loss," Proc. SPIE **8904**, 890416 (2013).
20. A. Oehler, T. Hauff, W. Heinlein, W. Stieb, and J. Schulte, "New field-matching technique for low-loss splices between conventional and dispersion-flattened single-mode fibres," in *Proceedings of the 14th European Conference on Optical Communication ECOC 88* (IEEE 1988), pp. 603–606.
21. N. Healy, E. McDaid, D. F. Murphy, C. D. Hussey, and T. A. Birks, "Low-loss single mode fibre 1 × 2 Y-junction," Electron. Lett. **42**, 740–742 (2006).
22. CorActive High Tech Inc., "Passive fibers brochure," www.coractive.com/pdf/brochures/PassiveFibers_BR0004r06.pdf.
23. D. Schulz, C. Glingener, M. Bludszuweit, and E. Voge, "Mixed finite element beam propagation method," J. Lightwave Technol. **16**, 1336–1342 (1998).
24. C. Geuzaine and J. F. Remacle, "Gmsh: a three-dimensional finite element mesh generator with built-in pre- and post-processing facilities," Int. J. Numer. Methods Eng. **79**, 1309–1331 (2009).
25. T. A. Birks and Y. W. Li, "The shape of fiber tapers," J. Lightwave Technol. **10**, 432–438 (1992).
26. A. W. Snyder and J. D. Love, *Optical Waveguide Theory* (Chapman and Hall, 1983), pp. 420–441.
27. A. D. Yablon, *Optical Fiber Fusion Splicing* (Springer, 2005), pp. 91–135.
28. D. Derickson, *Fiber Optic Test and Measurement* (Prentice-Hall, 1998), Chap. 9.

4.4. Monolithic Tm-Doped Fiber Laser at 1951 nm with Deep-UV Femtosecond-Induced FBG Pair

This chapter is a version of a published manuscript:

P. Peterka, P. Honzátko, M. Becker, F. Todorov, M. Písařík, O. Podrazký, and I. Kašík, "Monolithic Tm-Doped Fiber Laser at 1951 nm With Deep-UV Femtosecond-Induced FBG Pair," *IEEE Photonics Technology Letters*, vol. 25, no. 16, pp. 1623-1625, Aug.15, 2013.

Connection with my PhD. work:

The article provides summary of my research on novel design of an ultra-compact fiber laser and includes a successful demonstration of a combination of methods for fiber drawing with direct deep ultra-violent fiber Bragg grating writing at 266 nm pumped through newly developed FBC components – wavelength division multiplexers from powerful EDFA amplifier at 1611 nm using $^3F_4$ -> $^3H_6$ transition.

Monolithic Tm-Doped Fiber Laser at 1951 nm With Deep-UV Femtosecond-Induced FBG Pair

Pavel Peterka, Pavel Honzátko, Martin Becker, Filip Todorov, Michael Písařík, Ondrej Podrazký, and Ivan Kašík

***Abstract*— We report on a monolithic Tm-doped fiber laser emitting in the region ∼2 μm. A pair of fiber Bragg gratings (FBGs) was written into the Tm-doped fiber using a two-beam interferometry and a deep ultraviolet (DUV) femtosecond laser source at 266 nm. Such a monolithic setup allows a simple setup of the laser made of a single fiber only. This configuration also offers greater reliability because fusion splices inside the resonator cavity could eventually generate failure in the laser cavity. To the best of our knowledge, this is the first rare-earth-doped fiber laser with an FBG pair written by DUV femtosecond laser radiation. Laser characteristics are presented as well as compared with the fiber laser with external FBGs conventionally spliced to the Tm-doped fiber. Dependence of the laser wavelength on the pump power is investigated in detail.**

***Index Terms*— Thulium, fiber lasers, fiber Bragg gratings.**

I. Introduction

MONOLITHIC fiber lasers refer to compact laser cavities with Bragg gratings inscribed directly into the active fiber [1]. Such configuration improves the laser lifetime as the laser resonator is fully integrated and there are no splices with the fiber Bragg gratings (FBGs) which could generate a failure. Rare-earth doped fiber lasers with FBGs inscribed into the active fibers were reported using various methods, e.g., phase mask inscription using UV light [2] or femtosecond laser in visible [3] and infrared spectrum [4], and by point-by-point technique with infrared femtosecond radiation [5].

In this letter, we report on monolithic Tm-doped fiber laser (TDFL) emitting at 1951 nm. The preliminary results were presented in the conference abstract [6]. To our knowledge, this is the first rare-earth-doped fiber laser with a FBG pair written with DUV femto second laser radiation. DUV femtosecond lasers were used for FBGs inscription into passive fibers through phase mask technique [7]–[9]. The method with Talbot interferometer [10], [11] that we applied has advantages of grating inscription into germanium-free fibers while retaining versatility of the choice of the center wavelength of the FBG, and implementation of small refractive index changes, which makes the method suitable for 1st order FBGs. These features offer unique benefits for the intended application of the presented monolithic TDFL in laser arrays for component manufacturing and testing or in fiber sensing. In the array we need closely spectrally spaced TDFLs with a compact design. A resonator made out of FBG pair is advantageous for the required narrow bandwidth and for the higher stability of the laser upon moderate pumping, while for high-power applications the resonator can be formed by a single FBG and a perpendicularly-cleaved fiber [1], [11]. Moreover, only in the last years the measurement and characterization tools for FBGs in the 2 μm range appeared on the market, which are needed to inscribe well confined high- and lower-reflectivity (HR, LR) grating pairs in the Tm amplification band in non-photosensitive fibers. Laser characteristics of three TDFL samples are presented and compared to a TDFL consisting of the same active fiber but with external FBGs. We discuss the effect of temperature changes and resonant nonlinearity on the laser wavelength.

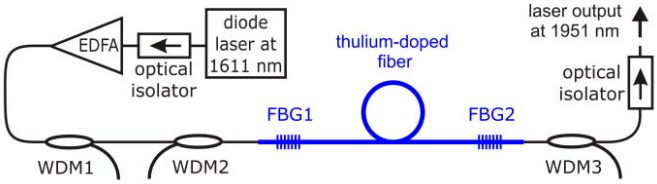

Fig. 1. Tm-fiber laser setup. EDFA: Er-doped fiber amplifier, WDM: wavelength-division multiplexer, FBG: fiber-Bragg grating.

II. Tm-Fiber Laser Setup and FBGs Characteristics

The experimental setup of the fiber laser is shown in Fig. 1 The monolithic TDFL is formed by the Tm-doped fiber (TDF) with two gratings inscribed into it 30 cm apart from each other to create the resonator. The TDF was fabricated by modified chemical vapor deposition (MCVD) and solution-doping methods. The thulium chloride was dissolved in the absolute ethanol together with alumina nanoparticles of <50 nm size. Such nanoparticle doping allows us to reach higher concentration of alumina in the fiber core compared to conventional production from chlorides [12]. The alumina content in the core is 11.2 mol % and no germanium oxide

Manuscript received May 17, 2013; revised June 27, 2013; accepted July 6, 2013. Date of publication July 11, 2013; date of current version July 31, 2013. This work was supported in part by the European Commission under the COST action under Grant TD1001: Novel and Reliable Optical Fibre Sensor Systems for Future Security and Safety Applications, in part by the Czech Science Foundation under Grants P205/11/1840 and P102/10/2139, and in part by the Czech Ministry of Industry and Trade under Grant FR-TI4/734.

P. Peterka, P. Honzátko, F. Todorov, O. Podrazký, and I. Kašík are with the Institute of Photonics and Electronics ASCR, Prague 18251, Czech Republic (e-mail: peterka@ufe.cz; honzatko@ufe.cz; todorov@ufe.cz; podrazky@ufe.cz; kasik@ufe.cz).

M. Becker is with the Department of Fiber Optics, Institute of Photonic Technology, Jena 07745, Germany (e-mail: martin.becker@ipht-jena.de).

M. Písařík is with Research and Development, SQS Vláknová optika a.s., Nová Paka 50901, Czech Republic, and also with the Department of Electromagnetic Field, Czech Technical University in Prague, Prague 16627, Czech Republic (e-mail: michael.pisarik@sqs-fiber.cz).

Color versions of one or more of the figures in this letter are available online at http://ieeexplore.ieee.org.

Digital Object Identifier 10.1109/LPT.2013.2272880

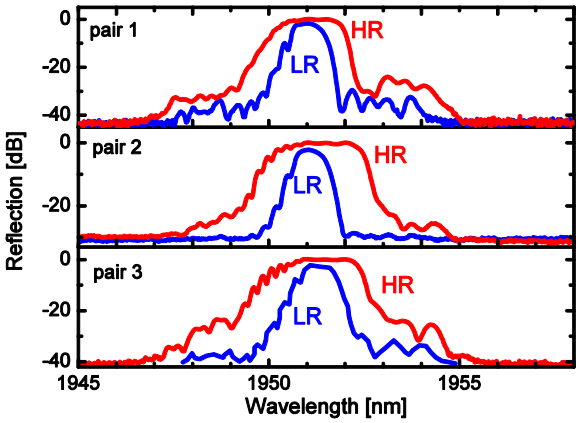

Fig. 2. Reflection spectra of the FBG pairs inscribed into the Tm-doped fiber. HR – high reflectivity grating, LR – lower reflectivity grating.

was added. The TDF has LP_{11} cutoff wavelength of 1520 nm, hence both pump at 1611 nm and signal at 1951 nm are propagating in the fundamental mode. The fiber absorption of 25 dB/m was measured at the pump wavelength. Mode field diameter at 1611 nm and 1951 nm is 5.6 μm and 6.3 μm, respectively.

A series of three monolithic TDFLs were prepared with FBGs nominal reflectivity of 99 % and 60 %, respectively. The nominal central wavelength is 1951 nm. The reflection spectra of the fabricated FBGs are shown in Fig. 2. The LR gratings are of 0.7 nm bandwidth while HR gratings exhibited larger bandwidths in the range of 1.6 to 2.3 nm. The gratings were inscribed using a two-beam Talbot interferometer with phase mask as a beam splitter [10]. The third harmonics from the Ti:sapphire femtosecond laser system was employed as a DUV source. It should be noted that with DUV femtosecond laser inscription a multiple-photon absorption occurs in contrary to the DUV cw laser inscription with a single-photon absorption only [10]. The different nature of the FBG inscription also lead to different features of these gratings, e.g., variation of their reflectivity with pump power and temperature was observed recently [11].

The TDF was pumped in the core at 1611 nm by a laser diode and an L-band erbium-doped fiber amplifier (EDFA). Most of the amplified spontaneous emission from the EDFA was filtered out by the first wavelength division multiplexer WDM1. The WDM2 can be used to monitor the laser output at around 2 μm generated backward to the pump. The WDM3 removes the unabsorbed pump radiation.

III. Experimental Results and Discussion

The output power characteristics of all three monolithic TDFLs are shown in Fig. 3. The laser output power for the FBG pair No. 1 is considerably lower than for the other two pairs. It is because the TDF length between the HR FBG1 and the standard single-mode fiber pigtail was about 32 cm while for the other pairs both pigtails were 10 cm long. Therefore, the actual pump power at the beginning of the TDFL resonator is lower by about 5 dB than for the other two pairs. The absorbed pump power in Fig. 3 refers

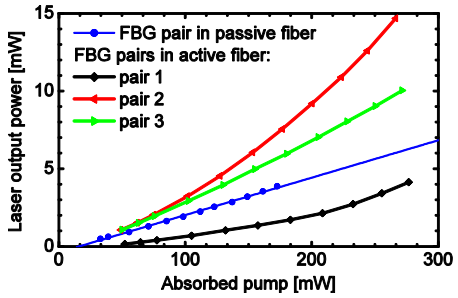

Fig. 3. Laser output vs. absorbed pump for the fiber laser with external FBG pair and for the monolithic configurations.

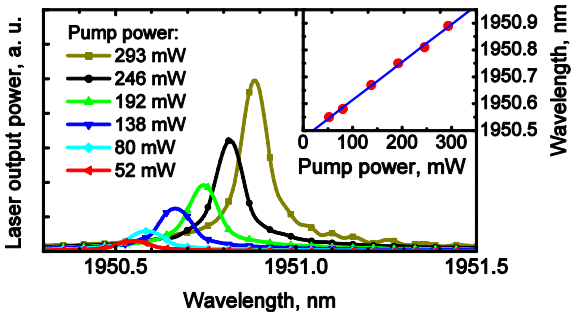

Fig. 4. Laser spectra of the monolithic TDFL with FBG pair No. 2 for various input pump power levels, Inset: Laser wavelength shift with the pump power together with linear fit.

to the total absorbed pump power in the TDF, i.e., in the monolithic fiber laser and the two residual sections of the TDF leading to the pigtails. The output power vs. pump power exhibits nonlinear behavior for all three. The most pronounced nonlinear dependence is for the pairs no. 1 and 3. Typical linear characteristics for the output power vs. pump power were found in the case of the TDFL with external FBG pair; see the line with circles in Fig. 3. The HR FBG with a bandwidth of 0.3 nm and reflectivity of 0.99 was placed at the pump end of the TDFL and the LR FBG with a bandwidth of 0.08 nm and reflectivity of 0.95 was used as output port of the laser. Since the output FBG reflectivity differs from that of the output mirrors inscribed directly into the active fiber, the slope efficiency is also different compared to the output FBG in the monolithic TDFL. The laser wavelength of the TDFL with external FBG pair was almost constant. The external FBGs were inscribed in rare-earth free optical fibers that exhibit no resonant nonlinearity (due to population inversion) and negligible temperature increase (due to rare-earth-ions absorption). But for the monolithic TDFL we have observed a wavelength shift with the pump power at the rate of $\delta\lambda_B/\delta P_{abs} \approx 1.41$ pm/mW, see Fig. 4, which is attributed to the change of the refractive index with absorbed pump power, as a result of changes of the temperature and the population inversion within the FBGs. Since the wavelength shifts of the two FBGs of the monolithic TDFL are generally different, their reflectivity varies differently resulting in nonlinear laser output power characteristics. Spectral variation of the thulium cross section should have negligible effect as the emission spectrum at the laser wavelengths is flat compared to the variation of the FBGs reflection spectra.

To evaluate the effect of temperature and population inversion let us consider the following analysis. The thermo-optic coefficient in silica based fibers is $\delta n/\delta T \approx 1 \times 10^{-5}$ per K [13]. The wavelength of reflection of the FBG is given by $\lambda_B = 2n_{eff}\Lambda_B$, where the n_{eff} is the effective refractive index of the fundamental mode of the TDF and Λ_B is the grating pitch (about 650 nm in our case). Therefore, the increase of the refractive index by Δn would cause a shift of the wavelength of reflection by $\Delta\lambda_B = 2\Delta n\Lambda_B$. If only the thermo-optic effect would be responsible for the wavelength shift, then from the relation: $\Delta\lambda_B/\Delta T = 2\Lambda_B \Delta n_{eff}/\Delta T$, one can find that in the thulium emission band the FBG wavelength shift with temperature is about 13 pm/K. Taking into account the observed laser wavelength shift of 1.41 pm/mW we can deduce that the temperature of the fiber core increased by 30 K for the 300 mW absorbed pump power. The observed FBG's wavelength shift is in good correspondence with 8 pm/K reported in ytterbium-doped fibers [11] and 13–30 pm/K recently reported in TDFL with FBG pair inscribed by different method [14].

If only resonant nonlinearity is taken into account, the shift of the FBG wavelength is $\Delta\lambda_B = 2\ \Lambda_B \Delta n_{eff} \approx 2\ \Lambda_B\ n_2\ P/A_{eff}$, where effective area A_{eff} is estimated from the mode-field diameter as 25 μm^2. Although the resonant nonlinearities in rare-earth doped fibers have been studied since nineties [15], only little information can be found about the resonant nonlinearity in TDFs. Kim et al. [16] have found nonlinear coefficient of germanosilicate fiber doped with tri- and divalent thulium ions of about $n_2 \approx 4 \times 10^{-15}$ m^2/W for the TDF with similar thulium concentration to our experiment. Attenuation of their TDF is about 50 dB/m at 1600 nm. Unfortunately, general analysis and required spectroscopic data have not been published yet about resonant nonlinearity for TDFs as it was done for the ytterbium-doped fibers [15]. Therefore, we cannot evaluate the nonlinear refractive index change in the strongly saturated regime of fiber lasers. To achieve the observed wavelength shift of 1.41 pm/mW only by the resonant nonlinearity, the nonlinear refractive index has to be at least 2.7×10^{-14} m^2/W. This number is an order of magnitude higher than the value reported in the literature [16]. It should be noted, that in laser regime the pump is converted mainly to the laser output and the effect of resonant nonlinearity can be much lower than it is in the case of a fiber without resonator studied in [16].

IV. Conclusion

In summary, we have demonstrated a monolithic fiber laser at 1951 nm. A good reproducibility of the gratings fabrication has been shown. We have found that the output wavelength of the monolithic fiber laser varies with the pump power as 1.41 pm/mW while negligible wavelength shift occurred for the TDFL with external FBG pair. We have confirmed that the shift of the laser wavelength with pump power is dominantly determined by the thermo-optic effect rather than resonant nonlinearity. Since the wavelength shifts of the two FBGs of the monolithic TDFL are generally different, their reflectivity varies differently resulting in nonlinear laser output power characteristics. The applied method of FBG inscription offers a great versatility of selection of the center wavelength of the FBG which makes presented monolithic lasers promising solution for compact arrays of lasers for component testing and optical fiber sensors.

References

[1] M. Becker, *et al.*, "Towards a monolithic fiber laser with deep UV femtosecond-induced fiber Bragg gratings," *Opt. Commun.*, vol. 284, no. 24, pp. 5770–5773, 2011.

[2] Z. Zhang, A. J. Boyland, J. K. Sahu, W. A. Clarkson, and M. Ibsen, "High-power single-frequency thulium-doped fiber DBR laser at 1943 nm," *IEEE Photon. Technol. Lett.*, vol. 23, no. 7, pp. 417–419, Apr. 1, 2011.

[3] M. Bernier, R. Vallée, B. Morasse, C. Desrosiers, A. Saliminia, and Y. Sheng, "Ytterbium fiber laser based on first-order fiber Bragg gratings written with 400nm femtosecond pulses and a phase-mask," *Opt. Express*, vol. 17, no. 21, pp. 18887–18893, Oct. 2009.

[4] E. Wikszak, *et al.*, "Linearly polarized ytterbium fiber laser based on intracore femtosecond-written fiber Bragg gratings," *Opt. Lett.*, vol. 32, no. 18, pp. 2756–2758, Sep. 2007.

[5] N. Jovanovic, M. Åslund, A. Fuerbach, S. D. Jackson, G. D. Marshall, and M. J. Withford, "Narrow linewidth, 100 W cw Yb^{3+}-doped silica fiber laser with a point-by-point Bragg grating inscribed directly into the active core," *Opt. Lett.*, vol. 32, no. 19, pp. 2804–2806, Oct. 2007.

[6] P. Peterka, *et al.*, "Monolithic thulium-doped fiber laser with UV femtosecond-laser-induced fiber-Bragg-grating pair," in *CLEO/Eur. EQEC Conf. Dig.*, May 2013, paper CJ-P.5.

[7] S. A. Slattery, D. N. Nikogosyan, and G. Brambilla, "Fiber Bragg grating inscription by high-intensity femtosecond UV laser light: Comparison with other existing methods of fabrication," *J. Opt. Soc. Amer. B*, vol. 22, no. 2, pp. 354–361, Feb. 2005.

[8] K. A. Zagorulko, P. G. Kryukov, E. M. Dianov, A. Dragomir, and D. N. Nikogosyan, "Fibre-Bragg-grating writing in single-mode optical fibres by UV femtosecond pulses," *Quantum Electron.*, vol. 33, no. 8, pp. 728–730, 2003.

[9] A. Dragomir, D. N. Nikogosyan, K. A. Zagorulko, P. G. Kryukov, and E. M. Dianov, "Inscription of fiber Bragg gratings by ultraviolet femtosecond radiation," *Opt. Lett.*, vol. 28, no. 22, pp. 2171–2173, Nov. 2003.

[10] M. Becker, *et al.*, "Fiber Bragg grating inscription combining DUV subpicosecond laser pulses and two-beam interferometry," *Opt. Express*, vol. 16, no. 23, pp. 19169–19173, Nov. 2008.

[11] M. Leich, J. Fiebrandt, S. Jetschke, M. Rothhardt, and M. Jäger, "In situ FBG inscription during fiber laser operation," *Opt. Lett.*, vol. 38, no. 5, pp. 676–678, Mar. 2013.

[12] O. Podrazky, I. Kasik, M. Pospisilova, and V. Matejec, "Use of nanoparticles for preparation of rare-earth doped silica fibers," *Phys. Status Solidi C*, vol. 6, no. 10, pp. 2228–2230, 2009.

[13] P. Peterka, J. Kanka, P. Honzatko, and D. Kacik, "Measurement of chromatic dispersion of microstructure optical fibers using interferometric method," *Opt. Appl.*, vol. 38, no. 2, pp. 295–303, 2008.

[14] C. C. C. Willis, *et al.*, "Highly polarized all-fiber thulium laser with femtosecond-laser-written fiber Bragg gratings," *Opt. Express*, vol. 21, no. 9, pp. 10467–10474, Apr. 2013.

[15] J. W. Arkwright, P. Elango, G. R. Atkins, T. Whitbread, and J. F. Digonnet, "Experimental and theoretical analysis of the resonant nonlinearity in ytterbium-doped fiber," *J. Lightw. Technol.*, vol. 16, no. 5, pp. 798–806, May 1998.

[16] Y. H. Kim, U.-C. Paek, and W.-T. Han, "Fabrication of germanosilicate glass optical fibers containing Tm^{2+} ions and their nonlinear optical properties," *J. Lightw. Technol.*, vol. 23, no. 2, pp. 543–550, Feb. 2005.

4.5. Thulium-doped fiber broadband source for spectral region near 2 micrometers

This chapter has been submitted and accepted as a version of the manuscript:

M. Pisarik,P. Peterka,J. Aubrecht,J. Cajzl,A. Benda,D. Mareš,F. Todorov,O. Podrazky,P. Honzatko,I. Kasik, *Opto-Electronic Review*, accepted for publication, 2016.

Connection with my PhD. work:

The article pertains to the methodology of the development of a 2 µm-amplified spontaneous emission (ASE) light source for various applications, such as in medicine or optical components characterization. Two novel concepts of thulium-doped fiber ASE sources were analyzed, optimized and experimentally evaluated. The thulium-doped fiber ASE sources offer higher stability, and lower complexity and costs compared to other broadband sources, namely the supercontinuum sources that are based on ultrafast, quasi-continuous lasers with a spectrum broadened in highly nonlinear fiber.

DE GRUYTER

OPTO-ELECTRONICS REVIEW **24**(4), 00–00

DOI: 10.1515/oere-2016-0022

Thulium-doped fibre broadband source for spectral region near 2 micrometers

M. PÍSAŘÍK[1,3], P. PETERKA[*2], J. AUBRECHT[2], J. CAJZL[2,4], A. BENDA[2], D. MAREŠ[1], F. TODOROV[2], O. PODRAZKÝ[2], P. HONZÁTKO[2], and I. KAŠÍK[2]

[1]Czech Technical University in Prague, Faculty of Electrical Engineering, Technická 2, 166 27 Prague, Czech Republic

[2]Institute of Photonics and Electronics of the Czech Academy of Sciences, v.v.i., Chaberská 57, 182 51 Prague, Czech Republic

[3]HiLASE Centre, Institute of Physics of the Czech Academy of Sciences, v.v.i., Za Radnicí 828, Dolní Břežany, 252 41, Czech Republic

[4]Institute of Chemical Technology, Faculty of Chemical Technology, Technická 5, 166 28 Prague, Czech Republic

We demonstrated two methods of increasing the bandwidth of a broadband light source based on amplified spontaneous emission in thulium-doped fibres. Firstly, we have shown by means of a comprehensive numerical model that the full-width at half maximum of the thulium-doped fibre based broadband source can be more than doubled by using specially tailored spectral filter placed in front of the mirror in a double-pass configuration of the amplified spontaneous emission source. The broadening can be achieved with only a small expense of the output power. Secondly, we report results of the experimental thulium-doped fibre broadband source, including fibre characteristics and performance of the thulium-doped fibre in a ring laser setup. The spectrum broadening was achieved by balancing the backward amplified spontaneous emission with back-reflected forward emission.

Keywords: fibre lasers, amplified spontaneous emission, thulium-doped fibres.

1. Introduction

Various applications, specifically those with a medical focus, have a great need for laser sources operating from 1.7 to 2.1 micrometers. For example, significant works with lasers were done in dermatology, cardiology, gynecology, urology and nephrology [1–3] and conclusion from this field of application shows that for most applications better results were achieved by a laser in a near 2 μm wavelength, because they had penetration depth lower than 0.5 mm, in comparison with 1 μm lasers which had a penetration depth up to 2 mm [4]. A pilot study of 15 patients who underwent zero-ischemia LPN using laser emitting at 2011 nm showed minimal blood loss, negative tumour margins, and preservation of renal function [5]. Thulium-doped fibre lasers (TDFLs) are compact continuous or pulsed solid state lasers that typically emit a wavelength of 1900–2040 nm and penetrates tissue to the depth of 0.5 mm [6]. Apart from medicine, the TDFLs at about 2 micrometers are becoming important tools also for many other applications ranging from chemical sensing, material processing, optical fibre component manufacturing, to defence and telecommunications. The TDFLs are the efficient source used to pump of holmium-doped active media [7,8] and praseodymium thin disk lasing media [9]. TDFLs offer high efficiency and high output power while reducing the risk of damage to the retina, as 2 μm radiation is highly absorbed in water compared to 1 μm radiation of Yb fibre lasers. Despite the fact that TDFLs require novel components to be designed and developed [10–12] and the thermal management issues are more serious than in ytterbium doped fibre lasers, the TDFLs are gradually becoming a mature type of the fibre laser [13–17].

Wideband light sources at wavelengths around 2 micrometers are of increasing interest in many applications like in TDFLs component fabrication [18], skin melanoma diagnostics [19], and ophthalmology [1]. There are a number of important chemical substances, such as carbon dioxide or

[*]e-mail: peterka@ufe.cz

water vapour, that have significant absorption bands around 2 micrometers and this can be used as fingerprints for the detection of these substances and for the determination of their concentrations, as well. Namely, high brightness, stable and broadband or tuneable sources in this spectral region are desired for such sensors of chemical substances. Apart from sensor systems, wideband sources could be used in manufacturing or testing components for a 2-micrometer spectral range. The first broadband source based on an amplified spontaneous emission (ASE) in a thulium-doped fibre (TDF) was reported by Oh *et al*. in multicomponent silicate fibre with 1 mW output power and 77 nm bandwidth centred at 1991 nm [20]. Relatively high slope efficiency of 15% of the TDF ASE sources has been soon after demonstrated experimentally in a low-phonon energy host material of the fluoride-based TDF [21]. Ultra-broad emission spectra were demonstrated in doubly-doped fibres, e.g., thulium- and ytterbium co-doped fibre with about 140 nm full-width at half-maximum (FWHM) [22] and thulium- and bismuth doped fibre with 167 nm wide spectrum [23] where energy transfer mechanisms between the dopants may extend the output spectrum and/or the pump wavelength range [24,25]. However, the total output power of these experimental results was very low, less than 100 μW. The record bandwidth achieved so far in a TDF ASE source was achieved in a thulium- and holmium-doped fibre with the so called 10-dB bandwidth of 645 nm [26]. The emission from the thulium ions was promoted at one of the fibre ends while the emission from holmium ions prevailed at the other end. The two outputs are combined together by an appropriate wavelength division multiplexer. In fact, this device acts similarly to a dual stage ASE sources with combined outputs [27–29]. The pumping schemes of TDF ASE sources include both core-pumping and cladding pumping. Recently, in-band core pumping was demonstrated in broadband sources with about 70 nm FWHM and 20 mW [30] and 40 mW [31] output powers. The cladding pumping arrangement with pump at 790 nm resulted in the output power of 120 mW and FWHM of 40 nm [32]. Remarkable progress has been achieved in the high-power double-clad TDF superfluorescent sources, where the output power is optimized, rather than the spectral width. Output power of 11 W, slope efficiency of 38% and FWHM of 35 nm was achieved in a configuration with bulk-optics pumping [33] and in an all-fibre master-oscillator power-amplifier configuration the output power of 25 W, slope efficiency of 49 % and FWHM of 22 nm was achieved [34].

In this paper we report on methods for optimization of broadband sources based on ASE in TDF. In the following section of this paper we present an analysis of the spectrally flattened TDF ASE source. Numerical analysis of possible spectral flattening of TDF ASE sources has not been published yet, to our knowledge. Theoretical analysis of the TDF ASE source appeared in two papers [35,36] where the numerical model was used to reveal the physical understanding of the power evolution in ASE sources based on TDFs rather than for optimization issues. The first paper contains a brief analysis that resulted in preference of the forward (in terms of the pump radiation propagation) ASE that should carry the most of the optical power. On the contrary, the latter analysis leads to the opposite findings that it is the backward ASE that carries the highest power in the most typical configurations. In the third section of this paper we present preliminary experimental results of TDF ASE source using TDF developed in house. TDF characteristics including its performance in ring-laser setup are included.

2. Numerical modelling of a Tm-doped fibre ASE source

For predicting the performance of various thulium doped fibre devices and their optimization, we developed a comprehensive, spectrally and spatially resolved numerical model, which is described in detail elsewhere [37–39]. For numerical simulations we set thulium ion concentration not higher than 1000 ppm mol. The pair-induced quenching processes among neighbouring thulium ions can still be assumed negligible at this concentration level provided that the thulium ions are homogeneously distributed in the core and not in clusters [37]. The emission and absorption spectra are taken from Ref. 37. The other parameters of the fibre used in the simulations are summarized in Table 1. The configurations of the broadband source for the numerical modelling are shown in Fig. 1. The pump source at 1611 nm is assumed because this wavelength is the closest wavelength to the Tm peak absorption $^3H_6 \rightarrow {}^3F_4$ at around 1630 nm and in the same time it falls within the amplification range of commercially available L-band EDFAs. In the case of in-band pumping at 1611 nm and neglecting the cooperative up-conversion processes thanks to the limited concentration of thulium, the numerical model of TDF with a rich energy level structure [37,38] is simplified to a system with two energy levels.

Table 1. Parameters of the Tm doped-fibre used in the numerical modelling.

Fibre parameter	Symbol	Value
Core radius	a	7 μm
Numerical aperture	NA	0.13
Fibre length	L	1.57 m
Fluorescence lifetime of $^3F_4$ level	τ_1	430 μs
Concentration of thulium ions	N^{Tm}	1000 ppm mol Tm^{3+}

Evolution of pump and ASE optical powers and relative population of the metastable $^3F_4$ level along the fibre is

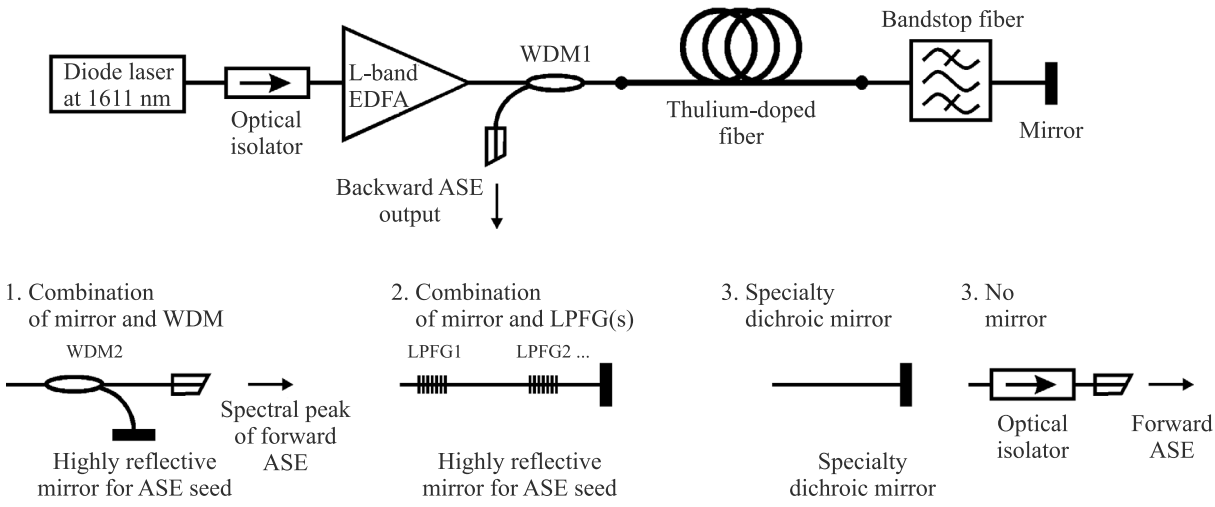

Fig. 1. Configurations of the TDF ASE source.

shown in Fig. 2 for the configurations with and without a mirror. The pump power level was set to 1 W. The pump is almost fully absorbed within the first meter of the fibre and the $^3F_4$ level population is close to zero beyond z = 1 m. For the configuration without reflection mirror (dashed lines in Fig. 2), the blue-edge of the spectrum of the forward ASE (FASE) is reabsorbed where a $^3F_4$ level population is low and the spectrally integrated FASE power is stagnating. The backward ASE (BASE) grows steadily towards the pump input end, benefiting from increasing pump power towards this fibre end. The BASE power may become strong enough to saturate its gain and lower the inversion population, as it was the case for the pump power level of 1 W shown in Fig. 2. Attachment of a mirror with spectrally flat reflection $R(\lambda) = 1$ at the z = L forms a seed for the BASE. Such an ASE seed promotes amplification of the BASE waves that deplete even more the inversion population at the beginning of the fibre, thus lowering the FASE power. The ASE output power *vs*. pump power for the two configurations and spectra corresponding to the pump power level of 1 W are shown in Fig. 3. As expected, the configuration with the mirror provides higher output power of the broadband source in one fibre pigtail than the mirror-less configuration. The higher output power is at the expense of narrower spectra. Notably, the blue edge of the ASE spectrum is suppressed due to reabsorption in the depleted part of the fibre close to the mirror end.

It should be noted out that the threshold pump power of the linear increase of ASE power depends on the fluorescence lifetime of the metastable level. The dependences of the ASE output power *vs*. pump power for different host materials are shown in Fig. 4. The other parameters were intentionally left the same in order to point out the effect of the host material. The longer fluorescence lifetime significantly decreases the pump power threshold while having

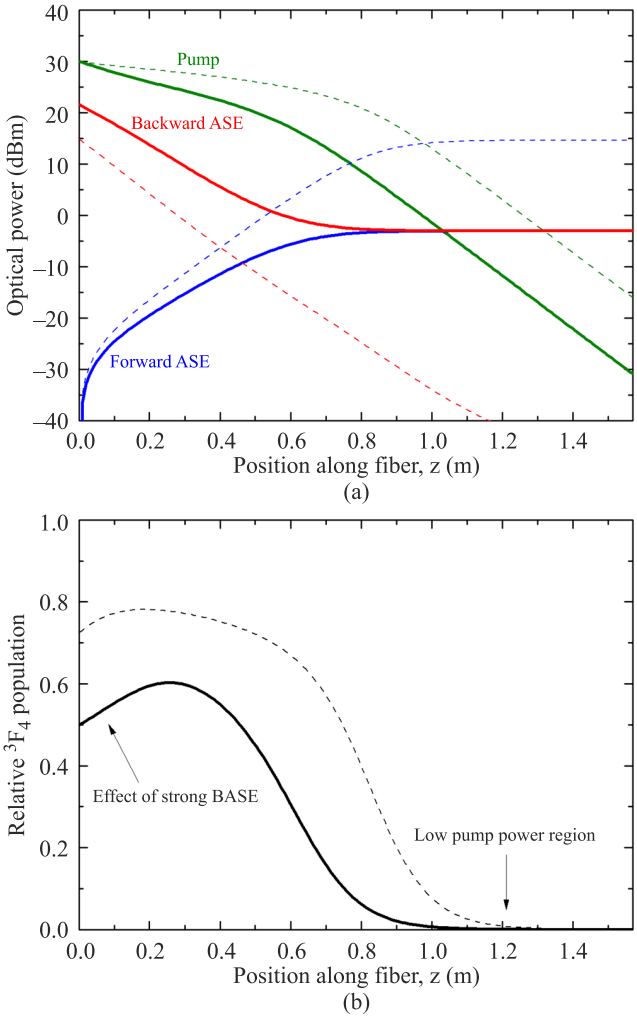

Fig. 2. (a) Optical power and (b) relative population of the thulium metastable level $^3F_4$ along the fibre with (solid line) and without mirror (dashed line).

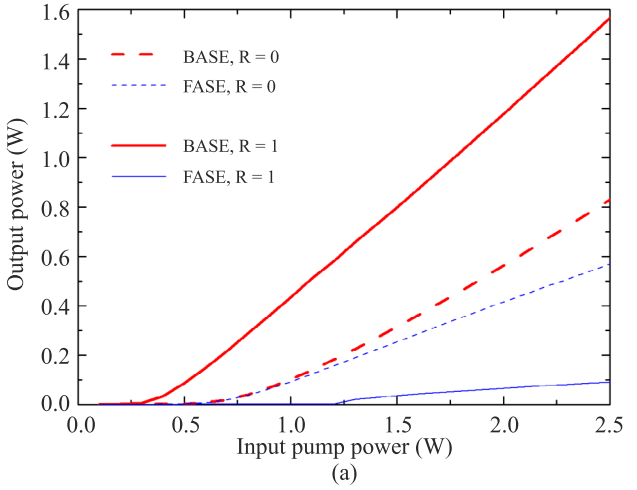

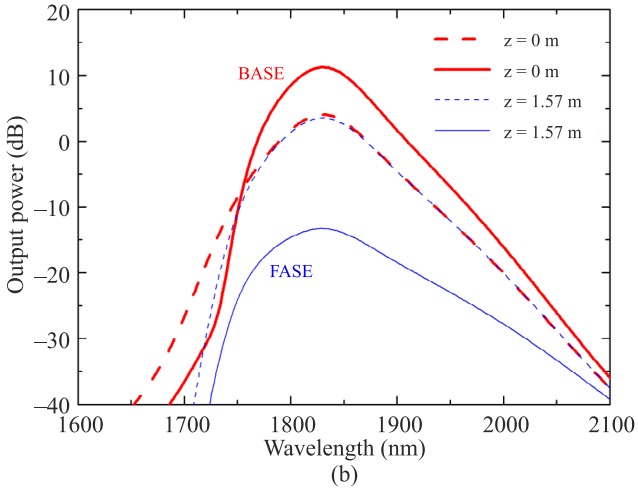

Fig. 3. (a) Output ASE power and (b) output ASE spectra.

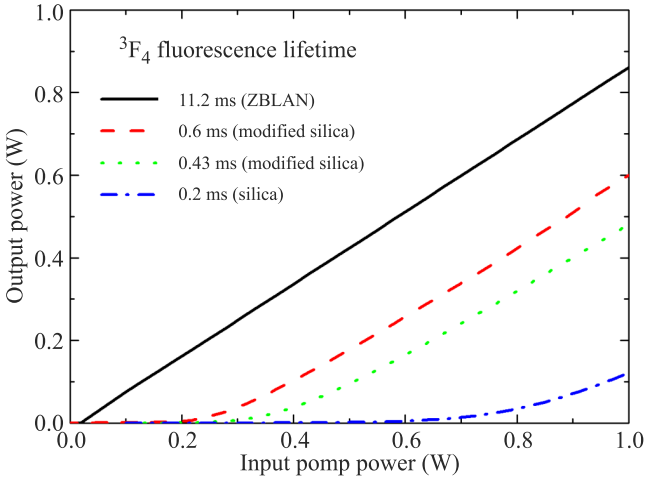

Fig. 4. Effect of fluorescence lifetime of the $^3F_4$ level on the output characteristics.

almost no effect on the slope. These trends are similar to the case of two-level fibre lasers where analytical expressions for the slope and threshold can be derived analytically [40]. The materials with low-phonon energy, like in the case of fluoride glass ZBLAN, are known for an excellent quantum conversion efficiency of almost 100% of the radiative transitions form the $^3F_4$ level. But fluoride fibres suffer from hygroscopicity, high cost and it is difficult to splice them with conventional silica fibres. On the other hand, silica-host materials pose higher phonon energy. Therefore, the quantum conversion efficiency is significantly lower, e.g., about 10% for the pure silica host. Figure 4 points out the importance of hosts with longer metastable levels of thulium for low- and medium- power applications like the broadband sources studied in this paper. TDFs with enhanced $^3F_4$ lifetimes of 400–700 μs have been reported in modified silica glasses [16]. A promising way to enhance the fluorescence lifetime is to modify locally thulium environment by the ceramic nanoparticle doping and MCVD methods [41–44].

The broadband sources are not being optimized only in terms of an output power but also in terms of the ASE output spectrum. Typically, the flat or Gaussian shapes are required for component characterization and optical coherent tomography systems; or one may require such a spectrum that balances the responsivity of the detector used [26,29]. In the following we present numerical optimization of the spectral shape of a band-stop filter in the setup in Fig. 1 in order to get the widest flat spectrum of the ASE source. We adopted an approach similar to the one presented earlier by Paschotta *et al*. [45] where the double-pass ytterbium-doped fibre ASE source is equipped at one end of the ytterbium-doped fibre with a bulk-grating-based filter and a mirror. In this method, the FASE output was collimated and sent to the mirror through a pair of gratings to disperse spatially the FASE spectrum. The dispersed spectrum traversed a mechanical comb made by a set of screws that protrudes the beam. The filter spectral shape can be finely tuned by a screwdriver; the higher protrusion of the screw into the beam, the higher the attenuation at the wavelength corresponding to that screw. On the contrary in our study, we use all-fibre components for spectral filtering so that the filter would be made by a combination of specially designed wavelength division multiplexer [18] and a mirror; by cascade of long-period fibre gratings [46]; or by a thin-film dichroic filter deposited on the perpendicularly cleaved fibre end, see Fig. 1. We tested the applicability of this approach in a TDF ASE source by means of a numerical model. The optimal spectral shape of the filter was searched iteratively. Starting shape mimics that of the emission spectrum and it is gradually modified unless the change of the full-width at half maximum of the output spectrum is less than a pre-set value. Examples of iterative steps are shown in Fig. 5, as well as the corresponding FWHM and output power values. The output spectra of the

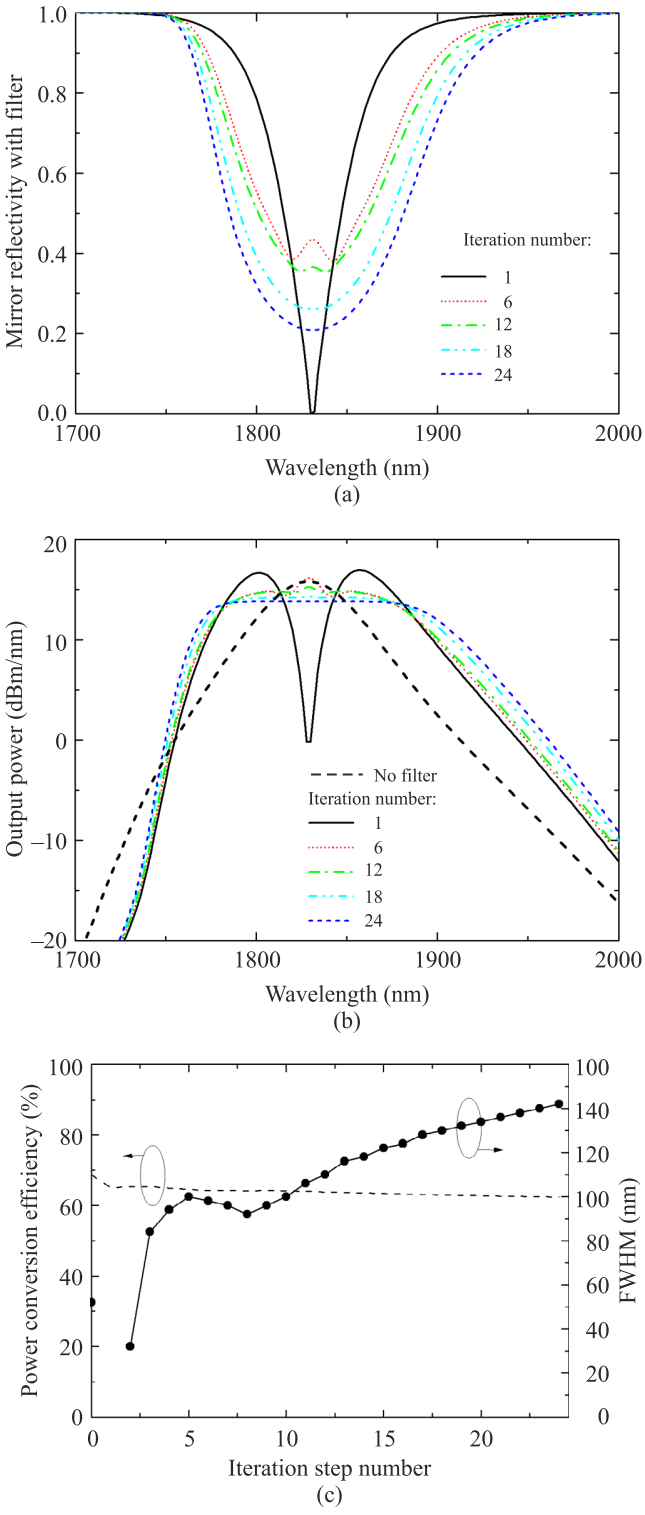

Fig. 5. (a) Reflectivities of the mirror with the preceding filter; and (b) the corresponding ASE spectra for several iteration-step examples of the iterative search of the optimal spectral shape of the filter. The ASE spectrum for the mirror without filter is shown for comparison. (c) Power conversion efficiency and spectral width of the output ASE spectrum with respect to the iteration step.

ASE source with and without filter are compared in Fig. 5(b). The FWHM can be broadened from 55 nm for the case without filter to more than 140 nm for the optimized filter shape. It means that the FWHM can be more than doubled at the expense of only little decrease of the output power.

3. Tm-doped fibre characteristics and performance in a ring-laser broadband ASE source

The thulium-doped preform was fabricated in house by using the MCVD (Modified Chemical Vapour Deposition) and solution doping methods. The fibre of 125 μm outer diameter was drawn from the preform. The fibre core had approximately step-index profile with a diameter of 7 μm and a numerical aperture of 0.17. The concentration profile of thulium followed that of the core refractive-index. Spectral shape of the $^3F_4$ level ground state absorption measured by cut-back method is shown in Fig. 6(a). The background losses were less than 0.1 dB/m. The attenuation due to absorption of Tm^{3+} ions is given by the product 4.34 $\Gamma\sigma_a(\lambda)$ N^{Tm} where Γ is the overlap factor accounting for the overlap of the guided optical mode with thulium ions. Overlap factor Γ can be calculated using the known refractive index and concentration profiles [39] and is of 0.95 at 1650 nm. Using the cross section at the peak ground state absorption of the $^3F_4$ level σ_a(1650 nm) = 4.4×10^{-25} m^2 [37] we determined that the thulium concentration was 6.3×10^{25} m^{-3}. It is about 1500 ppm mol Tm^{3+} assuming the density of the alumina-silicate core of 2.2 g/cm^3 [47]. The $^3F_4$ lifetime of 480 μs was determined from the fluorescence decay measurements. The normalized emission of the thulium-doped fibre is also shown in Fig. 6(a). The emission was measured in backward direction with respect to the pump at 1620 nm and using the WDM 1.6/2.0 μm. Note that the increased noise in the blue edge of the emission spectrum is due to the correction to the WDM 1600/2000 nm spectral transmission used in the measurement setup. Minimum WDM transmission was at 1610 nm. The spectral ripples in the emission spectrum in the interval of 1810–1930 nm were caused by water vapour absorption within the spectrum analyser, i.e., these ripples are not inherent to the TDF emission.

Fibre performance was tested in a ring laser cavity shown in the inset of Fig. 6(b). Length of the fibre was 1.8 m. In the setup we used the fused fibre components, i.e., the WDMs and the output coupler that were developed within a project EYESAFE2u sponsored by the Ministry of Industry and Trade of the Czech Republic (project No. FR-TI4/734). The fused fibre components fabrication and characteristics are described in detail elsewhere [18]. The laser output characteristics we measured for 90% and 10% output coupling, see

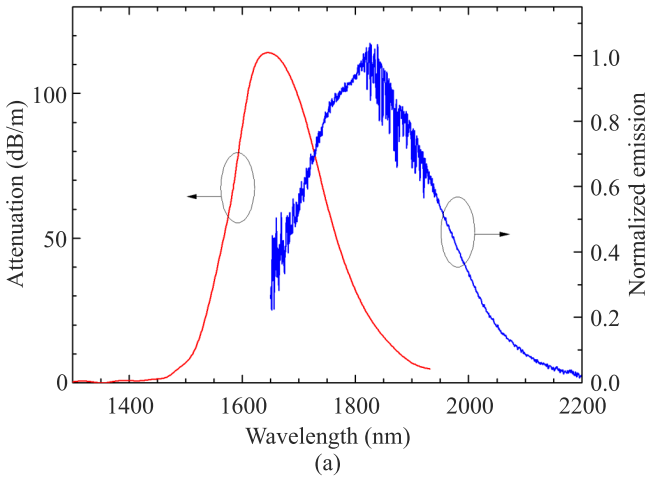

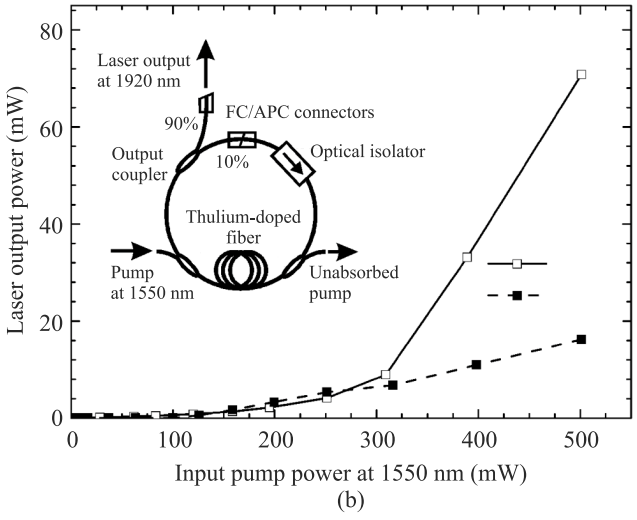

Fig. 6. (a) Absorption and emission spectra of the developed TDF. (b) Laser output characteristics for 90% and 10% output coupling. Experimental setup of the ring fibre laser is in the inset.

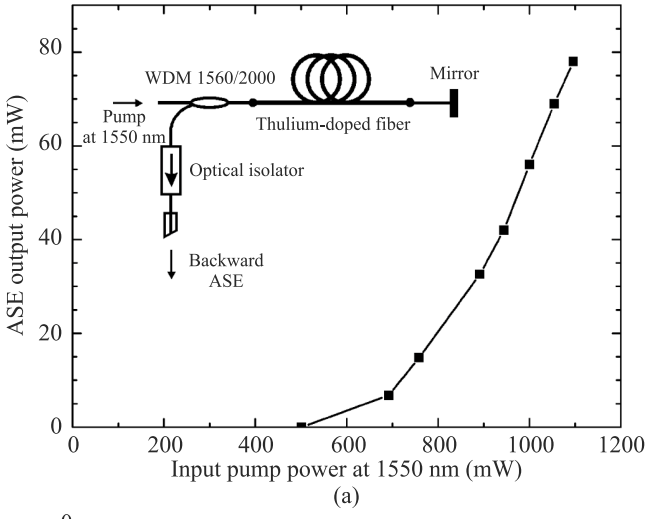

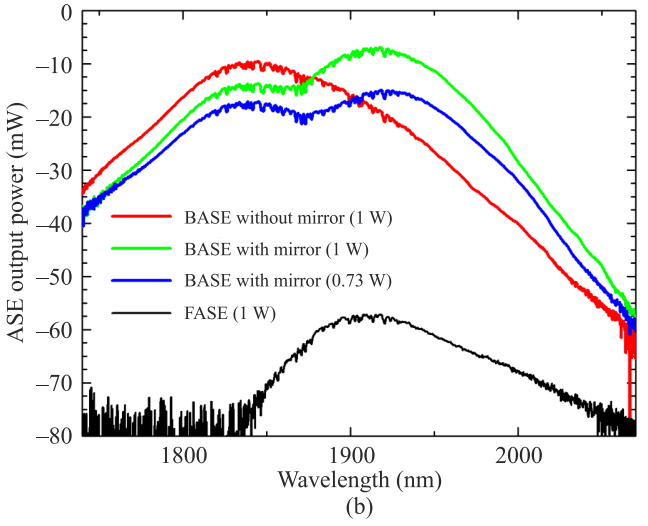

Fig. 7. (a) ASE output power *vs*. input pump power at 1550 nm. ASE source setup is shown in the inset. (b) Output spectra of the experimental TDF ASE source of various configurations and pump powers.

Fig. 6(b). The laser threshold of 170 and 290 mW and the slope efficiency of 32 and 4.4 % were found for the 90% and 10% output coupling, respectively. The higher slope efficiency was found for the case of higher output coupling as expected. Nevertheless, the slope efficiency is lower than the value of about 80% imposed by the quantum defect that is given by the ratio of the pump and the laser signal wavelength. This is mainly attributed to the insertion losses of the components used in the setup. Indeed, the overall insertion losses in the setup were estimated as high as 2 dB. Despite higher cavity losses and resulting lower slope efficiency, the ring-laser setup has an advantage of better stability thank to unidirectional propagation of the laser signal. In addition, the Tm^{3+} concentration is high enough to promote the cooperative upconversion to a $^3H_4$ level that would lead also to decrease of the laser slope efficiency.

The broadband ASE source was tested in the setup shown in the inset of Fig. 7(a). The fibre length was 3 m. The output power of the ASE source *vs*. the input pump power at 1550 nm is shown in Fig. 7(a). The output spectra for the pump powers of 0.73 and 1 W are shown in Fig. 7(b), as well as spectra of the backward and forward ASE when the mirror is removed from the setup. For the pump power level of 1 W, the peak wavelength, the 3-dB and 10-dB spectral widths of the double-pass arrangement were 1915 nm, 66 nm and 157 nm; while for the single-pass arrangement the corresponding values were 1842 nm, 60 nm, and 129 nm, respectively. Although no special spectral filter was used, the ASE spectrum was wider compared to the setup without mirror. It should be noted that most typical case is that double-pass ASE source built by the attachment of the mirror at one of

the fibre ends has opposite effect. The double-pass configuration leads to higher output power, but a narrower spectrum. It means that by proper selection of the pump power and fibre length one can optimize the width of the broadband source. Note that in our case the mirror promoted the longer-wavelength edge peak defined by the reflected FASE seed. The spectral shape of the FASE is shifted towards shorter wavelengths than the corresponding part of the ASE spectrum with attached mirror. This is an evidence of further reabsorption of the ASE seed (reflected by the mirror) in the depleted part of the thulium-doped fibre. The depleted section of the fibre and its length shaped the output ASE spectrum. The effect of ASE spectrum widening by combination of two distinct ASE peaks is somewhat similar to the widening of the ASE spectrum of ytterbium-doped double-clad fibres [29]. In contrast to the case described in our paper, the ytterbium ASE source was a single pass broadband source, i.e., without mirror, and the two distinct spectral peaks corresponded to typical ytterbium fibre laser wavelength regions around 1030 nm and 1070 nm.

4. Conclusions

We have described two methods of increasing the bandwidth of ASE source based on TDFs. Firstly, we have shown by means of the comprehensive numerical model that the FWHM of the ASE source can be more than doubled by using specially tailored spectral filter placed in front of the mirror in a double-pass configuration of ASE source. To our knowledge, it is the first report on numerical optimization of TDF ASE sources. Secondly, we reported initial results of experimental TDF ASE source, including fibre characteristics and performance of the TDF in fibre ring laser. We observed a counter-intuitive effect in the experimental ASE source that the spectrum in a double-pass configuration is broader than the spectrum of a single-pass ASE source. The broadening can be explained by the combination of shorter wavelength spectral peak of BASE and longer wavelength peak of the reflected FASE seed. By the proper combination of pump power and fibre length the two peaks may be set to similar optical powers and, in result, the output spectrum is broadened. The experimental and numerical optimization of the second approach is beyond the scope of this paper and it is a prospect of future work. It should be noted that numerical optimization of such device will require accurate spectroscopic characterization of the actual TDF, including absorption and emission cross-section spectra.

The TDF ASE sources offer higher stability and lower complexity and costs compared to other broadband sources, namely the supercontinuum sources that are based on ultrafast, quasi-continuous lasers with spectrum broadened in highly nonlinear fibre. Thus, the TDF ASE sources can substitute the SC sources in applications around 2 μm.

Acknowledgements

The authors thank Simon Hutchinson for careful reading of the manuscripts and his helpful comments. The authors acknowledge the company SQS Fibre Optics, Czech Republic, for cooperation in the development of fused fibre components for the spectral region around 2 μm. The research was supported by the Agency for Healthcare Research of the Czech Republic, under project No. 15-33459A.

References

1. B. Jean and T. Bende, "Mid-IR laser applications in medicine", in: *Solid-State Mid-Infrared Laser Sources*. pp. 530–565, Springer-Verlag, Berlin, 2003.
2. M. Grasso, "Experience with the holmium laser as an endoscopic lithotrite", *Urology* **48**, 199–206 (1996).
3. A. Sciarra, M. von Heland, F. Minisola, S. Salciccia, S. Cattarino, and V. Gentile, "Thulium laser supported nephron sparing surgery for renal cell carcinoma", *J. Urol.* **190**, 698–701 (2013).
4. Z.Q. Zhao and P.W. Fairchild, "Dependence of light transmission through human skin on incident beam diameter at different wavelengths", in Laser-Tissue Interaction IX, J. Lotz; S.L. Jacques, Editors, *Proc. SPIE* **3254**, 354–360 (1998).
5. A.Z. Thomas, L. Smyth, D. Hennessey, F. O'Kelly, D. Moran, and T.H. Lynch, "Zero ischemia laparoscopic partial thulium laser nephrectomy", *J. Endourol.* **27**, 1366–1370 (2013).
6. C.L. Tsai, J.C. Chen, and W.J. Wang, "Near-infrared absorption property of biological soft tissue constituents", *J. Med. Biol. Eng.* **21**, 7–14 (2001).
7. J. Kwiatkowski, "Highly efficient high power CW and Q-switched Ho:YLF laser", *Opto-Electron. Rev.* **23**, 165–171 (2015).
8. J. Sotor, M. Pawliszewska, G. Sobon, P. Kaczmarek, A. Przewolka, I. Pasternak, J. Cajzl, P. Peterka, P. Honzatko, I. Kasik, W. Strupinski, and K. Abramski, "All-fibre Ho-doped mode-locked oscillator based on graphene saturable absorber", *Opt. Lett*., **41**, 2592–2595 (2016).
9. L. Nagli, O. Gayer, and A. Katzir, "Middle-infrared luminescence of praseodymium ions in silver halide crystals and fibres", *Opt. Lett.* **30**, 1831–1833 (2005).
10. D. Sliwinska, P. Kaczmarek, and K.M. Abramski, "Pump and signal power combiners for high-power fibre amplifier applications", *Photonics Lett. of Poland* **7**, 29–31 (2015).
11. D. Stachowiak, P. Kaczmarek, and K. M. Abramski, "High--power pump combiners for Tm-doped fibre lasers", *Opto--Electron. Rev.* **23**, 259–267 (2015).
12. P. Koška, Y. Baravets, P. Peterka, J. Bohata, and M. Pisarik, "Mode-field adapter for tapered-fibre-bundle signal and pump combiners", *Appl. Opt.* **54**, 751–756 (2015).
13. J. Swiderski, M. Michalska, C. Kieleck, M. Eichhorn, and G. Maze, "High power supercontinuum generation in fluoride fibres pumped by 2 μm pulses", *IEEE Photonics Technol. Lett.* **26**, 150–153 (2014).

14. Z. Liu, Y. Chen, Z. Li, B. Kelly, R. Phelan, J. O'Carroll, T. Bradley, J.P. Wooler, N.V. Wheeler, A.M. Heidt, T. Richter, C. Schubert, M. Becker, F. Poletti, M.N. Petrovich, S. Alam, D.J. Richardson, and R. Slavík, "High-Capacity Directly Modulated Optical Transmitter for 2-μm Spectral Region", *J. Lightwave Technol.* **33**, 1373–1379 (2015).
15. P. Honzatko, Y. Baravets, F. Todorov, P. Peterka, and M. Becker, "Coherently combined 20 W at 2000 nm from a pair of thulium-doped fibre lasers", *Las. Phys. Lett.* **10**, 095104 (5pp) (2013).
16. P. Peterka, P. Honzátko, I. Kašík, O. Podrazký, F. Todorov, J. Cajzl, P. Koška, Y. Baravets, J. Aubrecht, and J. Mrázek, "Thulium-doped fibres and fibre-optic components for fibre lasers at around 2 μm", *Fine Mechanics and Optics* **60**, 174–177 (2015).
17. I. Kašík, P. Honzátko, P. Peterka, J. Mrázek, O. Podrazký, J. Aubrecht, J. Proboštová, J. Cajzl, and F. Todorov, "Special optical fibres – heart of thulium and holmium fibre lasers and amplifiers", *Fine Mechanics and Optics* **60**, 4–7 (2015). (IN CZECH)
18. M. Písařík, P. Peterka, S. Zvánovec, Y. Baravets, F. Todorov, I. Kašík, and P. Honzátko, "Fused fibre components for "eye--safe" spectral region around 2 μm", *Opt. Quant. Electron.* **46**, 603–611 (2014).
19. A.B. Seddon, " Mid-infrared (IR) – A hot topic: The potential for using mid-IR light for non-invasive early detection of skin cancer in vivo", *Physica Status Solidi (B)* **250**, 1020–1027 (2013).
20. K. Oh, A. Kilian, P.M. Weber, L. Reinhart, Q. Zhang, and T.F. Morse, "Broadband superfluorescent emission of the $^3H_4 \rightarrow {}^3H_6$ transition in a Tm-doped multicomponent silicate fibre", *Opt. Lett.* **19**, 1131–1133 (1994).
21. R.M. Percival, D. Szebesta, C.P. Seltzer, S.D. Perin, S.T. Davey, and M. Louka, "A 1.6-μm pumped 1.9-μm thulium--doped fluoride fibre laser and amplifier of very high efficiency", *IEEE J. Quantum Electron*. **31**, 489–493 (1995).
22. A. Halder, M.C. Paul, S.W. Harun, S.M.M. Ali, N. Saidin, S.S.A. Damanhuri, H. Ahmad, S. Das, M. Pal, S.K. Bhadra, "1880-nm broadband ASE generation with bismuth-thulium co-doped fibre", *IEEE Photonics J.* **4**, 2176–2181 (2012).
23. A. Halder, M.C. Paul, N.S. Shahabuddin, S.W. Harun, N. Saidin, S.S.A. Damanhuri, H. Ahmad, S. Das, M. Pal, S.K. Bhadra, "Wideband spectrum-sliced ASE source operating at 1900-nm region based on a double-clad ytterbium-sensitized thulium-doped fibre", *IEEE Photonics Journal* **4**, 14–18 (2012).
24. J. Zmojda, D. Dorosz, M. Kochanowicz, and J. Dorosz, "Active glasses as the luminescent sources of radiation for sensor applications", *Bull. Pol. Acad. Sci.-Tech. Sci.* **62**, 393–397 (2014).
25. J. Zmojda, M. Kochanowicz, P. Miluski, J. Dorosz, J. Pisarska,W.A. Pisarski, and D. Dorosz, "Investigation of up-conversion luminescence in antimony–germanate double--clad two cores optical fibre co-doped with Yb^{3+}/Tm^{3+} and Yb^{3+}/Ho^{3+} ions", *J. Luminescence* **170**, 795–800 (2016).
26. P. Honzatko, Y. Baravets, I. Kasik, and O. Podrazky, "Wideband thulium–holmium-doped fibre source with combined forward and backward amplified spontaneous emission at 1600–2300 nm spectral band", *Opt. Lett.* **39**, 3650–3653 (2014).
27. J.M. Sousa, M. Melo, L.A. Ferreira, J.R. Salcedo, and M.O. Berendt, "Product design issues relating to rare-earth doped fibre ring lasers and superfluorescence sources", *Proc. SPIE* **6102**, 610223 (2006).
28. I. Trifanov, P. Caldas, L. Neagu, R. Romero, M.O. Berendt, J.A.R. Salcedo, A.G. Podoleanu, and A.B. Lobo Ribeiro, "Combined Neodymium – Ytterbium-doped ASE fibre-optic source for optical coherence tomography applications", *IEEE Photonics Technol. Lett.* **23**, 21–23 (2011).
29. P. Peterka, F. Todorov, I. Kasik, V. Matejec, O. Podrazky, L. Sasek, G. Mallmann, and R. Schmitt, "Wideband and high-power light sources for in-line interferometric diagnostics of laser structuring systems", *Proc. SPIE* **8697**, 869718 (2012).
30. Q. Wang, J. Geng, T. Luo, and S. Jiang, "2 μm mode-locked fibre lasers [Invited]", *Proc. SPIE* **8237**, 82371N (2012).
31. Y.H. Tsang, A.F. El-Sherif, and T.A. King, " Broadband amplified spontaneous emission fibre source near 2 μm using resonant in-band pumping", *J. Modern Optics* **52**, 109–118 (2005).
32. Y.H. Tsang, T.A. King, D.-K. Ko, and J. Lee, "Broadband amplified spontaneous emission double-clad fibre source with central wavelengths near 2 μm", *J. Modern Optics* **53**, 991–1001 (2006).
33. D.Y. Shen, L. Pearson, P. Wang, J.K. Sahu, and W.A. Clarkson, "Broadband Tm-doped superfluorescent fibre source with 11 W single-ended output power", *Opt. Express* **16**, 11021–11026 (2008).
34. J. Liu and P. Wang, "High-power broadband Thulium-doped all-fibre superfluorescent source at 2 μm", *IEEE Photonics Technol. Lett.* **25**, 242–245 (2013).
35. G.-Y. Yu, J. Chang, Q.-P. Wang, X.-Y. Zhang, Z. Liu, Q.-J. Huang, "A theoretical model of thulium-doped silica fibre's ASE in the 1900 nm waveband", *Optoelectron. Lett.* **6**, 45–47 (2010).
36. M. Gorjan, T. North, and M. Rochette, "Model of the amplified spontaneous emission generation in thulium-doped silica fibres", *J. Opt. Soc. Am. B* **29**, 2886–2890 (2012).
37. P. Peterka, I. Kasik, A. Dhar, B. Dussardier, and W. Blanc, "Theoretical modelling of fibre laser at 810 nm based on thulium-doped silica fibres with enhanced $^3H_4$ level lifetime", *Opt. Express* **19**, 2773–2781 (2011).
38. P. Peterka, I. Kasik, V. Matejec, W. Blanc, B. Faure, B. Dussardier, G. Monnom and V. Kubecek, "Thulium-doped silica-based optical fibres for cladding-pumped fibre amplifiers", *Opt. Mat.* **30**, 174–176 (2007).
39. P. Peterka, B. Faure, W. Blanc, M. Karasek, and B. Dussardier, "Theoretical modelling of S-band thulium-doped silica fibre amplifiers", *Opt. Quant. Electron.* **36**, 201–212 (2004).
40. J. Chen, X. Zhu, and W Sibbett, "Rate-equation studies of erbium-doped fibre lasers with common pump and laser energy bands", *J. Opt. Soc. Am. B* **9**, 1876–1882 (1992).
41. O. Podrazký, I. Kašík, M. Pospíšilová, and V.Matμjec, "Use of alumina nanoparticles for preparation of erbium-doped

fibres", *IEEE Proc*. 20th Annual Meeting of the IEE LEOS, pp. 246–247, Lake Buena Vista, Florida, 2007.
42. D. Boivin, T. Föhn, E. Burov, A. Pastouret, C. Gonnet, O. Cavani, C. Collet, and S. Lempereur, "Quenching investigation on new erbium doped fibres using MCVD nanoparticle doping process", *Proc. SPIE* **7580**, 75802B, (2010).
43. W. Blanc and B. Dussardier, "Formation and applications of nanoparticles in silica optical fibres", *J. Optics* (India) **45**, 247–254 (2016).
44. I. Kasik, O. Podrazky, J. Mrazek, J. Cajzl, J. Aubrecht, J. Probostova, P. Peterka, P. Honzatko, and A. Dhar, "Erbium and Al_2O_3 nanocrystals-doped silica optical fibres", *Bull. Pol. Acad. Sci.-Tech. Sci.* **62**, 641–646 (2014).
45. R. Paschotta, J. Nilsson, A.C. Tropper, and D.C. Hanna, "Efficient superfluorescent light sources with broad bandwidth," *IEEE J. of Selected Topics in Quantum Electronics* **3**, 1097–1099 (1997).
46. P. Peterka, J. Maria, B. Dussardier, R. Slavik, P. Honzatko, and V. Kubecek, "Long-period fibre grating as wavelength selective element in double-clad Yb-doped fibre-ring lasers", *Laser Phys. Lett.* **6**, 732–736 (2009).
47. P. Koška, P. Peterka, J. Aubrecht, O. Podrazký, F. Todorov, M. Becker, Y. Baravets, P. Honzátko, and I. Kašík, "Enhanced pump absorption efficiency in coiled and twisted double-clad thulium-doped fibres", *Opt. Express* **24**, 102–107 (2016).

5. Conclusions

5.1 Contribution of the dissertation

This thesis provides insight into the methodology for design of key components leading towards stable 2 μm-high-power fiber lasers and amplifiers [A1, A2], novel fiber laser design [A3] and new 2 μm-sources for medical and industrial applications [A4]. In addition to articles targeting dissertation goals, it includes published articles on fiber optics and laser sources for sensing [A5,A7] and stability, and the reliability of laser sources in avionics and harsh environments [A6]. All works focus on high-power laser applications and the reliability of important laser sources for medicine, the avionics industry and high-power pulse laser sources which will be confirmed.

Certain aspects of my work deal with a fiber matrix design and measurements, as well as fiber lasers end-cap processing which is used in the European X-CAN project I participated in.

5.2 Future directions

I would like to continue in further experimental realizations of diode-pumped high-pulse energy solid-state lasers and fiber lasers, power amplifiers suitable for free space communication and high-energy lasers in the field of eye-safety.

At the HiLASE center, Institute of Physics of the CAS, where I am currently employed and which is in close cooperation with Institute of Photonics and Electronics CAS, I would like to develop high-pulse energy fiber delivery for a 1 to 100J-short and ultrashort pulse laser system which goes beyond single-fiber capacity to transfer metallic nanoparticles for lasing and modulation, and the implementation of 100W-fiber lasers for thin disk pumping of high energy lasers for industrial, medical and safety applications.

A tandem pumped layout is ideal for high-power Ho^{3+} fiber laser which could be important for ground-to-satellite and satellite-to-satellite optical communications because they emit in an atmosphere communication spectral window around 2.17 μm as described in chapter 2.1. A significant risk for NASA requirements is the absence of a high-power modulator. Multiple amplification and signal regeneration is reducing a possible modulation frequency. Transparent materials with oriented nanoparticles could be a possible way how to solve this problem. With the Institute of Chemistry at Prague and the Czech Technical University I would like to continue to transfer promising results from experiments to a final application.

6. References

[1] Maiman T., “Stimulated optical radiation in ruby,” Nature 187 (4736): 493–94. Bibcode:1960Natur.187..493M. doi:10.1038/187493a0 (August 6, 1960)..

[2] Snitzer E., "Optial MASER action of Nd+3 in a barium crown glass," Physical Review Letters, Volume 7, Number 12, pp. 444-446, December 15, 1961.

[3] Desurvire E., Simpson J.R., Becker P.C., “High-gain erbium-doped traveling-wave fiber amplifier,” Optics letters, Vol. 12, No. 11, November 1987.

[4] Gapontsev V. et al, U.S. Patent, No. 5,999,673, filed Dec. 28, 1994; Proc. CLEO 1996, 9, Anaheim (1996).

[5] Heidt A. M., Li Z., Sahu J., Shardlow P. C., Becker M., Rothhardt M., Ibsen M., Phelan R., Kelly B., Alam S. U., Richardson, D. J., “100 kW peak power picosecond thulium-doped fiber amplifier system seeded by a gain-switched diode laser at 2 μm,” Opt. Lett. 38, 1615-617 (2013)

[6] Jackson S. D., “Towards high-power mid-infrared emission from a fibre laser,” Nature Photonics 6, 423–431 (2012)

[7] Richardson D. J., Nilsson J., Clarkson W. A., “High power fiber lasers: current status and future perspectives [Invited],” J. Opt. Soc. Am. B 27, B63-B92 (2010)

[8] Nařízení vlády ze dne 12. prosince 2007 o ochraně zdraví před neionizujícím zářením, Sbírka zákonů č. 1/2008.

[9] Peterka P., Kanka J., “Erbium-doped twin-core fibre narrow-band filter for fibre lasers,” Opt. and Quantum Electron. 33, 571-581 (2001)

[10] Ehrenreich T., et al. "1-kW, all-glass Tm: fiber laser." Proc. SPIE. Vol. 7580. 2010.

[11] Clarkson W. A., Barnes N. P., Turner P. W., Nilsson J., Hanna D. C., "High-power cladding-pumped Tm-doped silica fiber laser with wavelength tuning from 1860 to 2090 nm," Optics Letters, Vol. 27, Issue 22, pp. 1989-1991 (2002)

[12] Kulkarni O. P., Alexander V.V., Kumar M., Freeman M. J., Islam M. N., Terry Jr. F. L., Neelakandan M., Chan A., “Supercontinuum generation from ~1.9 to 4.5 μm in ZBLAN fiber with high average power generation beyond 3.8 μm using a thulium-doped fiber amplifier,” J. Opt. Soc. Am. B **28**, 2486-2498 (2011)

[13] Noell W. K., Walker V. S., Kang B. S., Berman S., “Retinal damage by light in rats,” Investigative Ophthalmology & Visual Science, 5(5), 450-473(1966).

[14] Edwards B. L., et al. "Overview of the laser communications relay demonstration project." Proceedings of SpaceOps. Vol. 1261897. (2012).

[15] Boroson D. M., et al. "Overview and results of the lunar laser communication demonstration." SPIE LASE. International Society for Optics and Photonics, (2014).

[16] Grasso M., Caruso R., “Lasers in Urology,” Textbook of Surgery, eMedicine, February 2000

[17] Grasso M., “Experience with the holmium laser as an endoscopic lithotrite,” Urology. 1996 Aug. 48(2):199-206.

[18] Sciarra A., Von Heland M., Minisola F., Salciccia S., Cattarino S., Gentile V., “Thulium laser supported nephron sparing surgery for renal cell carcinoma,” J Urol. 2013 Jan 29.

[19] Wollin T. A., Denstedt J. D., “The holmium laser in urology,” Journal of Clinical Laser Medicine & Surgery. FEB 1998: 13-20

[20] Thomas A.Z., Smyth L., Hennessey D., O'Kelly F., Moran D., Lynch T.H., “Zero ischemia laparoscopic partial thulium laser nephrectomy,” J Endourol. 2013 Mar 8.

[21] John Y., Fitzgerald F., "Politics as law?: The anti-ballistic missile treaty, the separation of powers, and treaty interpretation." (2001): 851-915.

[22] Coffey V., "High-energy lasers: new advances in defense applications." Optics and Photonics News 25.10 (2014): 28-35.

[23] Staton R., Pawlak R., “Laser weapon system (LAWS) adjunct to the close-in weapon system (CIWS),” Naval surface warfare center Dahlgren DIV VA, 2012.

[24] Protz R., et al. "High-power beam combining: a step to a future laser weapon system." SPIE Security+ Defence. International Society for Optics and Photonics, 2012.

[25] Brocklesby W. S., et al. "ICAN as a new laser paradigm for high energy, high average power femtosecond pulses." The European Physical Journal Special Topics 223.6 (2014): 1189-1195.

[26] Shen D. Y., Pearson L., Wang P., Sahu J. K., Clarkson W. A., "Broadband Tm-doped superfluorescent fiber source with 11 W single-ended output power," Opt. Express 16, 11021 (2008).

[26] Bulgakova N.M., Panchenko A.N., Zhukov V.P., Kudryashov S.I., Pereira A., Marine W., Mocek T., Bulgakov A.V., “Impacts of Ambient and Ablation Plasmas on Short- and Ultrashort-Pulse Laser Processing of Surfaces,” Micromachines 2014, 5, 1344-1372.

[27] Digonnet M.J.F., “Rare-Earth-Doped Fiber Lasers and Amplifiers”, Second edition, ISBN 0-8247-0458-4

[28] Clarkson W. A., et al. “High-power cladding-pumped Tm-doped silica fiber laser with wavelength tuning from 1860 to 2090 nm,” Opt. Lett. 27,1989–1991 (2002).

[29] Jackson S. D., “Cross relaxation and energy transfer upconversion processes relevant to the functioning of 2 µm Tm3+-doped silica fibre lasers,” Opt. Commun. 230, 197–203 (2004).

[30] Schneider J., Carbonnier C., Unrau U. B., “Characterization of a Ho3+-doped fluoride fiber laser with a 3.9 µm emission wavelength,” Appl. Opt. 36, 8595–8600 (1997).

[31] Faucher D., Bernier M., Caron N., Vallee R., “Erbium-doped all-fiber laser at 2.94 µm,” Opt. Lett. 34, 3313–3315 (2009).

[32] Li J., Jackson S. D., “Numerical modeling and optimization of diode pumped heavily-erbium-doped fluoride fiber lasers,” IEEE J. Quant. Electron. 48, 454–464 (2012).

[33] Yamamoto, T., Y. Miyajima, and T. Komukai. "1.9 µm Tm-doped silica fibre laser pumped at 1.57 µm." Electronics letters 30.3 (1994): 220-221.

[34] Jackson S. D., et al. “High-power 83 W holmium-doped silica fiber laser operating with high beam quality,” Opt. Lett. 32, 241–243 (2007).

[35] Hemming A. V., et al. “Development of resonantly cladding-pumped holmium-doped fibre lasers,” Proc. SPIE 8237, 82371J (2012).

[36] Hanna D.C., Percival R.M., Smart R.G., Townsend J.E., “Continuous-wave oscillation of holmium-doped silica fibre laser,” Electronics letter, Volume:25 Issue:9 (1989)

[37] Kao K. C., Hockham G. A., "Dielectric-fibre surface waveguides for optical frequencies," Proc. IEE 113 (7): 1151–1158. doi:10.1049/piee.1966.0189 (1966).

[38] Malinowski A., Piper A., Price J. H. V., He F., Ibsen M., Nilsson J., Richardson D. J., "Short pulse high power fiber laser systems," In (CLEO). Conference on Lasers and Electro-Optics, 2005. (Vol. 3, pp. 1647-1649). IEEE.

[39] Vanda, J., et. al., " Laser induced damage threshold of optical fibers under ns pulses", Proc. SPIE vol. 10014, 10014-30, (2016).

[40] Škoda V., Vanda J., "A study of ps-laser-induced-damage-threshold in hybrid metal-dielectric mirrors," Proc. SPIE 9237, Laser-Induced Damage in Optical Materials: 2014, 92372E (October 31, 2014); doi:10.1117/12.2068237.

[41) Wang J. S., Vogel E. M., Snitzer E., "Tellurite glass: a new candidate for fiber devices," Optical materials 3.3 (1994): 187-203.

[42] Athanasiou G. S., Bereś-Pawlik E., Semczuk G., Furniss D., Seddon A. B., Benson T. M., "Large core, multimode, chalcogenide glass fibre coupler by side-polishing," Opt. and Quant. Electron. 45, 961-967 (2013)

[43] Peterka P., *et al.*, "Monolithic thulium-doped fiber laser with UV femtosecond-laser-induced fiber-Bragg-grating pair," in *CLEO/Eur. EQEC Conf. Dig.*, May 2013, paper CJ-P.5.

[44] Kane T. J., and Byer R. L.. "Monolithic, unidirectional single-mode Nd: YAG ring laser." Optics Letters 10.2 (1985): 65-67.

[45] Zhang Z., Boyland A. J., Sahu J. K., Clarkson W. A., M. Ibsen, "High-power single-frequency thulium-doped fiber DBR laser at 1943 nm," IEEE Photon. Technol. Lett., vol. 23, no. 7, pp. 417–419,Apr. 1, 2011.

[46] Fan T. Y., "Efficient coupling of multiple diode laser arrays to an optical fiberbygeometricmultiplexing,"Appl.Opt.,vol.30,pp.630–632,1991.

[47] Gapontsev, V. P., L. E. Samartsev, "High-power fiber laser," Advanced Solid State Lasers 6 (1990): LSR1.

[48] Fan T. Y., "Efficient coupling of multiple diode laser arrays to an optical fiber by geometric multiplexing", Appl. Opt., vol. 30, pp. 630-632, 1991

[49] Kosterin A., Temyanko V., Fallahi M., Mansuripur M., "Tapered fiber bundles for combining high-power diode lasers", Appl. Opt., vol. 43, pp. 3893-3900, 2004

[50] Ross T.S., Latham W.P., "Appropriate measures and consistent standard for high energy laser beam quality," J. Directed Energy, vol. 2, pp. 22–58, 2006.

[51] Brooker G., "Modern Classical Optics," New York, NY, USA: Oxford Univ. Press, 2003.

[52] Bohme S., Fabian S., Schreiber T., Eberhardt R., Tunnermann A., "End cap splicing of photonic crystal fibers with outstanding quality for high power applications", Proc. SPIE, vol. 8244, 824406, 2012

[53] Gapontsev .P. Valentin, et al. "Coupling arrangement between a multi-mode light source and an optical fiber through an intermediate optical fiber length." US PAT 5999673, 1999

[54] MacChesney J. B., DiGiovanni D. J., "Materials development of optical fiber," Journal of the American Ceramic Society 73.12 (1990): 3537-3556.

[55] Nisoli, M., De Silvestri S., Svelto O., "Generation of high energy 10 fs pulses by a new pulse compression technique," Applied Physics Letters 68.20 (1996): 2793-2795.

[56] Sun Z., Hasan T., Torrisi F., Popa D., Privitera G., Wang, F., Ferrari A. C., “Graphene mode-locked ultrafast laser,” ACS nano, 4(2), 803-810 (2010).

[57] Washburn B. R., Diddams S. A., Newbury N. R., Nicholson J. W., Yan M. F., Jørgensen C. G., “Phase-locked, erbium-fiber-laser-based frequency comb in the near infrared,” Optics letters, 29(3), 250-252 (2004).

[58] Tamura K., Ippen E. P., Haus H. A., Nelson L. E., “77-fs pulse generation from a stretched-pulse mode-locked all-fiber ring laser,” Optics letters, 18(13), 1080-1082 (1993).

[59] Stokes L. F., Chodorow M., Shaw H. J., “All-fiber stimulated Brillouin ring laser with submilliwatt pump threshold,” Optics Letters, 1982, 7.10: 509-511.

[60] Bernier M., Vallée R., Morasse B., Desrosiers C., Saliminia A., Sheng Y., “Ytterbium fiber laser based on first-order fiber Bragg gratings written with 400nm femtosecond pulses and a phase-mask,” *Opt.Express*, vol. 17, no. 21, pp. 18887–18893, Oct. 2009.

[61] Wikszak E., *et al.*, “Linearly polarized ytterbium fiber laser based on intracore femtosecond-written fiber Bragg gratings,” *Opt. Lett.*, vol. 32, no. 18, pp. 2756–2758, Sep. 2007.

[62] Jovanovic N., Åslund M., Fuerbach A., Jackson S. D., Marshall G. D., Withford M. J., “Narrow linewidth, 100 W cw Yb3+-doped silica fiber laser with a point-by-point Bragg grating inscribed directly into the active core,” *Opt. Lett.*, vol. 32, no. 19, pp. 2804–2806, Oct. 2007.

[63] Zervas M. N., Codemard C. A., "High power fiber lasers: A review," IEEE J. Sel. Topics Quantum Electron. , vol. 20 , no. 5 , 2014.

[64] Lehmberg R. H., Obenschain S. P., “Use of Induced Spatial Incoherence for Uniform Illumination on Laser Fusion Targets,” No. NRL-MR-5029. NAVAL RESEARCH LAB WASHINGTON DC, 1983.

[65] Zhao Baoyin, et al. "Experimental study on high power all-fiber laser." Chinese Optics Letters 8.4 (2010): 404-406.

[66] He B., Lou Q., Zhou J., Dong J., Wei Y., Xue D., Qi Y., Su Z., Li L., Zhang F., "High power coherent beam combination from two fiber lasers," Optics express 14.7 (2006): 2721-2726.

[67] Nilsson J., Payne D.N., "High-power fiber lasers." Science 332.6032 (2011): 921-922.

[68] Hecht J., "Beam combining cranks up the power," Laser Focus World 48.6 (2012): 41-43.

[69] Shirakawa A., Saitou T., Sekiguchi T., Ueda K., "Coherent addition of fiber lasers by use of a fiber coupler," Opt. Express 10, 1167-1172 (2002).

[70] Honzatko P., Baravets Y., Todorov F., Peterka P., Becker M., “Coherently combined power of 20 W at 2000 nm from a pair of thulium-doped fiber lasers,” Laser Physics Letters, 10(9), 095104 (2013).

[71] Jones D. J., Diddams S. A., Ranka J. K., Stentz A., Windeler R. S., Hall J. L., Cundiff S. T., "Carrier-envelope phase control of femtosecond mode-locked lasers and direct optical frequency synthesis." Science 288.5466 (2000): 635-639.

[72] Augst S. J., Redmond S. M., Yu C. X., Ripin D. J., Fan T. Y., Goodno G. D., Thielen P. A., Rothenberg J. E., Sanchez-Rubio A., "Coherent and spectral beam combining of fiber lasers," Proc. SPIE, 8237, 823704 (2012).

[73] Jérémy L. D., Antier M., Bourderionnet J., Larat C., Lallier E., Heilmann A., Fsaifes I., Daniault L., Bellanger S., Simon-Boisson C., Chanteloup J., and Brignon A., "Coherent beam combining of 19 fibers in femtosecond regime," in Conference on Lasers and Electro-Optics, OSA Technical Digest (2016) (Optical Society of America, 2016), paper STu1M.1.

[74] Quinn M. N., Jukna V., Ebisuzaki T., Dicaire I., Soulard R., Summerer L., Couairon A., and Mourou G., “Space-based application of the CAN laser to LIDAR and orbital debris remediation,” EPJ ST 224(13), 2645–2655 (2015).

[75] Yu C.X., Augst S.J., Redmond S.M., Goldizen K.C., Murphy D.V., Sanchez A., Fan T.Y., "Coherent combining of a 4 kW, eight-element fiber amplifier array," Opt. Lett., 36, 2686 (2011).

[76] Daniault, L., et al. "XCAN—A coherent amplification network of femtosecond fiber chirped-pulse amplifiers," The European Physical Journal Special Topics 224.13 (2015): 2609-2613.

[77] Kawasaki, B. S., Hill, K. O., Lamont, R. G., “Biconical-taper single-mode fiber coupler,” Opt. Lett. 6, 327-328 (1981).

[78] Tekippe V. J., “Passive fiberoptic components made by the fused biconical taper process,” Fiber Integrated Opt. 9, 97-123 (1990).

[79] Pal B. P., Chaudhuri P. R., Shenoy M. R., “Fabrication and modeling of fused biconical tapered fiber couplers,” Fiber Integrated Opt. 22, 97-117 (2003).

[80] Abebe M., Villarruel C. A., Burns W. K., “Reproducible fabrication method for polarization preserving single-mode fiber couplers,” J. Lightwave Technol. 6, 1191-1198 (1988).

[81] Birks T. A., Li, Y. W., “The shape of fiber tapers,” J. Lightwave Technol. 10:432-438 (1992).

[82] Mortimore D. B., Arkwright J. W., “Theory and fabrication of wavelength flattened 1 × N single-mode couplers,” Appl. Opt. 29, 1814-1818 (1990).

[83] Bures J., Lacroix S.,Lapierre J., “Analyse d’un coupleur bidirectionnel à fibres optiques monomodes fusionnées,” Appl. Opt. 22, 1918-1922 (1983).

[84] Du C.H., Chiou Y.P., “Beam propagation analysis using higher-order full-vectorial finite-difference method,” Opt. Quantum Electron. 45, 769–774 (2013).

[85] Chiang K. S., “Finite-element analysis of optical fibres with iterative treatment of the infinite 2-D space,” Opt. Quantum Electron. 17, 381-391 (1985).

[86] Jiang J.A., Hsu T.Y., Liao W.B., Liu M.Y., “Development of miniature optical fiber hybrid WDM coupler employing the FBT technology,” Opt. Fiber Technol. 17, 568-573 (2011).

[87] Theeg T., Hausmann K., Frede M., Sayinc H., Neumann J., Kracht D., “High power fused single mode optical fiber coupler,” Conference on Lasers and Electro-Optics Europe and 12th European Quantum Electronics Conference, CLEO EUROPE/EQEC 2011, art. no. 5943141(2011)

[88] Xiao Q., Yan P., He J., Wang Y., Zhang X., Gong M., “Tapered fused fiber bundle coupler capable of 1 kW laser combining and 300 W laser splitting,” Laser Phys., 21, 1415-1419 (2011).

[89] Zhu B., Taunay T. F., Yan M. F., Fini J. M., Fishteyn M., Monberg E. M., Dimarcello F. V., “Seven-core multicore fiber transmissions for passive optical network,” Opt. Express 18, 11117-11122 (2010).

[90] Saitoh F., Saitoh K., Koshiba M., “A design method of a fiber-based mode multi/demultiplexer for mode-division multiplexing,” Opt. Express 18, 4709-4716 (2010).

[91] Pelegrina-Bonilla G., Hausmann K., Liu K., Sayinc H., Morgner U., Neumann J., Kracht D., “Matching of the propagation constants in an asymmetric single-mode fused fiber coupler for core pumping thulium-doped fiber at 795 nm,” Opt. Lett. 37, 1844-1846 (2012)

List of author's publications related to the doctoral thesis

All authors contributed equally, unless otherwise stated.

- Papers in Peer-Reviewed Journals with Impact Factor

[A1] Písařík M., Peterka P., Zvánovec S., Baravets Y., Todorov F., Kašík I., Honzátko P. "Fused fiber components for "eye-safe" spectral region around 2 μm." Optical and Quantum Electronics 46.4 (2014): 603-611.

[A2] Koška P., Baravets Y., Peterka P., Bohata J., Pisarik M. "Mode-field adapter for tapered-fiber-bundle signal and pump combiners." Applied optics 54.4 (2015): 751-756.

[A3] Peterka, P., Honzátko P., Becker M., Todorov F., Písařík M., Podrazký O., Kašík I. "Monolithic Tm-doped fiber laser at 1951 nm with deep-UV femtosecond-induced FBG pair." Photonics Technology Letters, IEEE 25.16 (2013): 1623-1625.

[A4] Písařík, M., Peterka P., Aubrecht J., Cajzl J., Benda A., Mareš D., Todorov F., Podrazký O., Honzátko P., Kašík I. „ Thulium-doped fibre broadband source for spectral region near 2 micrometers ." Opto-Electronics Review 10/2016; DOI:10.1515/oere-2016-0022

- Patents

[P1] Koška P., Peterka P., Písařík M., "Adaptor element of field profile of signal mergers and pumping, merger and optical device", CZ20140030429U 20141212

- Papers and Abstracts in Conference Proceedings Listed in the Web of Knowledge

[C1] Koška P., Baravets Y., Peterka P., Bohata J., Pisarik M. "Optimized mode-field adapter for low-loss fused fiber bundle signal and pump combiners." SPIE LASE. International Society for Optics and Photonics, 2015.

[C2] Peterka, P., Honzátko P., Becker M., Todorov F., Písařík M., Podrazký O., Kašík I. "Monolithic thulium-doped fiber laser with UV femtosecond-laser-induced fiber-Bragg-grating pair." 2013 Conference on Lasers & Electro-Optics Europe & International Quantum Electronics Conference CLEO EUROPE/IQEC. 2013.

- Citations in Web of Knowledge and SCOPUS¨

A2 cited at Stachowiak, D., P. Kaczmarek, and K. M. Abramski. "High-power pump combiners for Tm-doped fibre lasers." Opto-Electronics Review 23.4 (2015): 259-264.

A2 cited at Sliwinska, Dorota, Pawel Kaczmarek, and Krzysztof Marek Abramski. "Pump and signal power combiners for high-power fiber amplifiers applications." Photonics Letters of Poland 7.1 (2015): pp-29.

A3 cited at Fengping Y., et al. "Dual-wavelength single-longitudinal-mode Tm-doped fiber laser using PM-CMFBG." Photonics Technology Letters, IEEE 27.9 (2015): 951-954.

A3 cited at Bureau B., et al. "Conference 9507: Micro-structured and Specialty Optical Fibres." TECHNICAL SUMMARIES•: 76.

List of author's publications non-related to main topic of the doctoral thesis

All authors contributed equally, unless otherwise stated.

- Papers in Peer-Reviewed Journals with Impact Factor

[A5] Weinzettla V., Shuklaa G., Ghoshc J., Melicha R., Paneka R., Tomesa M., Imriseka M., Naydenkovaa D., Varjua J., Pereirae T., Gomese R., Abramovicg I., Jaspersg R., Pisarik M., Odstrcilj T., Oost G. V. "High-resolution spectroscopy diagnostics for measuring impurity ion temperature and velocity on the COMPASS tokamak." Fusion Engineering and Design 96 (2015): 1006-1011.

[A6] Bohata J., Pisarik M., Zvanovec S., Peterka P. "Reliability of aircraft multimode optical networks." Optical Engineering 53.9 (2014): 096102-096102.

[A7] Kopacek I.,, Pisarik M. "Monitoring/sensing applications on AirPON." SPIE Security+ Defence. International Society for Optics and Photonics, 2012.

- Patents

[P2] Komanec M., Škoda P., Libich J., Písařík M., Zvánovec S., "Polarization-independent optical packet change-over switch", CZ20130000861 20131107

[P3] Písařík M., Kopáček I., Černík L., "Plug-in dedvice for connecting optical and/or electronic connectors and the method for this connecting", CZ20130419, US9086549, EP2811326, licensed

- Papers and Abstracts in Conference Proceedings Listed in the Web of Knowledge

[C3] Bohata, J., Pisarik M., and Zvanovec S. "Testing of optical fiber components for harsh environmets." Avionics, Fiber-Optics and Photonics Conference (AVFOP), 2013 IEEE. IEEE, 2013.

[C4] Bohata, J., Zvanovec S., and Pisarik M. "Outdoor atmospheric influence on polarization mode dispersion in optical cables." General Assembly and Scientific Symposium (URSI GASS), 2014 XXXIth URSI. IEEE, 2014.

- Citations in Web of Knowledge and SCOPUS

A7 cited at Herrera, L. Y., G. C. Amaral, and J. P. von der Weid. "Ultra-High-Resolution Tunable PC-OTDR for PON Monitoring in Avionics." Optical Fiber Communications Conference and Exhibition (OFC), 2015. IEEE, 2015.

A7 cited in do Amaral, Gustavo C., Luis Y. Herrera, and Jean Pierre von der Weid. "Ultra-High-Resolution Tunable PC-OTDR for PON Monitoring in Avionics." Optical Fiber Communication Conference. Optical Society of America, 2015.

Curriculum Vitae

Co-Applicant: Michael Pisarik (*1979)

Work experience:

2004 – 2016 SQS Vláknová optika a.s., Komenského 304, 509 01 Nová Paka

2015 – Technology Agency of the Czech Republic, Evropská 1692/37,160 00 Praha 6

2016 – HiLASE centre, Institute of Physics v.v.i., Academy of Sciences of the Czech Republic, Za Radnicí 828, 252 41 Dolní Břežany

Education

Ing. (MSc): 2003, Faculty of Electrical Engineering, Czech Technical University (CTU) in Prague,

Unfinished education

Ph.D.: 2012- doctoral thesis under final revision, Faculty of Electrical Engineering – Department of Electromagnetic Field, Czech Technical University (CTU) in Prague, doctoral thesis “Rare-earth doped fiber lasers for close to mid IR”

Research activities

Resent research focuses on optical fibers, fiber lasers and amplifiers, optical sensors and technical limits of optical fibers.

Professional activities

2016 – Senior Research Engineer HiLASE centre, Institute of Physics, The Czech Academy of Sciences
2014 – 2016 Chief of Research SQS
2013 - 2014 Deputy CTO SQS
2006 – 2013 Project Managers SQS
2004 – 2006 Development specialists SQS

2014 – 2016 Chairman of the Supervisory board of the SQS
2010 – 2013 Vice-chairman of the Supervisory board of the SQS
2010 – 2011 Member of Industrial Council
2013 – Member of RVVI HK committee
2013 – Member of RIS3 council
2015 – Authorized Consultant for Photonics under Technology Agency CR

Awards:
2013, Award of Technology Agency of the Czech Republic for Most Novel Result
2014, Nominated by Ministry of Education of the Czech Republic on Eureka Innovation Award

Bibliographic data

Author and co-author of 4 patents, 7 impacted scientific journal papers, more than 20 conference papers.

List of successfully finished projects till 2016

Cooperates on projects for telecommunications, sensing, fiber lasers and amplifiers, optoelectronics, biomedical devices, public transport and smart grids.

FR-TI4/734 - Fiber-optic components for "eye-safe" spectral region around 2 μm (Ministry of Industry and Trade of the Czech Republic), 2012-1015, principal investigator, project partners SQS and Institute of Photonics and Electronics

FR-TI3/797 – Polymer planar components for telecommunication and sensing (Ministry of Industry nad Trade of the Czech Republic), 2011-2014, principal investigator, project partners SQS, Czech Technical University at Prague and University of Chemistry and Technology, Prague

LF11001 / E!5838 – Fiber optic gas sensing (Ministry of Education of the Czech Republic), 2011-2014, principal investigator, project partners SQS, Institute of Photonics and Electronics, Gooche and Housego UK, CiS Erfurt DE

TA01011105 – Optical packet switch (Technology Agency of the Czech Republic), 2011-2013, principal investigator, project partners SQS, Institute of Photonics and Electronics, Czech Technical University at Prague

FP7 DAPHNE – Development of Aircraft Photonic Network (EK), 2010-2013, member of team (SQS team leader) , project partners Airbus, AugustaWestlend Helicopters, EADS, BAE and 13 other members

Other projects

LF13015 – Fiber Optic UV Sensing (Ministry of Education of the Czech Republic), 2011-2014, principal investigator, project partners SQS, Institute of Photonics and Electronics, Gemicon South Korea, CiS Erfurt DE

TA03010060 – Fiber optic detection of liquids (Technology Agency of the Czech Republic), project members SQS and Czech Technical University at Prague

TA03020439 – Safety of optical critical infrastructure (Technology Agency of the Czech Republic), project partners SQS, T-Mobile, Sitel, Kabex, Technical University of Ostrava

TA04010220 – Supercontinuum source made on soft glass modules (Technology Agency of the Czech Republic), project members SQS and Czech Technical University at Prague

TA04011400 – Optical pH sensing modules (Technology Agency of the Czech Republic), project members Institute of Photonics and Electronics, SQS and Safibra

TA04021007 – Surface Enhanced Raman Scattering (Technology Agency of the Czech Republic), project members University of Chemistry and Technology, Prague, SQS and Czech Technical University at Prague

TE02000202 – Advance sensors and methods for sensing (Technology Agency of the Czech Republic), main partner Czech Technical University at Prague, WG leader

TH01010567 – Volume optical modulators (Technology Agency of the Czech Republic), project members University of Chemistry and Technology, Prague and SQS

TH01010997 – Thulium fiber lasers for industry and medicine (Technology Agency of the Czech Republic), project members Institute of Photonics and Electronics, University of Chemistry and Technology, Prague, Matex and SQS

Annexes

[A5] Weinzettla V., Shuklaa G., Ghoshc J., Melicha R., Paneka R., Tomesa M., Imriseka M., Naydenkovaa D., Varjua J., Pereirae T., Gomese R., Abramovicg I., Jaspersg R., Pisarik M., Odstrcilj T., Oost G. V. "High-resolution spectroscopy diagnostics for measuring impurity ion temperature and velocity on the COMPASS tokamak." Fusion Engineering and Design 96 (2015): 1006-1011.

[A6] Bohata J., Pisarik M., Zvanovec S., Peterka P. "Reliability of aircraft multimode optical networks." Optical Engineering 53.9 (2014): 096102-096102.

Fusion Engineering and Design 96–97 (2015) 1006–1011

Contents lists available at ScienceDirect

Fusion Engineering and Design

journal homepage: www.elsevier.com/locate/fusengdes

High-resolution spectroscopy diagnostics for measuring impurity ion temperature and velocity on the COMPASS tokamak

Vladimir Weinzettl[a,*], Gaurav Shukla[a,b,d], Joydeep Ghosh[c], Radek Melich[a], Radomir Panek[a], Matej Tomes[a,d], Martin Imrisek[a,d], Diana Naydenkova[a,d], Josef Varju[a], Tiago Pereira[e,f], Rui Gomes[e], Ivana Abramovic[g], Roger Jaspers[g], Michael Pisarik[h,i], Tomas Odstrcil[j], Guido Van Oost[b]

[a] Institute of Plasma Physics ASCR, Prague, Czech Republic
[b] Department of Applied Physics, Ghent University, Ghent, Belgium
[c] Institute for Plasma Research, Bhat, Gandhinagar, India
[d] Faculty of Mathematics and Physics, Charles University in Prague, Prague, Czech Republic
[e] Instituto de Plasmas e Fusão Nuclear, Lisboa, Portugal
[f] Instituto Superior Técnico, Universidade de Lisboa, Lisboa, Portugal
[g] Eindhoven University of Technology, Eindhoven, The Netherlands
[h] SQS Vlaknova optika a.s., Nova Paka, Czech Republic
[i] Department of Electromagnetic Field, Faculty of Electrical Engineering, Czech Technical University in Prague, Czech Republic
[j] Max-Planck-Institut fur Plasmaphysik, Garching, Germany

HIGHLIGHTS

- We built a new diagnostic of poloidal plasma rotation on the COMPASS tokamak.
- Improvements in throughput via toroidal integration and fiber optimizations shown.
- Poloidal rotation and ion temperature measured in L- and H-mode and during RMP.
- Design and parameters of a new CXRS diagnostic for COMPASS are introduced.

ARTICLE INFO

Article history:
Received 19 September 2014
Received in revised form 12 March 2015
Accepted 6 April 2015
Available online 30 April 2015

Keywords:
Tokamak
Plasma spectroscopy
Plasma rotation
Ion temperature
CXRS

ABSTRACT

High-resolution spectroscopy is a powerful tool for the measurement of plasma rotation as well as ion temperature using the Doppler shift of the emitted spectral lines and their Doppler broadening, respectively. Both passive and active diagnostic variants for the COMPASS tokamak are introduced. The passive diagnostic focused on the C III lines at about 465 nm is utilized for the observation of the poloidal plasma rotation. The current set-up of the measuring system is described, including the intended high-throughput optics upgrade. Different options to increase the fiber collection area are mentioned, including a flower-like fiber bundle, and the use of micro-lenses or tapered fibers. Recent measurements of poloidal plasma rotation of the order of 0–6 km/s are shown. The design of the new active diagnostic using a deuterium heating beam and based on charge exchange recombination spectroscopy (C VI line at 529 nm) is introduced. The tool will provide both space (0.5–5 cm) and time (10 ms) resolved toroidal plasma rotation and ion temperature profiles. The results of the Simulation of Spectra code used to examine the feasibility of charge exchange measurements on COMPASS are shown and connected with a selection of the spectrometer coupled with the CCD camera.

1. Introduction

High-resolution spectroscopy is a powerful tool for the measurement of plasma rotation as well as ion temperature using the Doppler shift of the emitted spectral lines and their Doppler broadening, respectively [1]. Eq. (1), using SI units, describes a shift of the

* Corresponding author. Tel.: +420 266052947.
E-mail address: vwei@ipp.cas.cz (V. Weinzettl).

http://dx.doi.org/10.1016/j.fusengdes.2015.04.006
0920-3796/

rest wavelength of the emission line λ_0 with respect to the observed wavelength λ_D, which is caused by motion of the ion with velocity v at angle α between the observer and ion motion:

$$v = \frac{c}{\cos(\alpha)} \frac{\lambda_D - \lambda_0}{\lambda_0} \quad (1)$$

where c is the speed of light. Assuming Gaussian line profiles, ion temperature T_i can be derived from the observed line's full-width at half of maximum $\Delta\lambda_{FWHM}$ using Eq. (2) with quantities given in SI units:

$$T_i = \frac{m_i c^2}{8 \ln 2 \cdot k_B} \frac{(\Delta\lambda_{FWHM})^2 - (\Delta\lambda_{FWHM,instr})^2}{\lambda_0^2} \quad (2)$$

where m_i is the ion mass, and $\Delta\lambda_{FWHM,instr}$ is the instrumental broadening at the measured wavelength, k_B is Boltzmann constant.

Passive diagnostics monitor spectral lines emitted as a result of spontaneous decay of excited atoms or ions in the plasma. Active diagnostics use the neutral beam to induce processes of charge exchange, and therefore, observations are well localized but limited by the attenuation of the beam. Both passive and active variants of this diagnostic for the COMPASS tokamak [2], a device of the ITER-like divertor plasma geometry (major radius 0.56 m, minor radius 0.23 m, toroidal magnetic field 1.15 T, plasma current up to 330 kA, electron temperature about 1 keV, discharge duration about 300 ms, auxiliary heating 2× NBI 300 kW, linear size ratio to ITER plasma 1:10), are introduced in the next sections.

2. Plasma rotation measurements on COMPASS

2.1. Poloidal rotation diagnostic

The passive diagnostic focused on the carbon triplet, i.e. C III lines at 464.742 nm, 465.025 nm and 465.147 nm [3], is used to measure the poloidal rotation of the edge plasma on COMPASS. The setup consists of: (1) an objective, (2) a fiber bundle, (3) focusing optics for coupling the fiber to the spectrometer, (4) a high-dispersion two-grating spectrometer [4] (2700 grooves per mm, f = 0.5 m, f/#∼10) and (5) a scientific CCD camera, see Fig. 1.

The objective, mounted on a vertical tokamak port, is composed of two spherical lenses and focuses plasma radiation onto the optical fiber bundle, with a demagnification of 4, which corresponds to a coverage of up to 50 mm on the plasma (typically from 10 mm outside up to 40 mm inside the separatrix).

The fiber bundle (see Fig. 2) consists, on the tokamak side, of 7 flower-like arrangements of 7 optical fibers each, with a total of 49 fibers. On the spectrometer side, the 49 fibers are arranged as a one-dimensional array, with a size of 3080 μm × 50 μm. The specifications of each fiber are: fused silica, core diameter of 50 μm, cladding diameter of 62.5 μm and numerical aperture of 0.22. The purpose of such an arrangement of fibers is to increase the amount of collected light, by reshaping hexagonal groups of 7 fibers into a linear array, which has a shape of the entrance slit of the spectrometer.

The light from the fiber is coupled into the spectrometer by an optical setup, consisting of 2 spherical lenses, with a total magnification of 5. This setup is necessary because the fiber and spectrometer numerical apertures are quite different (0.22 and 0.06, respectively). With this setup, the image of the end face of the fiber bundle appears magnified by a factor of 5 (15 mm × 250 μm) at the entrance slit of the spectrometer, but with a numerical aperture of 0.07 (measured), which is appropriate for coupling into the spectrometer. If necessary, the amount of gathered light can be increased, by way of increasing the width of the slit up to 250 μm (the height of the slit is 20 mm and the width is variable from 0 to 400 μm) at the expense of wavelength resolution. This was not the case though, as a slit width of 100 μm (which was the width used

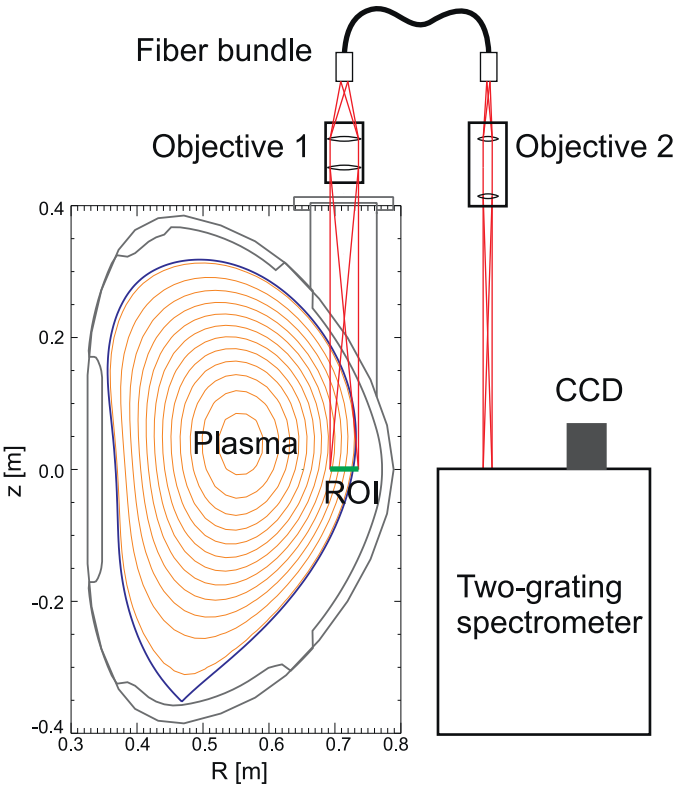

Fig. 1. Scheme of the experimental set-up of poloidal rotation measurements on COMPASS. Region of interest (ROI) is indicated in the poloidal cut of the vessel with the plasma. Objective 1 focuses plasma radiation onto the fiber bundle, from which it is projected by Objective 2 onto the entrance slit of the two-grating spectrometer equipped with a camera.

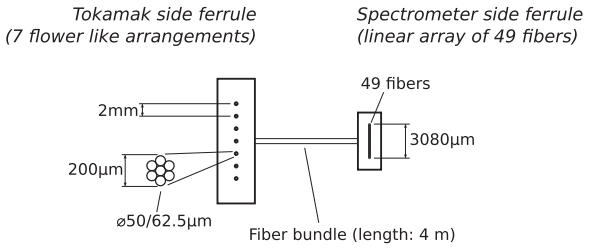

Fig. 2. Depiction of the arrangement of fibers in the fiber bundle.

for most acquisitions) was enough to obtain acceptable signal to noise ratio, and a further degradation of the wavelength resolution was not necessary.

The scientific CCD camera (model ANDOR iXon DU-897) is attached at the output of the spectrometer. Its main characteristics are: thermoelectrically cooled to −50 °C, back illuminated EMCCD, 512 × 512 pixels, pixel size of 16 μm × 16 μm, frame transfer and quantum efficiency of 80% in the region of interest.

Typically, shots are acquired using an exposure time of 20 ms at a rate of 40 frames per second, with a vertical binning of 32 pixels and using the frame transfer capability of the camera. This last feature enables the readout of the frame without any smearing. The main constraint limiting the acquisition frame rate is low light intensity.

Usually, the throughput of the system is limited by non-optimized fiber coupling on the tokamak side caused by the use of sets of circular lenses only. Consequently, there is the same magnification factor in both the radial and toroidal directions. While radial resolution is the requested parameter, the toroidal direction can be strongly integrated with respect to highly toroidally

symmetric plasmas in tokamaks. We propose the optical solution based on a combination of standard circular lenses and a set of cylindrical lenses, which allows having different magnification in radial and toroidal directions. A conventional (off-the-shelf) objective based on circular lenses (focal distance of 50 mm), which defines radial zoom (8× for the plasma-objective distance of 450 mm) and in which the iris will be adjusted to meet the numerical aperture of used fibers, will be connected to the custom-made anamorphic conversion lens, which improves the toroidal magnification two times. The conversion lens is a compound of a doublet of cylindrical lenses made of poly-methyl-methacrylate material and manufactured by the Single Point Diamond Turning technique. The throughput of system is increased accordingly to an increase of toroidal magnification, i.e. about two times by this improvement.

Besides the focusing optics upgrade we also evaluated different options of increasing the fiber collection area being inspired by astronomer's tests in [5]. Since the spectrometer's slit width masters the spectral resolution and the slit height is also limited (by the detector size), tapered fibers could seem to be one of the most interesting choices, also with respect to the economic effect: price divided by effective fiber collection area. But conservation of etendue in combination with typical *f*/# of high-resolution spectrometers suppresses both the advantages of a big collection area and a fiber narrowing. For example, even for NA as low as 0.12, we have the equivalent *f*/# about 4.2. Decreasing the fiber diameter to fit the slit size, the solid angle is even higher and exceeds the grating size. Scaling of the positive effects is the same or weaker than scaling of expected light losses (always with fiber size squared), moreover, an additional attenuation must be taken into account. Also, microlenses (small lenses applied to each fiber individually) are ineffective there, especially in comparison with conventional optics. They cannot reach an equivalent collection area, and must be applied separately to each fiber, which makes them also economically unattractive. Therefore, we focused on a comparison of fiber bundles of different fiber sizes filling the slit height, namely the fibers of NA = 0.12 and core/cladding size of 105/125 μm, 200/220 μm, 400/440 μm, 800/880 μm, and similar fibers starting from 50/125 μm for NA = 0.22. Calculating throughput of the whole detection system, a decisive parameter depending on the fiber core diameter and the shape of the spectrometer's slit has been derived and called the effective fiber light collection area. We defined it as a product of (1) the total area of the fiber cores, and (2) the ratio of the light passing through the spectrometer's slit and the light transmitted through the fiber bundle. Since the price of the bundle slowly decreases with fiber size, the effective fiber light collection area strongly increases up to the fiber diameter two times bigger than the slit size. Above this limit, an optical improvement is in the range of few per cent only. The effect is scalable, and can be used for any combination of slit width and fiber size. We choose the bundle composed of 34 fibers of 200/220 μm (NA = 0.12) due to easy handling and reasonable value (weighted fibers area) for the money. The fibers form a linear array in both the ferrules. On the tokamak side, centers of the fibers are equidistantly spaced by 310 μm. It allows getting the light from 80 mm of the edge plasma by using a new 8 times magnifying objective. On the spectrometer's side, the fibers are placed in touch with each other. Two of them will serve for spectral calibration purposes and are connected to the bundle only on spectrometer's side. Throughput of system is increased nearly by one order by optimizing a number, thickness and numerical aperture of the fibers with respect to the slit of the spectrometer. In the case of bundles composed from thinner fibers, flower-like fiber structures on the tokamak side reorganized into one dimensional array on the spectrometer's side are a good option. Often, they can be directly combined with the spectrometer without the use of both additional optics and the entrance slit. The flower-like set of thin fibers can be also put together into a thicker fiber, if the decisive parameter is the bundle price. But then the throughput is lower than in the case of equivalent separate fibers.

2.2. Calibration and poloidal rotation measurements

The strong zinc spectral calibration lamp, which provides three useful Zn I lines at 468.014 nm, 472.215 nm, and 481.053 nm [3], is used for a coarse alignment of both the gratings in the spectrometer, and also for a raw estimation of the linear dispersion at the detector plane. Since the nearest spectral line is about 3 nm away from the spectral region of interest but CCD covers only about 1.3 nm, the zinc lamp cannot directly provide the final calibration. Instead, a much weaker hollow cathode iron lamp filled by neon is used having many lines there. The final camera alignment is done using an estimated linear dispersion and expecting Fe I lines at 464.743 nm, and overlapping lines at 465.450 nm, 465.461 nm, and 465.463 nm, and Ne I lines at 464.542 nm, 464.990 nm, 465.210 nm, and 465.370 nm [3]. The spectral calibration is performed repeatedly several times a day to eliminate thermal expansion effects, which can also partly influence shifts of spectrum, and therefore the derived plasma rotation. The linear dispersion, as well as the spectral offset, are obtained from a multi-line analytical fit of the calibration spectrum by Gaussian curves. The calculated value of the linear dispersion is 0.162 nm/mm. The instrumental width for 100 μm spectrometer slit width is $\Delta\lambda_{FWHM,instr} \sim 0.029$ nm.

The spectrometer is operated routinely during campaigns on COMPASS, in which poloidal rotation measurements (realization of the upgraded configuration is scheduled for 2015) are requested. Measured spectra from high-temperature discharges contains already mentioned CIII triplet, and a bit weaker O II line in between the carbon peaks at 464.914 nm [3], see the typical spectrum in Fig. 3. The poloidal plasma rotation and ion temperature are derived according to Eqs. (1) and (2), and their typical time evolution is plotted in Fig. 4. As an illustration, we show changes of both quantities in three shots representing the diverted, ohmically heated low-confined plasma evolving to ELM-free H-mode with (#7860) and without (#7866 and #7867) application of edge magnetic perturbations (MP). It is clearly seen, how L–H transition changes the edge poloidal plasma rotation from the electron diamagnetic to ion diamagnetic drift direction and how the ion temperature increases there. It also appears that the application of the edge magnetic perturbations decreases this effect.

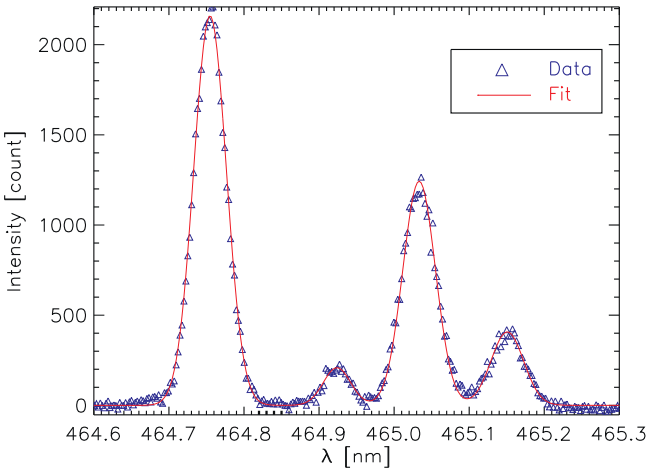

Fig. 3. Measured spectrum near the CIII triplet at (1006 ± 13) ms in the diverted ohmically heated low-confinement plasma in the shot #5852 on the COMPASS tokamak. The second peak from the left is O II line at 464.914 nm.

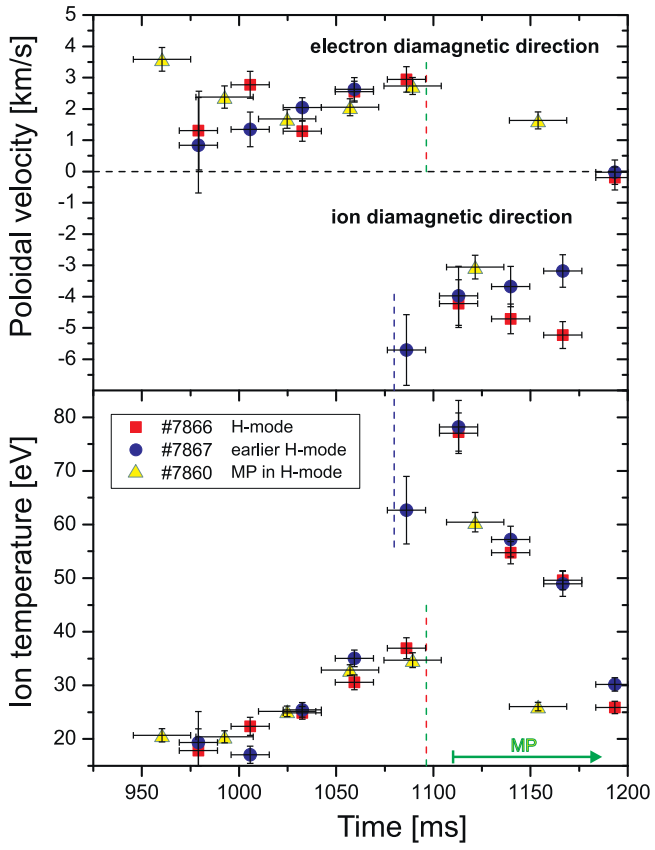

Fig. 4. Temporal evolution of poloidal plasma rotation and ion temperature on COMPASS in a diverted ohmically heated plasma in the shots with the transition to ELM-free H-mode (from 1096 ms in #7860 and #7866, from 1080 ms in #7867) and with edge magnetic perturbations (MP) (from 1110 ms in #7860).

3. Charge exchange diagnostic on COMPASS

3.1. Introduction to CXRS

Charge exchange recombination spectroscopy (CXRS) is one of the most successful tools for the measurements of impurity rotation and ion temperature profiles [6–9]. This technique has been used since the early 1990s for measurements of both the edge and core ion temperature and rotation of impurity ions, which are among key parameters for better understanding of physics of transport barriers [10]. On COMPASS, CXRS should provide a deeper insight into physics of the observed L–H transitions as well as the effects connected with the application of the edge magnetic perturbations [11] by the measurement of radial profiles of both the toroidal plasma rotation and the ion temperature.

CXRS on COMPASS will use the light emitted during the interaction of impurity ions with neutrals injected by a heating neutral beam; this yields information on local values of both the impurity ion temperature and the rotation using Doppler broadening and the shift of the measured line. Since carbon is the most common impurity in COMPASS, the CXRS diagnostic is proposed for C VI line at 529 nm ($n = 8 \rightarrow 7$) there. The deuterium beam, one of two heating neutral beams (NBI) installed on COMPASS, will be used as a source of fast neutrals, which penetrate up to the plasma core. The diagnostic comprises the collection optics coupled with an array of fibers. Light from the plasma will be led to a single spectrometer–CCD camera system.

3.2. Design of CXRS

3.2.1. Geometrical arrangement

The geometrical arrangement of the new CXRS diagnostic for the COMPASS tokamak is shown in Fig. 5. The equatorial port, with inner diameter of 150 mm, located in the sector between toroidal field coils 10 and 11 was selected for the installation of the collection optics. COMPASS has two NBIs, operated at beam current up to 10 A and beam energy of 40 keV, and capable of delivering 300 kW heating power in either deuterium or hydrogen atoms. The beams are injected tangentially in the equatorial plane and travel a distance of about 1 m before reaching the beam dump at the vessel wall. The beam diameter at focus is 5.5 cm and the beam divergence is about 0.7°. A better CXRS performance is reached for NBI1, for which the optical design will be introduced.

3.2.2. Collection optics and fibers

The collection optics will be used to image the plasma onto the optical fibers that couple the light to the spectrometer. The first version of the optics design consists of the in-vessel stainless steel mirror and a pair of convex lenses (focal distance of 100 mm, $f/2.2$) located outside the vessel. During glow discharges or other vacuum chamber conditioning processes, the mirror will be rotated to face the optical window and the back of the mirror, protected by a graphite block, will serve as a shutter for the window. The lenses image the carbon charge exchange emission onto 15 fibers of NA = 0.22, and 600/660 μm core/cladding diameter mounted on a plate. However, the port and hence the optical head diameter restrict the magnification that can be achieved through the collection optics. In the mentioned case, the magnification is considered to be about 17. Consequently, the minimum spot size of 10 mm is generated for each line of sight at the intersection with the neutral beam. Using the known spot size, the calculated radial resolution of the CXRS system varies from 5 to 0.5 cm from the plasma core towards the edge as shown in Fig. 6.

With the proposed collection optics, the CX emission is expected to be imaged by the lens system onto a linear array of fibers so as to fill the collection optics with f-number of the fibers. Then,

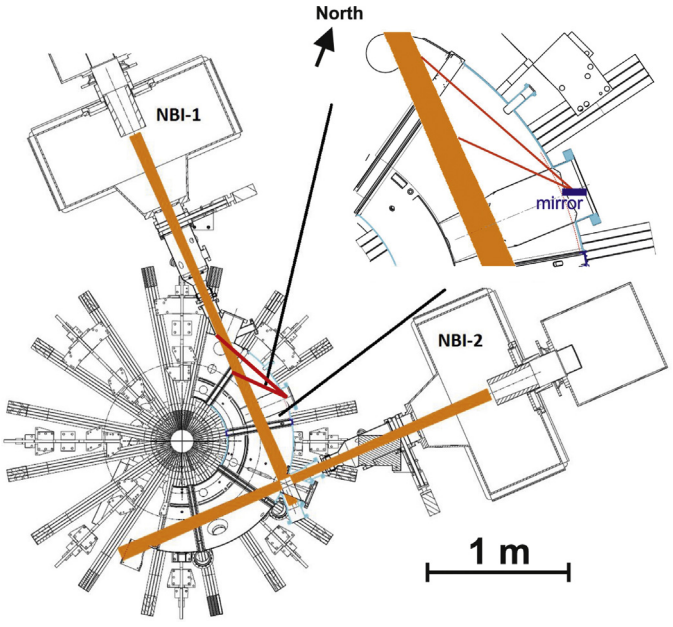

Fig. 5. Geometrical arrangement of the new CXRS diagnostic on COMPASS. The edge line-of-sights of the CXRS diagnostic are indicated in the figure.

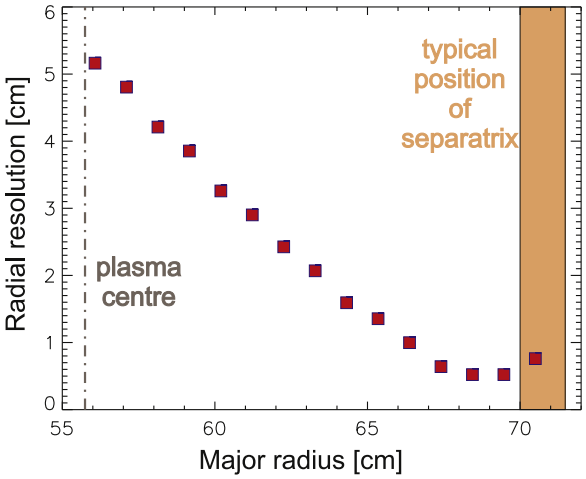

Fig. 6. Radial resolution of CXRS using NBI1.

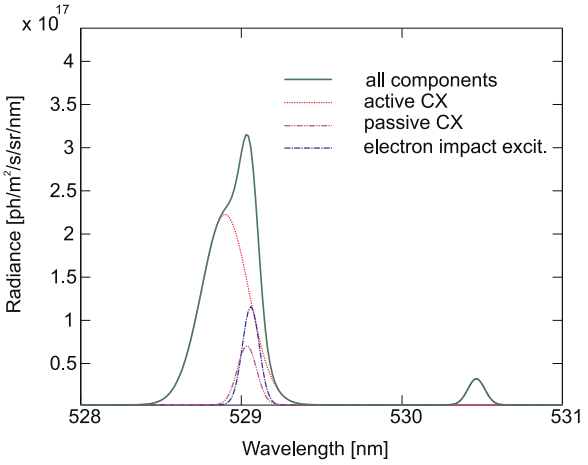

Fig. 7. Simulated spectra generated by the SoS code for COMPASS using plasma parameters from the shot #6133. The left peak is composed from the active charge-exchange (beam dependent), passive charge-exchange and electron excitation components of C VI line at 529 nm. The small peak on the right is C II line at 530.5 nm.

the light is transferred 20 m away from the tokamak hall to a low radiation area, where the fibers will be coupled to a high resolution Czerny–Turner spectrometer. A prototype of the proposed periscope has already been tested in the optical laboratory for an engineering feasibility study.

3.2.3. Spectrometer and CCD system

For the CXRS diagnostic, which will be used for H-mode studies on COMPASS, a high dispersion spectrometer is required for achieving an adequate accuracy of toroidal rotation measurements of about 10 km/s. If it is combined with an observation angle for the edge plasma of 52°, a linear dispersion of the spectrometer should be at least 0.83 nm/mm for the typical pixel size of the camera of 13 μm. At the same time, a lower limit of the spectral region to be covered by the spectrometer–camera system is given by the maximum ion temperature expected in the region of interest. Assuming temperature values of 0.3–1 keV, the C VI line broadening calculated according to Eq. (2) sets this limit to 0.20–0.37 nm. Based on these parameters, the spectrometer and the camera have been chosen.

However, the selection of the camera, the spectrometer, and the fiber optics is not independent since the spectrometer resolution, the covered spectral region, the pixel size of the camera, the number of pixels in both directions of the camera, and the spectrometer slit height are mutually coupled.

For the present CXRS diagnostic, the 0.67 m Czerny–Turner McPherson 207 spectrometer has been purchased equipped with a holographic grating of 1800 grooves/mm optimized for visible wavelength range. The grating size is 120 mm × 140 mm. The system accepts light up to *f*/4.7. The fibers used in the collection optics can be vertically stacked in one column and coupled to the spectrometer system. The spectrometer resolution lies at the above mentioned limit.

The imaging plane of the spectrometer is covered by a charge couple device (CCD) as the detector. We purchased the newest model of ANDOR's EMCCD cameras, iXon Ultra 888. The camera has 1024 × 1024 pixels in the active area, and a pixel size of 13 μm; thus creating active area of 13.3 mm × 13.3 mm. The camera has a readout speed of up to 30 MHz, which, in combination with the binning options, allows measurements well below 5 ms. Moreover, it is equipped with a frame-transfer readout. Due to limitations of the exposure time given by a low light intensity, we can also gain from a high quantum efficiency of about 90% for the used spectral region. The system is expected to provide pixel resolution of about 0.011 nm at the mentioned linear dispersion of the spectrometer.

3.2.4. Implementation of CXRS diagnostic

Feasibility of the proposed CXRS diagnostic based on measurements of the C VI line at 529 nm (n = 8 → 7), which will be implemented on the COMPASS tokamak, has been numerically examined in different project phases by the Simulation of Spectra (SoS) code, which has been developed for these purposes at the University of Technology, Eindhoven (http://fusion.phys.tue.nl). The code takes main plasma and beam parameters, including the real geometry of both the plasma and NBI, the beam attenuation, the instrumentation specifications of the spectrometer and CCD, and plasma emission rates to provide the simulated 'observed' CX spectrum. The code generates both the active and passive CX components of the spectra. Simulated spectra indicate a dominating active charge-exchange signal over a passive one. A realistic simulated case corresponding to the final set-up mentioned above is shown in Fig. 7. The plasma parameters used there were taken from the realized shot on the COMPASS tokamak with the number #6133: central electron temperature was 0.6 keV, line-averaged density $3.7 \times 10^{19}\,m^{-3}$, 40 keV neutral (deuterium) beam of current of 10 A with the beam composition of the full, half and one-third energy ratios of 47% (E), 26% ($E_{1/2}$) and 27% ($E_{1/3}$), respectively. The profiles of electron density and temperature were incorporated from the Thomson Scattering diagnostic. Independently of the simulations, a simple set-up based on the low-resolution HR2000+ spectrometer (spectral range of 458–663 nm, $\Delta\lambda \sim 0.1$ nm), presently available on COMPASS, was successfully realized to check the presence of both the passive and active components of the investigated CX line at 529 nm.

The spectral calibration of the system is planned to be done by the hollow cathode samarium lamp. The absolute calibration will be performed using the quartz tungsten halogen lamp to allow reconstructions of the carbon (C^{6+}) concentration profile.

4. Conclusion

Both passive and active variants of the plasma rotation diagnostic on the COMPASS tokamak have been introduced. For successful implementation, poloidal rotation measurements require as high spectral dispersion of the system as 0.16 nm/mm to resolve typical values of the poloidal rotation of the order of several km/s. Toroidal measurements can be realized with dispersions of only

about 0.8 nm/mm. A passive diagnostic should also be optimized for a high-throughput; otherwise, time measurements are limited by low intensity of the signal. When the beam is available on the device, CXRS can provide well spatially resolved measurements of profiles of plasma rotation, ion temperature, and impurity concentration.

Acknowledgments

This work was partly funded by the Czech Science Foundation under the grants GA14-35260S (H-mode studies) and GAP205/11/2341 (magnetic perturbation studies) and the MSMT CR project LM2011021. The doctoral grant of G. Shukla is financed by the EU (Erasmus Mundus Svaagata project).

References

[1] R.C. Isler, Nucl. Fusion 24 (12) (1984) 1599.
[2] R. Panek, O. Bilykova, V. Fuchs, M. Hron, P. Chraska, P. Pavlo, et al., Czech. J. Phys. 56 (Suppl. B) (2006) 125.
[3] A. Kramida, Yu. Ralchenko, J. Reader, NIST ASD Team, NIST Atomic Spectra Database (ver. 5.2), 2014, http://physics.nist.gov/asd
[4] R. Gomes, C. Varandas, J. Cabral, E. Sokolova, S. Reyes Cortes, Rev. Sci. Instrum. 74 (2003) 2071.
[5] G. Avila, Fiber Optics in Astronomy, 1988, pp. 63.
[6] R.C. Isler, Plasma Phys. Control. Fusion 36 (1994) 171.
[7] K.H. Burrell, P. Gohil, R. Groebner, D. Kaplan, J. Robinson, W. Solomon, et al., Rev. Sci. Instrum. 75 (2004) 3455.
[8] R.P. Seraydarian, K. Burrell, N. Brooks, R. Groebner, C. Kahn, Rev. Sci. Instrum. 57 (1986) 155.
[9] R.J. Fonck, D. Darrow, K. Jaehnig, Phys. Rev. A 29 (6) (1984) 3288.
[10] K. Crombe, Y. Andrew, M. Brix, C. Giroud, S. Hacquin, N. Hawkes, et al., PRL 95 (2005) 15003.
[11] R. Panek, J. Stockel, J. Havlicek, F. Janky, M. Hron, V. Weinzettl, et al., ECA, vol. 37D, P4.103.

Optical Engineering

OpticalEngineering.SPIEDigitalLibrary.org

Reliability of aircraft multimode optical networks

Jan Bohata
Michael Písařík
Stanislav Zvánovec
Pavel Peterka

SPIE.

Reliability of aircraft multimode optical networks

Jan Bohata,[a,*] Michael Písařík,[a,b] Stanislav Zvánovec,[a] and Pavel Peterka[c]
[a]Czech Technical University in Prague, Department of Electromagnetic Field, 2 Technicka, 16627 Prague, Czech Republic
[b]SQS Vlaknova Optika a.s., Komenskeho 304, 509 01 Nova Paka, Czech Republic
[c]Academy of Sciences of the Czech Republic, Institute of Photonics and Electronics, v.v.i., Chaberská 57, 182 51 Prague, Czech Republic

Abstract. Results from tests and analyses of multimode optical fibers for an avionic optical network under a variety of stress conditions are presented. Experiments revealed vibrational and temperature changes of distinct multimode fibers. Results lead to the discussion of influenced insertion losses and especially reduced bandwidth corresponding to modal distribution changes. It was determined that these crucial parameters could affect system reliability when an airplane network intersects thermal and vibrational variable environments. [DOI: 10.1117/1.OE.53.9.096102]

Keywords: optical fiber; optical connectors; multimode; photonic network; avionics; harsh environment.

Paper 140831 received May 22, 2014; revised manuscript received Aug. 1, 2014; accepted for publication Aug. 1, 2014; published online Sep. 3, 2014.

1 Introduction

New developments in the construction of aircrafts result in a multitude of demands on digital and analog networks placed inside airplanes. Needs such as infrastructure weight recalculated during fuel consumption, power consumption, available bandwidth, electromagnetic resistance, and the ability to implement the next generation of sensors cannot be satisfied by currently utilized copper links, therefore, a massive development of optical systems for civil aircraft is foreseen.[1]

Due to flight safety requirements,[2] the avionic industry is a conservative area that harbors a wariness for new technologies; therefore, there must be convincing reasons to change well-tested, reliable technologies.[3] One of the most important reasons to modify technologies results from newly revealed composite materials being used, such as in the gigantic A380 shell.[4] The absence of a common ground brings serious problems with electromagnetic interference since the cost of additional shielding for cables rapidly increases the fixed mass of aircrafts.[5] The weight difference between optical and copper cables, assuming all necessary shielding and coating within the A380, was investigated in Refs. 5 and 6 and revealed a decrease of ∼3000 kg when optical infrastructure is implemented. Another notable reason to switch to fiber optics is the increased bandwidth for advanced nodes such as hi-resolution cameras. Lowering power consumption for transmission, which was investigated by the DAPHNE consortium where simulations revealed savings of up to 10 kW of power on analog antenna systems alone,[5] is another promising area. Optical fiber structures offer other benefits, including their ability to monitor fiber Bragg grating (FBG) stress and temperature[7] (already implemented in military aircraft and civil rotorcraft), gas and humidity, and the photonic network itself,[8] not to mention the wide bandwidth suitable for transmission of modulated analog signals for antennas [radio frequency over glass (RFoG)] based on Raman or Brillouin scattering. Several such aspects dealing with optical infrastructures were investigated within the DAPHNE consortium, a project of the European Union Framework Program 7 (EU FP7).[5,6]

Civil aircrafts are introducing a complex network system with many slave nodes and one centralized mainframe node with backup. There are several common aspects in the fiber of the x broadband network and optical backbone systems within aircraft that could prove to be interesting for future implementation within avionics. All aircraft systems/infrastructures were closely investigated within the EU FP7 DAPHNE consortium where different network types were identified. The most promising designs investigated were (1) passive star with single-mode optical fibers (PON), (2) active star with multimode optical fibers, and (3) daisy chain with single-mode and multimode optical fibers.[5] Star topologies for single-mode fiber networks and their potential and robustness in terms of scalability limits at different crossing traffic loads were analyzed in Ref. 9, revealing the trade-offs between latency, system complexity, and scalability.

Despite the potentials mentioned above, fiber optics deployment on civil aircrafts still has not overcome all the challenges yet and proper discussions, especially on the selection of fibers and their behaviors under in-flight conditions, have yet to be held. That said, single-mode fiber 8/125 μm is used in military aircrafts, like rotorcrafts,[10] and developed FBG stress and temperature sensors are used in some critical parts of the aircraft.[8] The advantage of a single-mode fiber is demonstrated by the stability of power couplers, filters, and multiplex elements for dense wavelength division multiplexing; therefore, single-mode fibers are implemented for communication links and infrastructures. Nevertheless, multimode fibers were historically preselected due to a larger diameter, which should be less difficult for connections and more resistant to vibrations and temperature changes. Although they have already been integrated in A340 and A380 aircrafts for hi-definition digital cameras to assist landing (landing camera),[1] their utilization within aircrafts is still being debated.

*Address all correspondence to: Jan Bohata, E-mail: bohatja2@fel.cvut.cz

0091-3286/2014/$25.00 © 2014 SPIE

A photonic network falls under the auspice of ground operations and has to fulfill most requests over the long term as specific, rigid aircraft conditions require a closer reconsideration of every aspect of fiber optics and their particular influences. It has to be emphasized that temperature changes during ground operations are more than 1000 times slower than during in-flight conditions. Multimode fibers were stable in combination with a light-emitting diode light source, but most systems (high data rate systems and RFoG) use laser sources such as vertical cavity surface emitting laser. Some network components are, or will be, installed in unpressurized zones with high temperature differences. Unpressurized zones should be considered as a harsh environment because temperatures close to the engine range from 80 up to 120°C can be found in some places, but can drop to ~ -60°C (Ref. 11) only a few meters away, which could result in a change of the stress and basic parameters, including reflection loss and insertion loss.[5]

This paper closely investigates the influences of temperature cycling and vibrations on multimode fibers and some basic optic components, such as the connectors used in aircrafts, and their impact on the optical network. The impact of launch conditions in combination with failures on fiber splice was also closely investigated. The paper is organized as follows. Section 2 introduces simulation results for misaligned multimode fibers in terms of modal distribution. Section 3 presents the experiment laboratory setup to investigate thermal and vibrational influences during in-flight and results from these measurements are discussed. Key findings for the entire aircraft network are introduced and discussed in Sec. 4, with concluding remarks given in Sec. 5.

2 Simulation Results

To determine transmission characteristics, changes in field distribution for propagating modes were analyzed for typical cases of aerial influences, especially vibrational changes. Fiber misalignment brings an additional extrinsic loss to connections. To assess them, our studies focus on transverse offset considering loss due to a displacement δ (μm) while assuming uniformly distributed power in the first fiber. Insertion loss (IL) can be expressed by[12]

$$L = 10 \log\left\{\frac{1}{\pi}\left[2\cos^{-1}\frac{\delta}{2a} - \frac{\delta}{a}\sqrt{1-\left(\frac{\delta}{2a}\right)^2}\right]\right\}, \quad (1)$$

where $2a$ introduces the diameter of the core.

Another definition for IL, computed with mode field diameter (MFD), originates from misalignment of the field distribution. Figure 1 shows how shifting cores with various MFD according to Ref. 13 could depend on IL.

It is obvious that the narrower the mode field, the smaller the IL. However, it is necessary to consider the tendency of producing a narrower laser beam loaded to a fiber core with just a few modes guided to achieve better bandwidth.

Simulations were carried out featuring a shifting of the forehead by 50/125 multimode × (MM) fibers with a parabolic refractive index and distribution of the mode field being observed at a wavelength of 1310 nm. Three modes, LP_{01}, LP_{11}, and LP_{02}, were chosen to illustrate the influence of shifting fibers. Two multimode fibers are connected (spliced) with different shiftings to simulate vibrating conditions. The positional range was changed from 0 to 3.5 μm. Chosen results are shown in Fig. 2 corresponding to the LP_{01}, LP_{11}, and LP_{02} modes with the position of the vibration-affected connector denoted. Multimode fibers were fed from below.

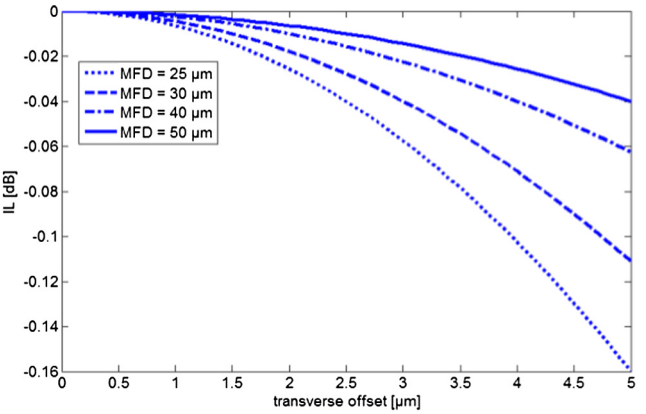

Fig. 1 Insertion loss (IL) dependent on transverse offset with different mode field diameter.

The influence was investigated on two spliced MM fibers, typical of an airplane camera infrastructure, and how the modes become distorted behind the connection (in figures placed 200 μm from bottom) is clearly illustrated.

Under recommendation ITU-T G.651.1,[14] related to the MM fiber characteristics of a 50/125 μm multimode graded-index optical fiber cable for the optical access network, the tolerance of the core size can be up to ± 3 μm. We have also performed simulations for connecting two MM fibers from different manufacturers with distance limits of core diameter tolerance containing modes LP_{01} and LP_{11}. Multimode 52/125 μm fiber joined to 48/125 μm is described. The impact on mode structure was tested again with shifting cores from 0 to 3.5 μm. In this case, mode distribution has become more distorted and covers a larger area in the core. An evanescent wave also radiates more power. The recommendation allows for ~ 1 μm higher tolerance of core than was actually used. Distribution of power in a three-dimensional view for two selected modes with a 3.5 μm radial shifting of cores is also shown in Fig. 3. Results represent shifted eccentricity cores (52 to 48 μm) for basic modes.

Dependence of vibrational shifting was also modeled by simulation software with the simulation scheme in Fig. 4 referring to the vibrational measurement setup. It contains a continuous wave laser of 1310 nm with an output power of 0 dBm, three spatial connectors with variable connections, and an optical power meter placed at the end of the setup. The connectors are joined by graded-index MM 50/125 fibers with the movement of the fibers being realized within two principal axes. The forehead shift was set from 0 to 4 μm in the x axis, from 0 to 4 μm in the y axis in the second connector, and combinations up to 2.2 μm in both x and y axis in the third connector to achieve different shifting directions. The difference in IL per connection was up to 0.034 dB for the maximum shift with reference power −0.632 dBm. Three connectors were joined by two 1-m-long MM fibers and connected by 20-m-long MM fibers to the source and detector. With dependence on the number of modes, shifting, rotation, and performance of the connectors, these impacts could lead to an additional attenuation of up to 0.1 dB for the case of three connectors.

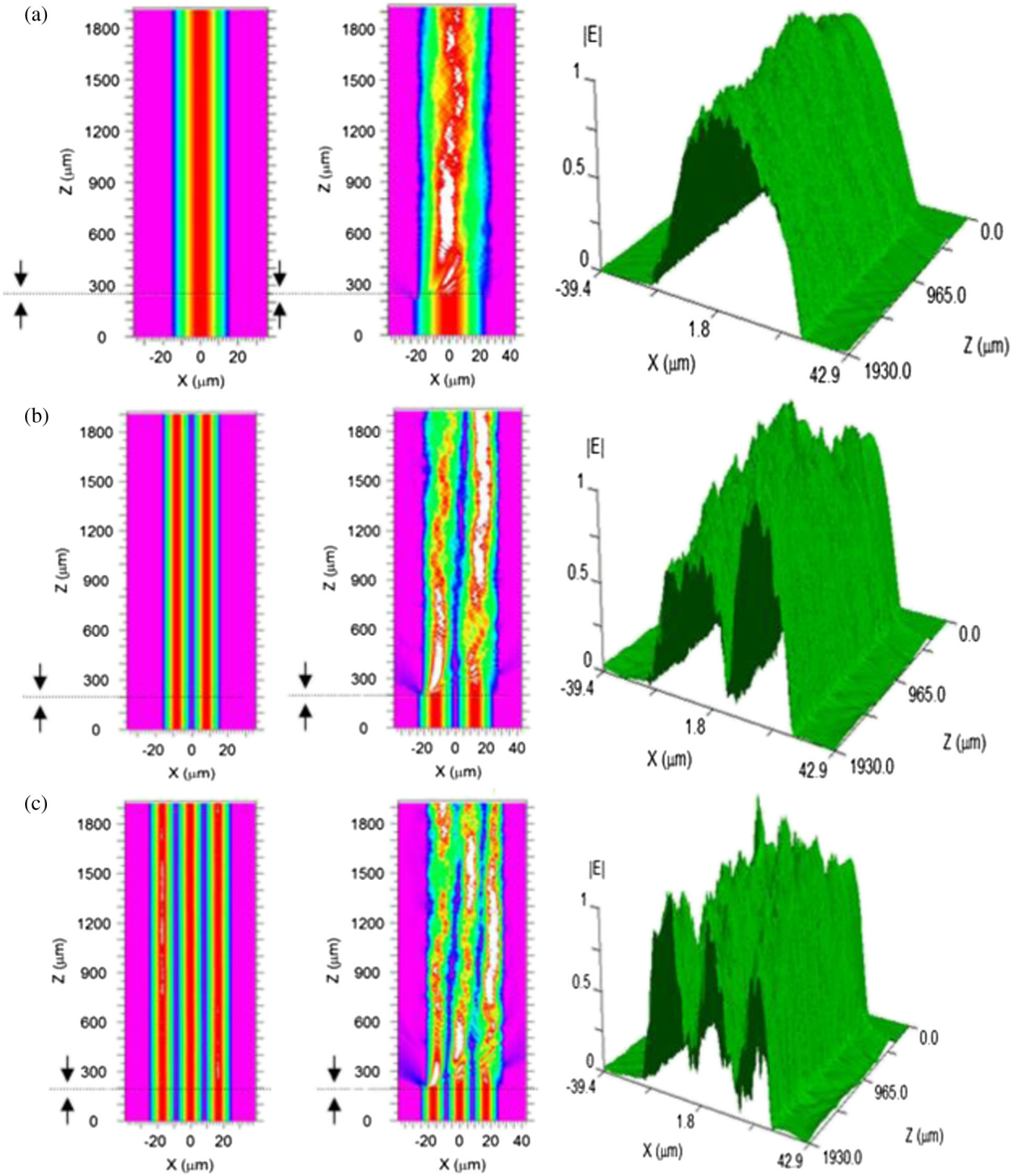

Fig. 2 Dependence of modes LP_{01}, LP_{11}, and LP_{02} (from top to bottom) on shifting fibers with three-dimensional illustration of distributed power: (a) LP_{01}, (b) LP_{11}, and (c) LP_{02}.

3 Experimental Setup and Results

We carried out several measurement tests for 50/125 MM fiber and their connections for avionic applications. Contrary to the first generation of multimode fibers (OM1/OM2), novel MM fibers OM3 and OM4 (known as laser-optimized fibers) are utilized for their enhanced bandwidth. The fibers are designed for a laser-based high bit-rate transmission, working in a few-modes' regime. Modern OM3/OM4 fibers differ from the first generation by an almost ideal graded refractive index, which rapidly reduces the differential mode delay (DMD) and increases the bandwidth.[15] We investigated the resistance of connected MM graded-index fibers OM3 and OM4 against temperature changes and vibration set to identical in-flight conditions.

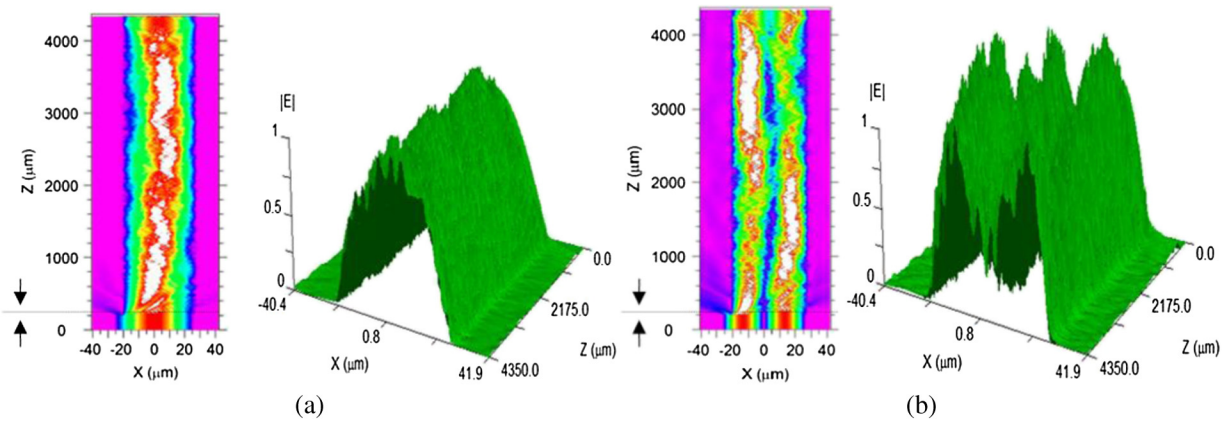

Fig. 3 Dependence of modes LP_{01} on shifting fibers with core eccentricity 48/52 μm: (a) LP_{01} and (b) LP_{11}.

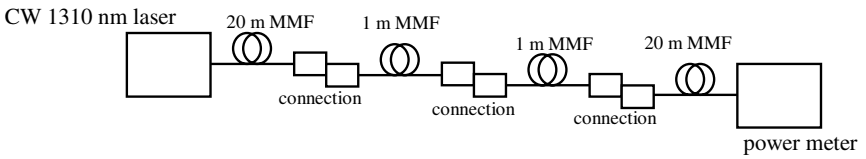

Fig. 4 Simulation setup of fiber shifting.

3.1 *Thermal Tests*

First, a measurement setup having various temperature sections was realized as shown in Fig. 5. Two MM fibers types OM3 and OM4 are connected by four FC/PC connectors. Two types of optical sources were used: a polychromatic halogen lamp (Ocean Optics H2000, Dunedin, Florida) and a distributed feedback laser (DFB) 1310-nm laser, respectively. Fluctuations of IL were observed at a wavelength of 1310 nm with changing temperature conditions. The optical link, having a total length of 6 m, passed through an open space section (22°C), temperature chamber 1 (temperatures up to 85°C), another open space section (22°C), cycling temperature chamber 2 (temperature set from −60 to 20°C), and via the last open section without a connector splice.

The first case contained a polychromatic source with a constant temperature of 22°C away from the chamber, a constant temperature of 85°C in chamber 1, and a continuously changing temperature in chamber 2. The temperature decreased from 22 to −60°C and back to 22°C in 10-min steps within a 6-h duration. It simulated different thermal conditions along an airplane and their changeability from take-off until landing. Results of the measurements are depicted in Fig. 6(a). It is obvious that parameter Δ IL (green curve) follows temperature changes. The highest deviation of IL was ∼0.13 dB and it is evident that the lower the temperature, the higher the IL. Detection of the received power at 1550 nm clearly duplicates the received power at 1310 nm. We presented a more detailed process to capture a more precise correlation between the temperature change and IL change than in previous results.

The second measurement was performed with a DFB 1310 nm source. The temperature was changed only in chamber 1, which was heated to 85°C and then cooled down. All remaining parts of the setup had the same temperature of 22°C. We observed the highest change in IL of ∼0.024 dB after fluctuating the temperature as seen in Fig. 6(b), where the difference between thermal conditions of 85 and 22°C is easily discernible. During both thermal changes (chamber 1 and chamber 2), the total Δ IL fluctuated around a range of 0.025 dB.

3.2 *Vibrational Tests*

The impact of vibrations of optical connections on insertion loss was investigated next. The whole optical setup, consisting of optical connectors, was placed on a special vibration membrane with a flexible pad as shown in Fig. 7. The rest of the deployment was loosely gripped. The acoustic tester platform allowed the undertaking of vibrational tests within a frequency range from 10 Hz up to 2 kHz. The total length of the fiber setup was 6 m with OM3 and OM4 fibers connected by three FC/PC connectors. Connectors with OM3 and OM4 fibers, manufactured on the limits of recommendations from the standards for MM fibers, such as ISO/IEC

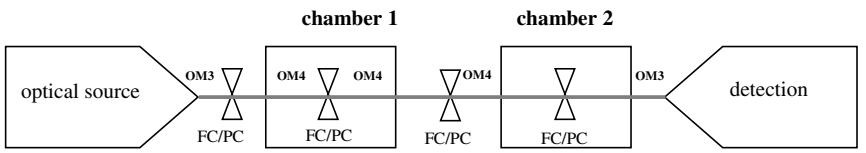

Fig. 5 Schematic of temperature measurement.

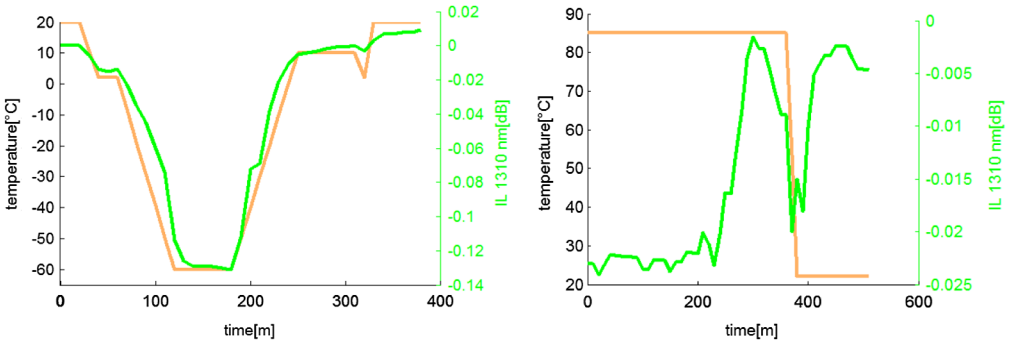

Fig. 6 (a) IL by chamber 2 temperature cycling with polychromatic source. (b) IL by chamber 1 temperature cycling with distributed feedback laser (DFB) laser source.

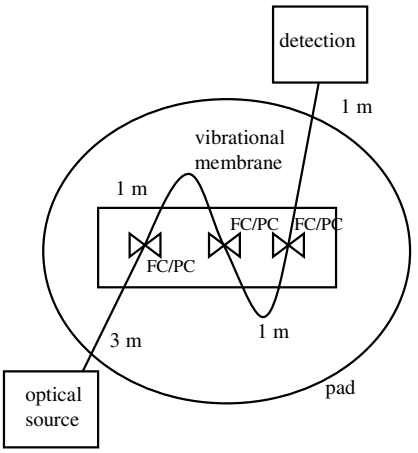

Fig. 7 Schematic of vibrational measurement.

11801, IEC 60793-2-10, TIA/EIA, and ITUG 651.1, were used to simulate the worst-case scenarios that can occur. Recommendations allow, for example, maximum span distances for 40G/100G systems of 100 m in OM3 and 150 m in OM4, respectively.[15]

To achieve realistic properties of the optical link, the same two sources were used as in the previous measurement. The vibration frequency was changed from 5 Hz to 2 kHz and the Δ IL of the whole link was observed. Three cases were used to determine the influence due to MM fibers. Only a standard OM3 was involved in the first measuring case. The second case contained a combination of OM3-OM4-OM4-OM3 and the third case was, unlike the first case, realized by using only OM4 fibers. The fibers had a 900 μm tubing instead of a 20-cm section next to the optical source and only had a 250 μm coating.

All connectors and fibers gripped on the membrane were drifted as given by the acceleration in a particular frequency which causes an overload even over 20 G. The measured dependence of the acceleration on frequency is shown in Fig. 8(a). It is very possible to find an almost linear growth up to 200 Hz. The characteristic of the acceleration was related to the measured results described below. The first test was performed with only OM3 fibers with a polychromatic H2000 source. Δ IL increased up to 0.003 dB in the first test and up to 0.006 dB in the second case. The progress of the first test is shown in Fig. 8(b), with the blue curve representing the increase in frequency from 5 Hz to 2 kHz and the green line covering the decrease in frequency from 2 kHz to 5 Hz.

The second test contained a combination of OM3 and OM4 fibers. Two 1-m-long OM4 fibers were placed on the membrane and connected to the OM3 fibers. See two results for polychromatic and monochromatic sources in Figs. 9(a) and 9(b), respectively. We measured four series of tests with the highest Δ IL equal to 0.042 dB at a frequency of 1 kHz with a polychromatic source and 0.007 dB with a monochromatic source. All shapes contain a decrease of IL around a frequency of 200 Hz; then the IL increased rapidly and became more stable, according to the accelerative process.

Only OM4 fibers were measured during the third test as seen in the results in Fig. 10. The IL evidently changes and

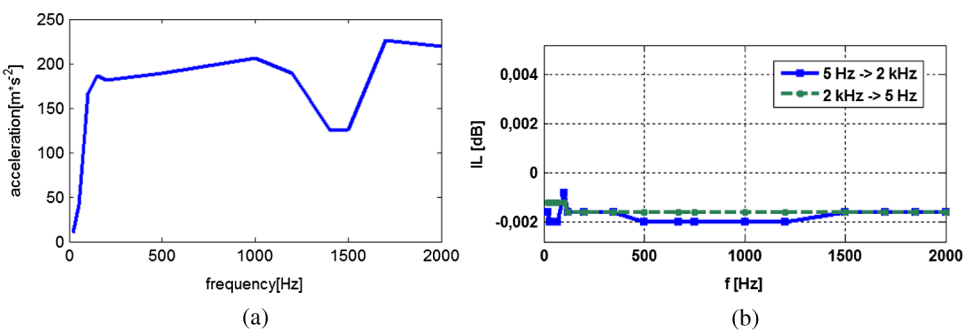

Fig. 8 (a) Dependence of acceleration influencing the connectors. (b) OM3 connection test with halogen lamp.

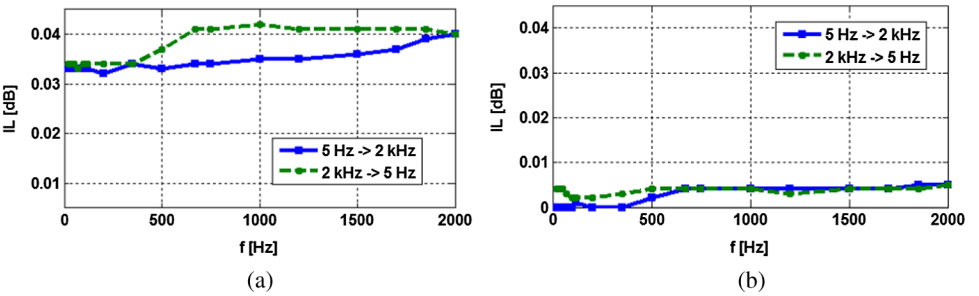

Fig. 9 OM3-OM4 connection test with (a) halogen lamp and (b) DFB 1310 laser.

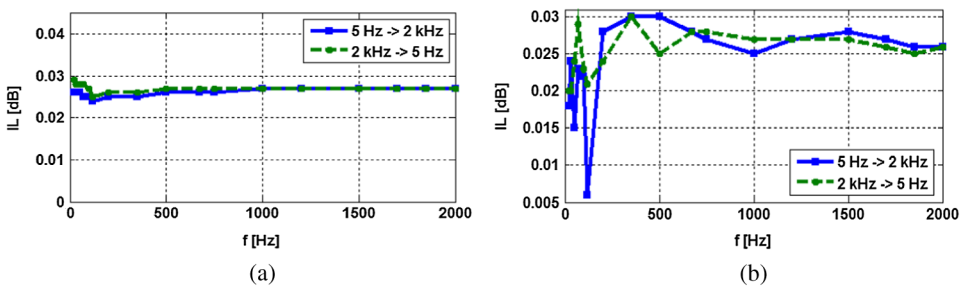

Fig. 10 OM4 connection test with (a) halogen lamp and (b) DFB 1310 laser.

decreases around 200 Hz and then increases behind this point within all performed series. Δ IL reached a maximum of 0.038 and 0.03 dB for the polychromatic and monochromatic sources, respectively.

The progress of Δ IL for all tests has oscillations around a frequency of 200 Hz where the smallest attenuation can also be found, and the shape of Δ IL becomes more linear and constant behind this point. The measured stability of the setup was ±0.001 dB, which implies the results were correct. Three connectors were tested with a total length of 6 m for the setup. An entire aircraft optical network would have ∼10 connectors[5] and a length of optical link in the hundreds of meters causing attenuation of at least three times that in the performed tests, possibly worsening the optical signal-to-noise ratio. If we considered both thermal and vibrational changes, Δ IL would be ∼1 dB for the worst case scenario with a dependence on wavelength, source, fiber recommendations, etc.

4 Whole Network Analyses

According to the temperature and vibrational measurements, the influence of the spliced IL was further exploited and demonstrated via simulations of the whole airplane network. There are many requirements for sensor systems, including landing cameras, which are already placed on Airbus aircrafts. An optical multimode link is led through various sections, including connectors, as proper maintaining reconfiguration tools for supervising. The connectors bring a potential additive loss to the network and can be less resistant to harsh conditions. The entire network is built on the concept of point-to-point links led from a central unit at the head of the airplane to particular landing cameras as shown in Fig. 11. The longest distance, led from the central unit to the tail camera, measures ∼250 m long with stressed occurrences seriously limiting possible transfer bandwidth (e.g., OM3 fibers allow 10 G systems for 300 m and 40 G systems for only 100 m).[15]

The impact of a harsh environment, such as thermal and vibrational changes, was observed when increasing the bit error rate (BER), decreasing the Q-factor and deformed eye diagram. Several cases were considered with continuously increasing IL due to a harsh environment from 0 to 1 dB for all connections in the link. The link was analyzed for 10 Gbps nonreturn to zero (NRZ) with results illustrated in Fig. 12.

Increasing BER was registered from $1.19 \cdot 10^{-6}$ to $8.59 \cdot 10^{-5}$ for 10 Gbps NRZ and increasing Q-factor with a difference of 0.96. Raising the optical power brought an improved error rate, but at the expense of higher demands on the transmission systems.

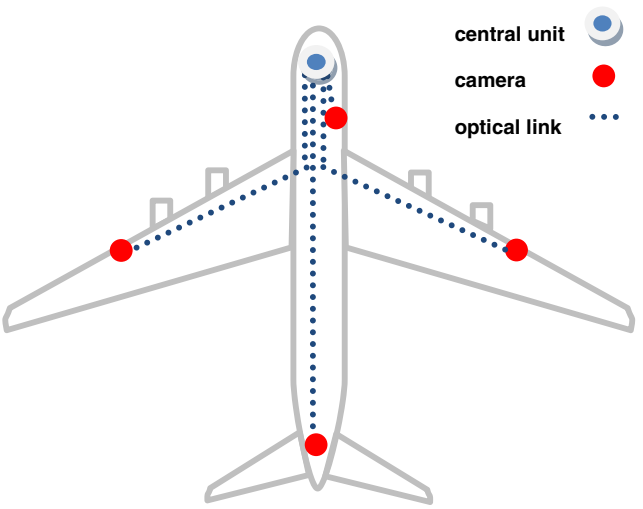

Fig. 11 Airplane MM camera network.

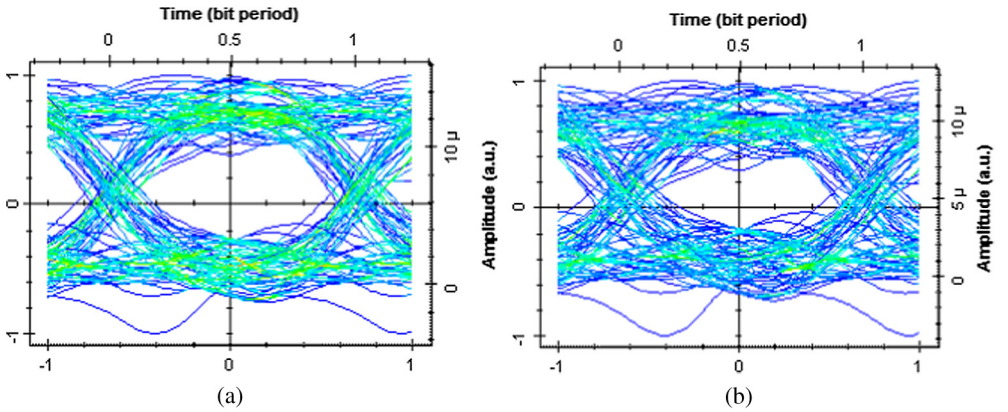

Fig. 12 Eye diagrams for 10 Gbps nonreturn to zero: (a) IL = 0 dB and (b) IL = 1 dB.

The most limiting factor reducing the bandwidth of multimode fibers is modal dispersion.[16] Dispersion could be highly suppressed by the proper performance of the refractive index, but due to the radial shifting of the fiber end faces, a different modal distribution can result in bandwidth reduction. We carried out a simulation on an OM3 measured, refractive, and profiled fiber to investigate the statistics of DMD, the number of guided modes, and changes in the bandwidth.

Simulation of DMD was performed with radial shifting of the transmitted beam coupling with a beam featuring a 5 μm profile and a step of movement of 1 μm. A test was performed at a wavelength of 850 nm to investigate convenient conditions for transmission. Pulse broadening and bandwidth reduction was observed at each point of the shift. The simulation scheme corresponds to the vibrational scenario described in Sec. 2.

Significant changes in transmission characteristics were observed in the case of maximal shifts. This can be clearly shown via pulse broadening in Fig. 13, which starts with beams guided closer to the cladding. In other words, the figure shows how the DMD affects the duration of the launched pulse in respect to radial position. Figure 14 depicts a comparison of the bandwidth in MHz·km for the used fiber section with a drop for radial offsets >10 μm during vibrational influence.

Both figures demonstrate how the DMD influences modal bandwidth (directly or indirectly). In a steady state, the pulse broadening starts approximately before the 15 μm shift, but during vibrational conditions, the broadening starts approximately before 11 μm and achieves >0.7 ps higher broadening compared to the steady state. Pulse broadening was observed within fibers having a set length of 22 m. The situation is similar in the case of the shape of bandwidth statistics. The useful bandwidth continually (without considering peak values) decreases to zero. A connection offset causes a similarly useful bandwidth (~1000 MHz · km in the range of 0 to 10 μm and then it drops). The visible step determines where most of the optical power should be guided and limits the transmitted bandwidth. The bigger the radial shift of the launched beam, the more the modes

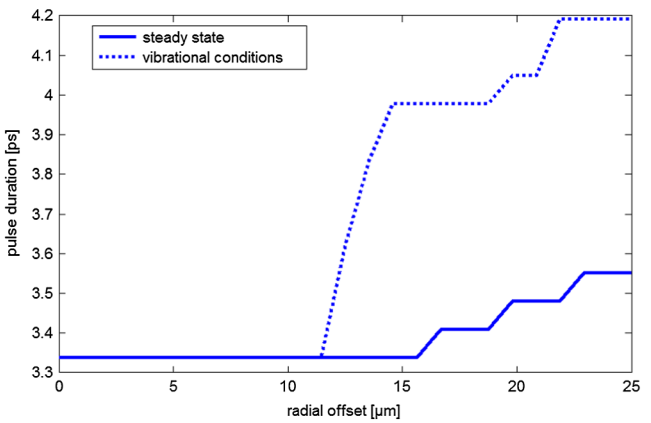

Fig. 13 Pulse broadening due to radial shifting.

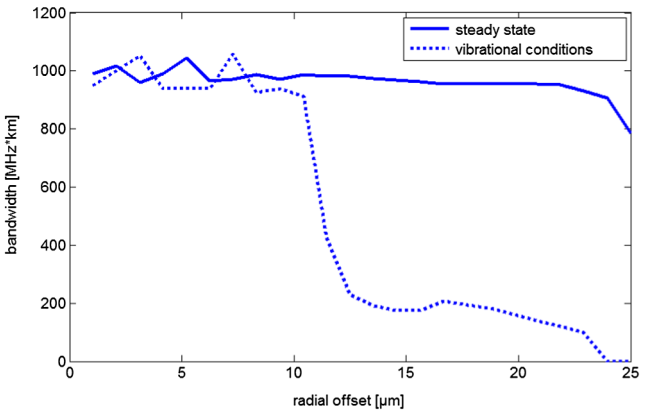

Fig. 14 Reduction of bandwidth due to radial shift.

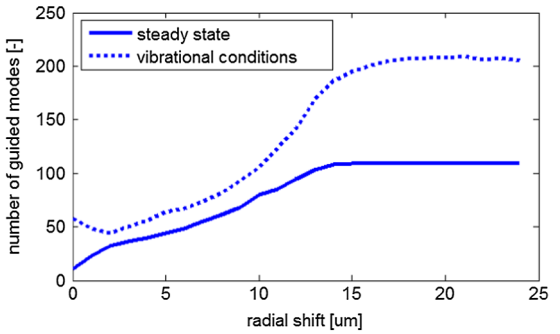

Fig. 15 Number of guided modes in fiber related to radial shift.

were guided in fibers and the higher the impact the DMD had on transmission characteristics. The dependence of guided modes on the radial shift is shown in Fig. 15 with the solid line representing a steady state and the discontinued line representing a situation with connection offsets due to vibrations.

Increasing the number of modes before the offset of ~10 μm corresponds to an increase in DMD and a bandwidth reduction.

Simulation results imply that a harsh environment (from the point of view of temperature and vibrational changes) can easily modify the connection profile of fibers, especially for MM fibers with high tolerable recommendations and norms.

5 Conclusion

We have demonstrated the influences of MM class OM3 and OM4 optical links within a harsh environment, in particular in the field of avionics. Tests were designed to determine the impacts of thermal and vibrational changes on connectors and intersections. Simulation and experimental results show that although these effects could lead to slight changes of IL up to 1 dB for the whole optical link including various sections joined by connectors, the influence on bandwidth reduction has to be considered. Vibrational conditions, together with a low tolerance for fiber industry standards, lead to deformed mode-field characteristics and an increase of DMD. This substantially reduces the bandwidth to <20%. Every additional connector joint (in aircraft, this is occasionally inevitable due to assembly) can randomly increase bandwidth reduction. Understanding mode distribution changes and substantial bandwidth reduction in a harsh environment is a key phenomenon that has to be considered to assure the consistently high reliability of aircraft optical networks.

Acknowledgments

This work was supported by the Czech Technical University Grant No. SGS14/190/OHK3/3T/13. The authors would like to thank SQS, Fiber Optics for providing access to the vibrational testing laboratory.

References

1. A. A. R. Lee and S. D. Rayner, "Avionic architectures incorporating optical fibre technology," in *IEEE Conf. on Avionics Fiber-Optics and Photonics*, pp. 10–11, IEEE, New York, NY(2006).
2. C. V. Oster, Jr., J. S. Strong, and C. K. Zorn, "Analyzing aviation safety: problems, challenges, opportunities," *Res. Transport. Econ.* **43**(1), 148–164 (2013).
3. R. Pirich and J. Mazurowski, "Engineering of fiber optics infrastructure," in *Systems, Applications and Technology Conf.*, pp. 1–4, IEEE, New York, NY(2012).
4. P. Jérôme, "Composite materials in the Airbus A380—from history to future," 2013, http://www.iccm-central.org/Proceedings/ICCM13proceedings/SITE/PAPERS/paper-1695.pdf (8 August 2014).
5. DAPHNE project, "Developing aircraft photonics networks," http://www.fp7daphne.eu/ (August2011).
6. K. Schulze et al., "Model-based design and evaluation of fault-tolerant fibre-optical networks for avionics," 2011, https://www.tu-ilmenau.de/fileadmin/public/sse/Veroeffentlichungen/2012/PSAM_ESREL_2012_Final.pdf (8 August 2014).
7. J. Gomez et al., "Comparing polymer optical fiber, fiber Bragg grating, and traditional strain gauge for aircraft structural health monitoring," *Appl. Opt.* **48**(8), 1436–1443 (2009).
8. N. Takeda, "Embedded fiber optics shed light on aircraft damage," 2008, http://spie.org/x20265.xml (8 August 2014).
9. Q. Li et al., "Scaling star-coupler-based optical networks for avionics applications," *J. Opt. Commun. Netw.* **5**(9), 945–956 (2013).
10. H. J. White et al., "Developing aircraft photonic networks for airplane systems," *Proc. SPIE* **8720**, 87200V (2013).
11. J. C. Williams and E. A. Starke Jr., "Progress in structural materials for aerospace systems," *Acta Mater.* **51**(19), 5775–5799 (2003).
12. C.-L. Chen, *Elements of Optoelectronics & Fiber Optics*, Irwin Professional Publishing, Illinois (1996).
13. J. M. Anderson et al., "Report: lightwave splicing and connector technology," *AT&T Tech. J.* **66**(1), 45–64 (1987).
14. ITU-T Recommendation G.651.1, "Characteristics of a 50/125 μm multimode graded index optical fibre cable for the optical access network," 2007, http://cds.cern.ch/record/1393442 (8 August 2014).
15. A. V. Bourdine, "Design of refractive index profile for multimode optical fibers with low differential mode selay," *J. Optoelectron. Eng.* **1**(1), 5–13 (2013).
16. D. H. Sim et al., "High-speed multimode fiber transmission by using mode-field matched center-launching technique," *J. Lightwave Technol.* **27**(8), 1018–1026 (2009).

Jan Bohata is a researcher at Czech Technical University (CTU) in Prague, Department of Electromagnetic Field. He received BS and MS degrees in electrical engineering from CTU in Prague in 2010 and 2012, respectively, where he is continuing his PhD studies. He has been involved in a few research projects focused on fiber optics problematics, including investigation of harsh environments for optical fibers. His current research interests include fiber optics, radio over optic systems, harsh environment for communications, and radio wave propagation.

Michael Písařík is a senior project manager at SQS. He received his MSc in 2002 from CTU in Prague. He leads the research department and R&D teams from SQS. His current research interest includes optical sensors, optics for harsh environment, fiber lasers, and modulators.

Stanislav Zvánovec is an associate professor and vice-head of the Department of Electromagnetic Field at the CTU in Prague. He received his MSc and PhD in 2002 and 2006, respectively, from CTU in Prague. He leads an optical team from Faculty of Electrical Engineering, CTU. His current research interests include fiber optical systems, sensors, and wireless optical communications.

Pavel Peterka received his MSc degree in physical engineering in 1993 and PhD degree in radioelectronics in 2000 from CTU in Prague. He is currently a senior research scientist in the Institute of Photonics and Electronics, Academy of Sciences of the Czech Republic. He has over 15 years of experience on design, characterizing, and development of specialty fibers and fiber lasers and amplifiers.